SEDIMENTOLOGY the journal of the International Association of Sedimentologists

Sedimentology (2015) doi: 10.1111/sed.12209

Comparison of lacustrine successions and their palaeohydrological implications in two sub-basins of the Triassic Cuyana rift, Argentina

CECILIA BENAVENTE*, ADRIANA MANCUSO*, NORA CABALERI† and ELIZABETH GIERLOWSKI-KORDESCH‡

*Instituto Argentino de Nivología, Glaciología y Ciencias Ambientales (IANIGLA), CCT-Mendoza, CONICET, Av. Adrián Ruiz Leal s/n, Parque General San Martín CC 330 (CP 5500), Mendoza, Argentina (E-mail: cebenavente@gmail.com)

†Instituto de Geocronología y Geología Isotópica (INGEIS), CONICET, Pabellón INGEIS – Ciudad Universitaria (C1428EHA), Ciudad Autónoma de Buenos Aires, Argentina

‡Department of Geological Sciences, Ohio University, 316 Clippinger Labs, Athens, OH 45701-2979, USA

Associate Editor – Daniel Ariztegui

ABSTRACT

Continental carbonates are rich in palaeoclimatic, palaeoenvironmental and palaeontological information. While carbonate accumulation mechanisms have been described for many types of continental environments, especially in extensional basins, there are still uncertainties that existing facies models fail to address. The Triassic Cerro de las Cabras and Cerro Puntudo formations are alluvial–fluvial–lacustrine sequences that represent a part of the sedimentary infill of two sub-basins of the Cuyana Basin during the early stages of the Triassic rift in west-central Argentina. Previous work has provided absolute dates, confirming that these deposits are coeval (Anisian) allowing a comparative study of carbonate sedimentation in an extensional tectonic context. The description and origin of freshwater carbonate deposits and their surrounding siliciclastic sediments in specific areas of the Cuyana rift, gives insight into the major factors that control carbonate precipitation in all rift basins, including the characterization of the palaeohydrology and the importance of provenance. The Cerro de las Cabras Formation represents an ephemeral, playa-lake depositional system with subaerial exposure and pedogenesis. Its aggradational succession corresponds to the evaporative facies association lake type, diagnostic of underfilled lake basins where persistently closed surface hydrology can lead to thick evaporites. However, this formation lacks thick evaporites and has microbialitic limestones, pointing to an open groundwater supply. The Cerro Puntudo Formation represents an alkaline playa-lake system fed by groundwater and ephemeral surface-water input. The unit is an aggradational–minor progradational succession, pointing to a fluctuating profundal facies association, suggesting a balanced-filled lake type. These two synchronous, lacustrine depositional systems were influenced by tectonics and climate. Provenance and hydrology are key controls in carbonate accumulation in continental rift basins that must be included in future facies models for continental carbonates. Comparison with other rift basins suggests that application of lake-type characterizations coupled with palaeohydrology and provenance patterns will aid in developing new sedimentation models for freshwater limestones in extensional settings.

Keywords Continental carbonates, limnogeology, microbialites, palaeontology, sedimentology, tectonics.

INTRODUCTION

Continental carbonates are rich in palaeoclimatic, palaeoenvironmental and palaeontological information; they are found within all types of land-based sedimentary systems all over the world (Alonso-Zarza & Wright, 2010; Gierlowski-Kordesch, 2010; Jones & Renaut, 2010; Gierlowski-Kordesch *et al.*, 2013), especially in extensional basins (Alonso-Zarza *et al.*, 2012). Reports on continental carbonate deposits in the geological record in South America are scarce and belong mainly to Jurassic and Cretaceous deposits (Bertani & Carozzi, 1985; Suárez & Bell, 1994; Rouchy *et al.*, 1996; Camoin *et al.*, 1997; Cabaleri & Armella, 1999, 2005; Gómez-Pérez, 2003; Tunik, 2003; Beraldi-Campesi *et al.*, 2004; Cabaleri *et al.*, 2005, 2013; Cabaleri & Benavente, 2013). Reports of Triassic continental carbonates, however, have been non-existent until now.

The exact nature and location of continental carbonate accumulation in association with microbialites has been linked tentatively with basin hydrology, especially in rifts (Gierlowski-Kordesch, 2010; Gierlowski-Kordesch *et al.*, 2013; Renaut *et al.*, 2013). Many facies models involving microbialitic carbonates within rift infill in the geological record, as well as in modern rifts, have failed to address the hydrology in a basin, most importantly groundwater influence and provenance as important controls (e.g. Wright, 2012; Harris *et al.*, 2013; Hargrave *et al.*, 2014). The aim of this contribution is to present results of a high-resolution study of continental carbonates from two sub-basins of the Triassic Cuyana rift basin in Argentina with a focus on the factors, most importantly palaeohydrology, which determined and influenced carbonate precipitation at the ramp or platform margin and transfer zone of these half-grabens. This will provide insight for establishing a facies model combining sedimentological and hydrological controls for determination of the exact origin of microbialitic facies in rift basins globally.

Geological setting

The Triassic sedimentary basins of Argentina formed during extension that caused fragmentation of Gondwana along its south-west margin (Uliana & Biddle, 1988). Of those basins, the Cuyana Basin is well-known for its extensive outcrops, palaeontological content and hydrocarbon reservoir potential (Spalletti, 1997; Chebli *et al.*, 2001; Stipanicic, 2001). The Cuyana is a rift basin oriented north-west/south-east, comprising several asymmetrical half-grabens along which the border faults for each half-graben alternate (Legarreta *et al.*, 1992; Kokogian *et al.*, 1993; López-Gamundí & Astini, 2004; López-Gamundí, 2010; Barredo *et al.*, 2011). In the northern area of the basin, the border fault is in the east, and in the south, the border fault lies to the west (Fig. 1; Ramos & Kay, 1991; Legarreta *et al.*, 1992; Barredo, 2005; López-Gamundí, 2010).

In the northern part of the basin, the Cerro Puntudo Formation outcrops are located in the Western Precordillera, San Juan province (S 30°59′52.20″, W 69°16′58.83″; Fig. 2) in the Cerro Puntudo sub-basin (north half-graben). In the southern part of the basin, the outcrops of the Cerro de las Cabras Formation are found at the foot of the Cerro de las Cabras hill (S 30°56′54.3″, W 69°17′22.9″; Fig. 2) in the Potrerillos sub-basin (south half-graben). The basement in both sub-basins is the Permian–Triassic volcanic deposits of the Choiyoi Group (Llambías, 2001). Surrounding each sub-basin, there are abundant Palaeozoic and Cenozoic sedimentary rocks within the palaeodrainage area. Palaeozoic deposits include volcanic rocks of late Permian age, and siliciclastic and carbonate marine formations. Cenozoic sedimentary units are continental siliciclastics (Folguera & Etcheverría, 2004; Fig. 2).

Both of the formations studied (Cerro Puntudo and Cerro de las Cabras) are dated as Anisian. The Cerro de las Cabras was dated by U–Pb (SHRIMP) as 243 ± 5 Ma (Ávila *et al.*, 2006), as was the Cerro Puntudo (243·8 ± 1·9 Ma; Mancuso *et al.*, 2010). Both successions represent infill of the basin during the first synrift stage (Fig. 3), allowing a comparative study in two different locations of the basin during the same rift stage.

METHODS

High-resolution sedimentary logs were measured in both sub-basins and facies were identified as siliciclastic facies from coarse to fine grain size

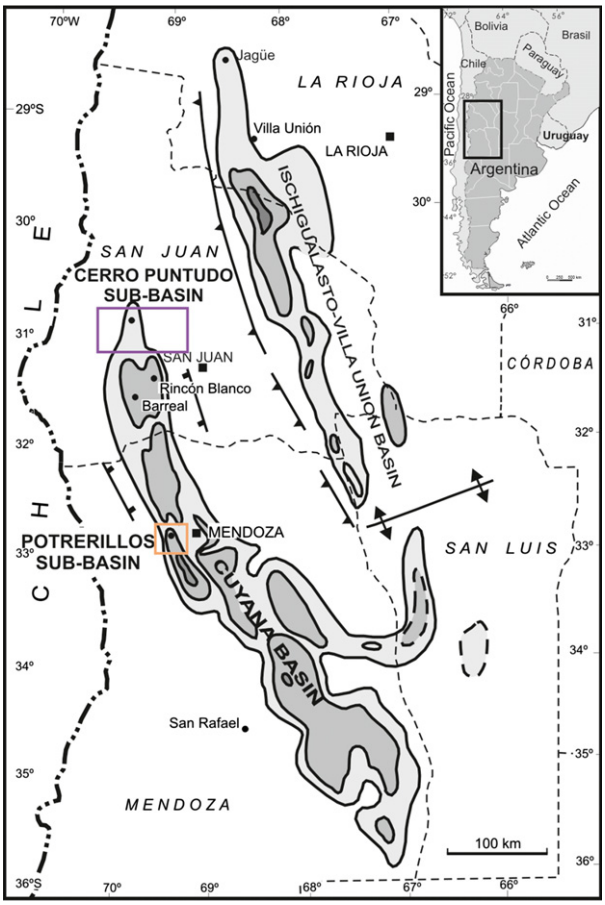

Fig. 1. Map of the sedimentary Triassic basins of the west-central region of Argentina showing the location of the Cerro Puntudo and Potrerillos sub-basins in the Cuyana rift basin. Coloured boxes indicate location of studied sub-basins and corresponding geological maps in Fig. 2. Modified from Stipanicic & Marsicano (2002).

(a) to (f) and carbonate-dominated facies from (g) to (m). Hand samples were collected for further analysis and facies were identified. Samples were named with an abbreviation of the formation (CC stands for Cerro de las Cabras and CP for Cerro Puntudo) plus a correlative number. Polished slabs of hand samples made at the Secretaría de Minería of Mendoza were analysed under a low-magnification microscope (Nikon NI-150 SMZ 1000; Nikon Corporation, Tokyo, Japan) at the Instituto de Nivología, Glaciología y Ciencias Ambientales (IANIGLA). These samples are part of the IANIGLA-ES collection under the following registration numbers: 1 to 42. Thin sections of hand samples, produced at the Instituto de Geocronología y Geología Isotópica (INGEIS), were studied using a petrographic microscope (Olympus BX-51; Olympus, Tokyo, Japan). The Rock Color Chart of the Geological Society of America was used for colour descriptions. Thirty grams of selected mudstones and siltstones were subjected to X-ray diffraction analysis (total fraction and finest fraction <62 μm) with an X-ray diffractometer (Philips X′Pert MPD; PANalytical, Almelo, The Netherlands) at the Instituto Tecnológico Minero (INTEMIN) of the Servicio Geológico Minero Argentino (SEGEMAR) of Buenos Aires. Patterns and cycles in sedimentation were tested using Markov Chain analysis (Krumbein & Dacey, 1969; Parks *et al.*, 2000), based on facies transitions in the studied successions. Matrix data were analysed by the χ^2 Statistical Frequency Test (see Supporting Information).

RESULTS

Sedimentology

Cerro de las Cabras Formation

The Cerro de las Cabras Formation at its type locality in the south half-graben overlies the Río Mendoza Formation in a transitional contact that is composed of conglomerates representing an alluvial-fan system. From base to top, the Cerro de las Cabras succession contains conglomerates, pebbly sandstones, sandstones in channel bodies, and sandstones that interfinger with mudstones, siltstones and limestones (Figs 4 and 5A). These deposits have been interpreted as sheetfloods and ephemeral fluvial systems (Toledo, 1987; Bellosi *et al.*, 2001). The middle section of the unit with its thickest outcrops reaching 900 m is dominated by carbonates associated with volcaniclastic deposits. Two facies associations (Table 1) have been recognized.

Sandflat and mudflat facies association: Pebbly sandstones (a) form units 90 cm thick with erosive bases and tabular geometry. They have faint planar cross-stratification (Sp); sets and cosets are 10 and 30 cm thick, respectively (Fig. 5B). These sandstones are medium-grained to coarse-grained and dusky red (5R 3/4) with well-sorted dispersed clasts up to pebble size (10 cm long). Lag gravels are observed on lower contacts.

Interpretation: The Sp indicates traction flows and the dominant clast size implies a highly competent flow producing migration of sandy bedforms (Fisher *et al.*, 2007a,b, 2008). Thickness of sets and cosets points to a waning flow

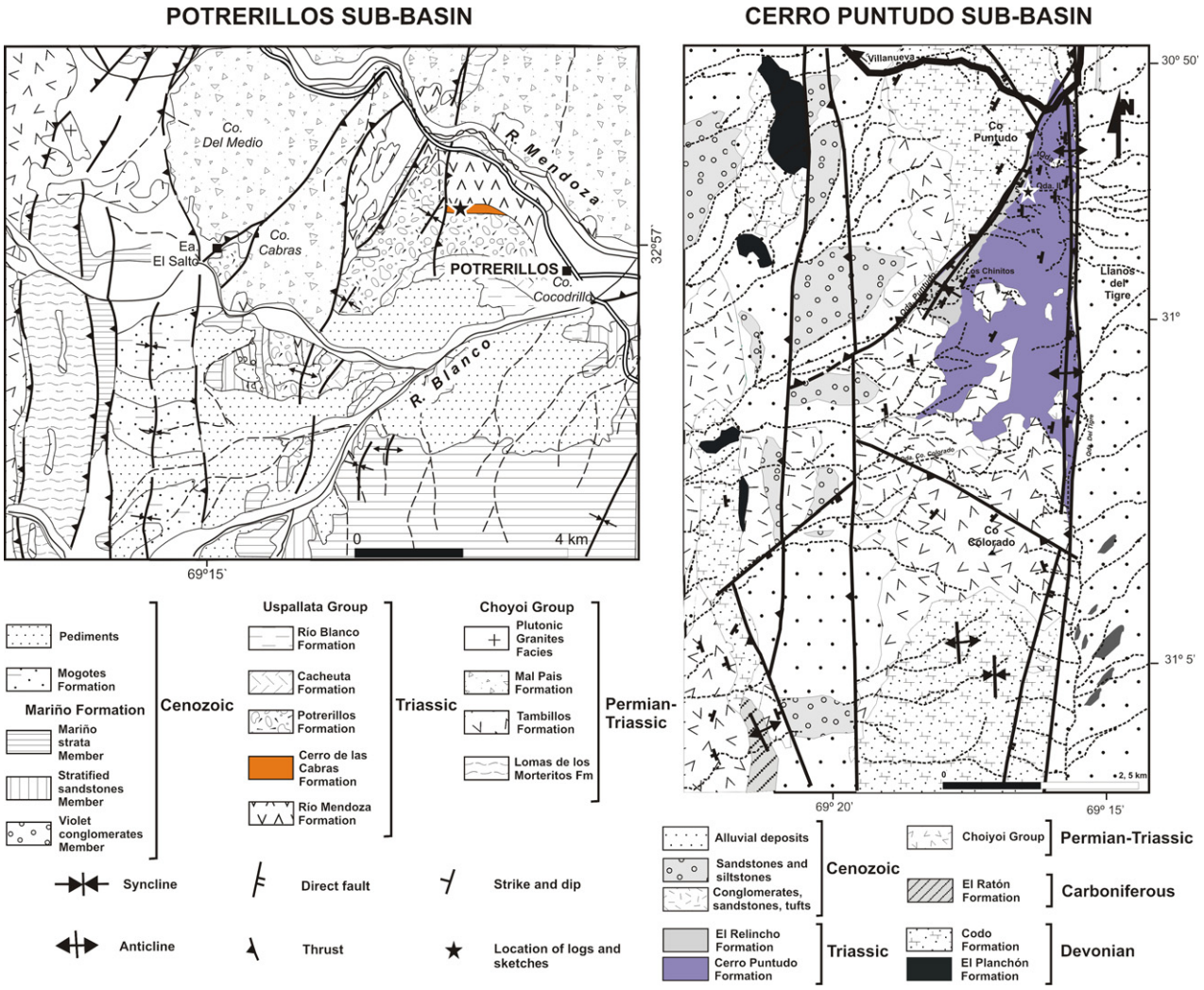

Fig. 2. Geological maps of the Cerro Puntudo sub-basin, in the San Juan province and of the Potrerillos sub-basin, in the Mendoza province; Triassic Cuyana rift basin, Argentina. The location of these maps is indicated in Fig. 1. Modified from Mancuso (2009) and Folguera & Etcheverría (2004).

regime where flows become unconfined (Smoot & Lowenstein, 1991) at the base of alluvial fans. This is common during sheetfloods (Young *et al.*, 2003; Fisher *et al.*, 2008) and is characteristic of erosional sandstone sheets (Fisher *et al.*, 2007a,b) in which the principal transport mechanism is unconfined tractive flow.

Massive intraclastic sandstones (b1) form units 60 cm thick. The sand is fine-grained to medium-grained and is dark reddish brown (10R 3/4) with a mottled fabric (Fig. 5C) of faint halos. There are subangular to subrounded calcitic intraclasts up to 3 cm long (Fig. 5D). Towards the top of units, carbonate nodules (5 cm wide) occur and the fabric colour changes towards greyish red purple (5RP 4/2) upwards. In thin section, the siliciclastic sand grains include quartz, biotite, hematite and lithic fragments (claystones and mudstones; Fig. 5D). Calcite spar is present as cement infilling in all intergranular spaces; there is no matrix (Fig. 5D).

Interpretation: The massive fabric of the sandstones is due to post-depositional pedogenic processes (Retallack, 1994; Ghosh, 1997; Kraus & Aslan, 1999). Angular clasts indicate moderate transport. The changes in colour of the units were produced by gleying, caused by the water table fluctuations that redistributed Fe (Kraus & Aslan, 1999). These fluctuations in the phreatic level also caused early spar precipitation by supplying Ca-rich fluids. Diffuse halos are interpreted as rhizohalos (Kraus & Hasiotis, 2006) and their grey colour characterizes Fe-depleted

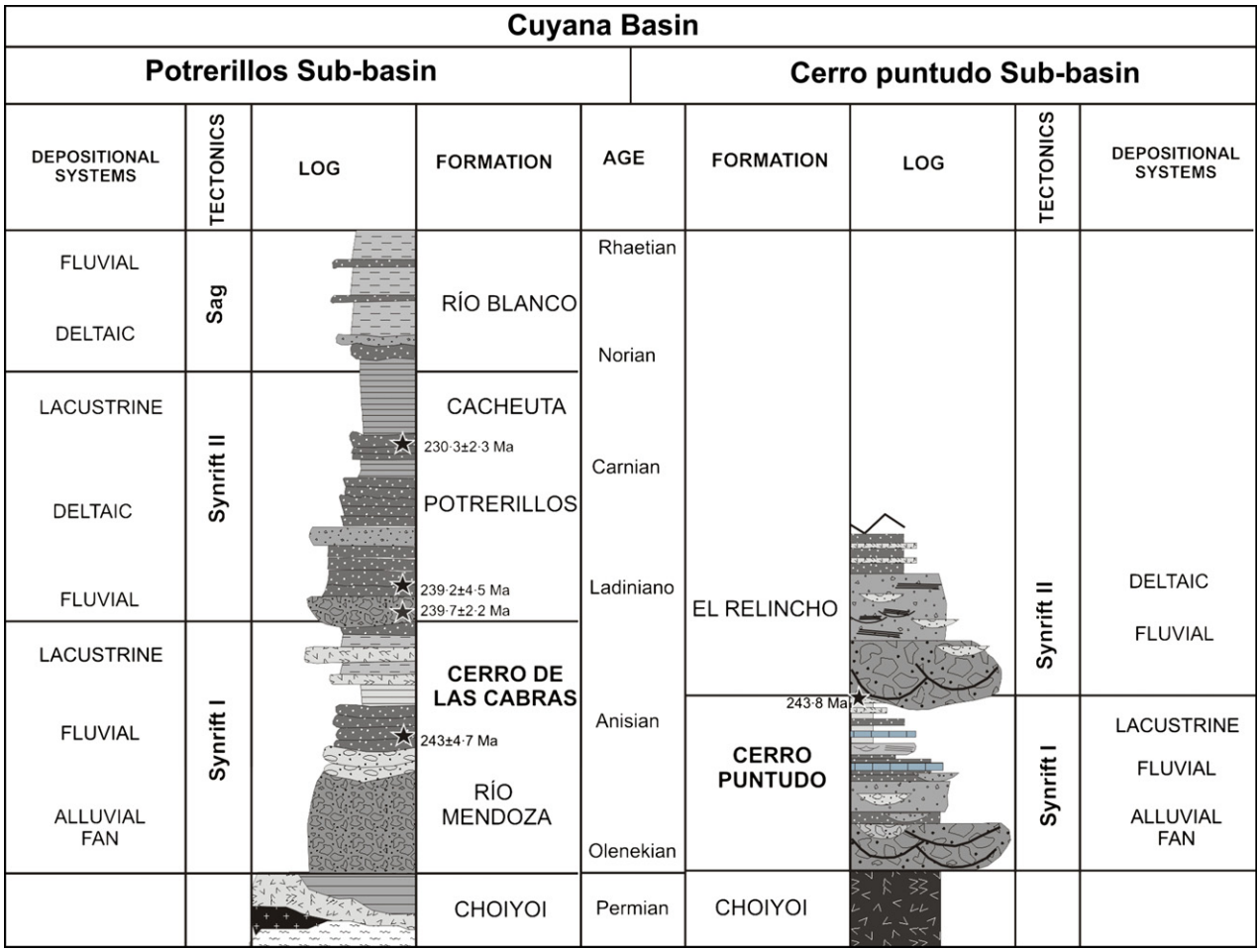

Fig. 3. Stratigraphic and palaeoenvironmental comparative chart of the Cerro de las Cabras (60 to 900 m in thickness) and Cerro Puntudo (90 m in thickness) formations, Middle Triassic (Anisian), Cuyana Basin. Both successions represent the infilling of the basin during the synrift I stage. Black stars indicate absolute dates for the sections.

zones of the rhizosphere. Therefore, the deposits are interpreted as the result of waning traction flows that were later affected by pedogenesis, developing incipient palaeosols during periods of low sedimentation. Similar, poorly developed sandy palaeosols have been described by Retallack (1994) from Cretaceous palaeosols in Montana, USA.

Mudrocks (e) form tabular siliciclastic units 20 to 90 cm thick that are greyish brown (5YR 3/2), dusky green (5G 3/2) and very dark red (5R 2/6). In a few cases, stratal geometry is lenticular. The fabric is mottled and nodular with faint horizontal lamination (Fl) to vague ripple cross-lamination (Fr). Nodules are carbonate and ellipsoidal and measure 1 to 7 cm in diameter; they are randomly dispersed in the units. Vertical, horizontal and circumgranular cracks are observed (Fig. 5E). Abundant vertical cracks at the top of the unit are infilled by spar, coated by 1 mm thick laminae of organic matter (OM) or clay lines and measure 0·2 to 3 cm wide and 9 cm long. They can also have fragments of mudstone up to 4 mm long as infill. Horizontal cracks are 0·1 cm wide by 5 cm long. Circumgranular cracks are 5 mm in diameter (Fig. 5E) and are lined with OM. Mottling consists of faint ellipsoidal halos, darker than the general rock fabric, which are 2 cm wide and 1·5 cm long. In general, the fabric changes to a dusky red (5R 3/4) at the top of the units. Large-scale features that resemble wavy horizonation 1 m in thickness, and shrink and swell textures showing broken and twisted centimetre-scale clay layers are found in these mudrocks (cf. Wilding & Tessier, 1988).

Two rhizohalo colour patterns are distinguished. Pattern 1 consists of red and violet halos in a grey matrix. Pattern 2 is represented by green to orange halos in a red fabric,

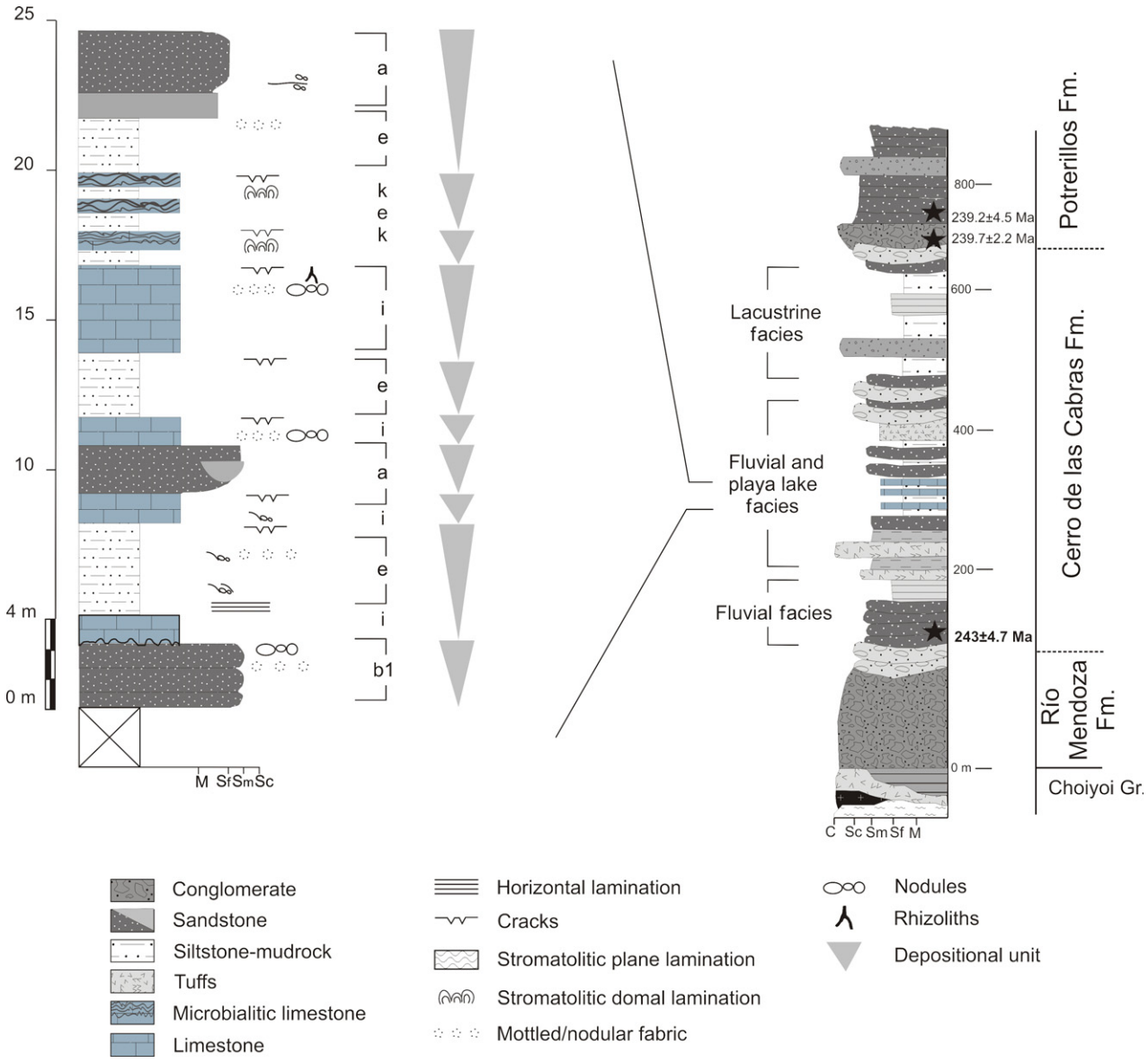

Fig. 4. Log section of the Cerro de Las Cabras Formation (Anisian) and detailed log of the middle section in the Potrerillos sub-basin, Cuyana Basin. Facies codes used can be found in Table 1. Absolute dates from Ávila *et al.* (2006) and Spalletti *et al.* (2008). General stratigraphic log has been modified after Kokogian *et al.* (1993).

commonly with carbonate nodules (Fig. 6). In thin section, siliciclastic grains are mainly quartz, biotite and lithic fragments, cemented by calcitic spar. Dominant minerals are calcite cement and quartz. The clay fraction is mainly smectite (Table 2).

Interpretation: The massive fabric is interpreted to be the result of pedogenesis (Kraus & Aslan, 1999; Kraus & Hasiotis, 2006; Krause *et al.*, 2010) with relict lamination and ripple cross-lamination, indicating a depositional origin. Fine lamination indicates suspension settle-out within mudflats (Smoot & Lowenstein, 1991; Gierlowski-Kordesch & Rust, 1994) and the ripple cross-lamination points to muddy sheetflood deposits (Maroulis & Nanson, 1996; Wright & Marriott, 2007). The relatively thick units could have been transported as bedload by sheetfloods and later altered by soil processes. Generally, these processes characterize alluvial plain environments in semi-arid to arid regions associated with alkaline volcanic provenance (Gierlowski-Kordesch, 1998; Huerta & Armenteros, 2004). Basal lags of small clasts indicate reactivation of sheetflows and erosion of older deposits.

Filled vertical tubules at the top of units are rhizotubules (Ghosh, 1997; Kraus & Hasiotis, 2006) indicating palaeosol development of this unit. Crack systems with lined clays resulted from root bioturbation or pedoturbation (Kraus & Aslan, 1999). Cracks without clays resulted from subaerial exposure and desiccation (Kraus, 1999). Colour changes are attributed to alternating wet and dry conditions (Kraus & Aslan, 1999; Krause *et al.*, 2010). The mottled fabric is related to rhizohalos (Ghosh, 1997; Kraus & Hasiotis, 2006) that indicate root activity. Palaeosol colour pattern 1 characterizes palaeosols that lack Fe oxides (Fig. 6) and is associated with preserved OM in the strata that is interpreted as rhizoliths (Klappa, 1980; Kraus & Hasiotis, 2006). These palaeosols represent very poor drainage and dysoxic to anoxic conditions. The red colour of pattern 2 rhizohalos indicates palaeosols with good drainage and high hematite content. Carbonate nodules formed in the vadose zone by precipitation induced by root activity in the rhizosphere (Ghosh, 1997; Owen *et al.*, 2008). In the succession, the tendency observed is from pattern 1 to pattern 2 (Fig. 6), which suggests a rise in the water table related to local climate variations (Meléndez *et al.*, 2009). Abundant pedogenic features support the periodic and ephemeral nature of the floodplain hydrology (Smoot & Lowenstein, 1991).

Presence of smectitic clays, of metre-scale wavy horizonation (possibly gilgais), and of possible shrink–swell features of broken clay layers indicate the development of palaeoVertisols (Wilding & Tessier, 1988; Lynn & Williams, 1992; Gierlowski-Kordesch & Rust, 1994; Gierlowski-Kordesch, 1998; Gierlowski-Kordesch & Gibling, 2002). Smectites are abundant in semiarid regions of the East Africa rift and eastern Australia, where the provenance includes alkaline volcanic rocks (Scott *et al.*, 2007) and the climate is seasonal (Wakelin-King & Webb, 2007). Vertisols are characterized by expandable clays that generate sand-sized pedogenic mud aggregates with wetting and drying cycles (Rust & Nanson, 1991; Gierlowski-Kordesch & Rust, 1994). These aggregates are commonly preserved in bedforms (i.e. ripple cross-lamination) in sheetflood deposits (Gierlowski-Kordesch, 1998; Wright & Marriott, 2007). However, preservation of these aggregates in this Cuyana facies is difficult since there are no large quartz or feldspar grains to protect them from compaction (Gierlowski-Kordesch & Gibling, 2002). However, calcite cement can aid in preservation (see Müller *et al.*, 2004).

Palustrine limestones facies association: Mottled-nodular mudstones (i) are micritic and yellowish grey (5Y 8/1) forming units 75 cm thick with a fabric containing mottles and nodules. Unit geometry is lenticular to tabular with a limited areal extent of 30 m. Vertical, horizontal and circumgranular cracks infilled by spar are common. Vertical cracks branch towards the base of the units and are 0·1 cm wide and 3 cm long. Horizontal cracks measure 0·2 cm wide and 1·5 cm long. Circumgranular cracks are up to 2 mm in diameter and are lined with clay. Vertical tubules 1 cm in diameter and 5 cm long are present at the tops of units. They are infilled by concentric calcitic spar and coated by silica (Fig. 7A). The mottled fabric exhibits diffuse brown and red halos associated with the cracks. These micritic mudstones contain a siliciclastic component (20%) and cross-sections of mineralized (calcite) concentric structures can be seen (Fig. 7B). Predominant siliciclastic grains are angular quartz, biotite, feldspar and lithic fragments. Two diagenetic stages are recognized with the first consisting of the precipitation of calcitic spar and microspar cements. The second stage is observed as corrosion of the micrite with spar and microspar cements by silicification.

Interpretation: Disruptive features in the fabric indicate subaerial exposure and pedogenesis (Freytet & Plaziat, 1982; Armenteros & Daley, 1998; Alonso-Zarza, 2003). Crack systems associated with OM, with a branching pattern that tapers downwards, are the result of rhizobrecciation (Freytet & Plaziat, 1982; Alonso-Zarza, 2003). Cracks that lack branching features are interpreted as desiccation cracks (Smoot & Lowenstein, 1991). Brown-reddish halos are rhizohalos (Kraus & Hasiotis, 2006) that indicate zones of Fe removal from the rhizosphere by roots. Vertical tubules filled by spar and coated by silica (Fig. 7A and E) are rhizoliths (Klappa, 1980; Huerta and Armenteros, 2005). These features support a primary subaqueous, Ca-rich and shallow depositional setting with subsequent exposure and pedogenesis. Siliciclastic grains were supplied by sheetflooding from the distal alluvial-fan system; no evidence for aeolian-linked processes has been found. Corrosion in calcite is associated with silicification during early diagenesis that commonly alters continental carbonates (Bustillo & Alonso-Zarza, 2007; Bustillo, 2010).

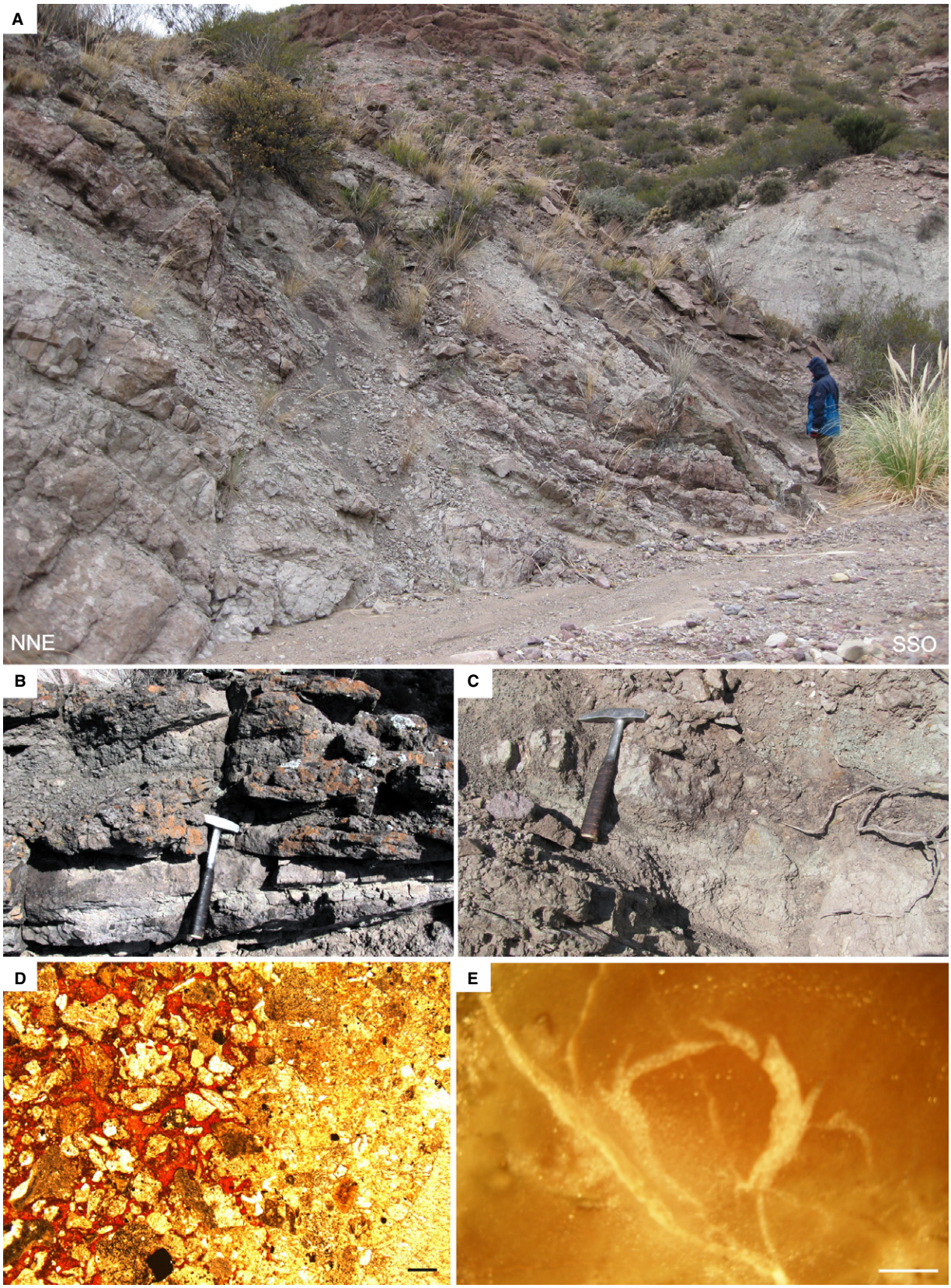

Fig. 5. Outcrop, polished slabs and thin section photographs of the facies of the Cerro de las Cabras Formation (Anisian) in the Potrerillos sub-basin (South), Cuyana Basin. (A) General view of the outcrop section of this formation 2 to 10 m of the log in Fig. 4 showing mottled–nodular limestone (i) and mudrock facies (e). Person is 1·7 m tall. (B) Outcrop photograph of pebbly sandstone facies (a) showing planar cross-stratification (Sp; 25 m, Fig. 4). Hammer is 35 cm long. (C) Outcrop photograph of massive intraclastic sandstone facies (b1) overlying mudrock facies (e) (4 m, Fig. 4). Hammer is 35 cm long. (D) Thin section microphotograph showing clastic fabric of massive intraclastic sandstone facies (b1; 0 m, Fig. 4) where the intergranular space is filled by spar cement and silt-sized matrix, calcite enhanced in red by Alizarin Red S staining. Framework grains are lithic fragments (claystone), quartz, feldspar, biotite and rutile. Parallel light (10×). Scale is 2 mm. (E) Polished slab photograph of mudrock facies (e; 12 m, Fig. 4) showing a circumgranular crack filled by spar (10×). Scale is 5 mm.

Laminated limestone (k) forms tabular strata 30 cm thick with plane to domal lamination and overlies massive mudstone (c) (Fig. 7C). Lamination is characterized by alternation of micritic crenulated laminae (olive grey; 5Y 4/1), that are laterally discontinuous and 1 to 3 mm thick, with carbonate mudstone laminae (greyish red; 5R 4/2) that are 3 mm thick. Lamination is disrupted by concave-upward structures (microtepees; Fig. 7D) and tubules and vertical cracks. In thin section, the laminae form sets 20 μm thick of homogenous micrite. Tubules are 20 μm wide, taper and branch downwards, and are up to 400 μm long and associated with peloids and clay linings (interpreted as cutans; Fig. 7E). Cracks disrupting lamination are 10 μm wide; they also branch and taper downwards. Vertical structures 300 μm wide exhibit rounded margins and are filled by spar. Also present are abundant fenestrae that are parallel to the lamination and measure 50 μm wide. These fenestrae are associated with peloids 20 to 40 μm in diameter. Bioclasts are scarce and consist of articulated ostracode valves 4 μm wide and 40 μm long. Quartz clasts are abundant, measure 80 μm in diameter, and are randomly dispersed. Silicification of these limestones with chalcedony crystals forms patches between calcitic laminae. Under a gypsum plate, the chalcedony shows high birefringence in the north-east and south-west quadrants of the microscope, indicating a length slow chalcedony.

Interpretation: Lamination of the facies is interpreted as biogenic (Riding, 1991a; Freytet & Verrecchia, 1998; Arp *et al.*, 2005; Dupraz *et al.*, 2009), most probably caused by bio-induced precipitation to form stromatolites. Tubular structures filled by spar and coated by silica are root moulds (Gómez-Gras & Alonso-Zarza, 2003). Fabric disruption by cracks and microtepee structures resulted from subaerial exposure and pedogenesis (Smoot & Lowenstein, 1991; Durand *et al.*, 2006). Microtepees formed when the biofilm was exposed, subsequent desiccation killed the micro-organisms, triggering the cracking and curling upwards of the margins (Flügel, 2004; Taher & Abdel-Motelib, 2014). Fenestral fabric resulted from the death and decay of micro-organisms (algae and cyanobacteria) in areas of the microbialite under subaqueous conditions (Flügel, 2004). Evidence for subaqueous deposition and subaerial disruption indicates that this was a palustrine subenvironment (Alonso-Zarza, 2003). It is possible that subaerial exposure was the result of a low water table (Meléndez *et al.*, 2009). Siliciclastic grains were most probably supplied by sheetflooding, although wind deposition is also possible. Localized silicification and the presence of length slow chalcedony indicate that this process occurred during early diagenesis of the limestones (Benavente *et al.*, 2015), involving sulphate-rich waters (Bustillo, 2010). Silicification can result from spontaneous precipitation in alkaline water (Platt, 1989) and length slow chalcedony precipitates from sulphate-rich fluids. This silicification suggests that the possible chemical composition of the secondary inflowing waters was sulphate-rich (Scholle & Ulmer-Scholle, 2003; Bustillo, 2010).

Cerro Puntudo Formation

The lower part of the Cerro Puntudo Formation is composed of red conglomerates and sandstones that represent alluvial-fan deposits. Upwards, the succession contains braided fluvial system deposits characterized by alternating dusky red (5R 3/4) conglomerates and medium-grained to coarse-grained, poorly sorted sandstones. The middle section of the succession is interpreted as a fluvial system of finer deposits: fine-grained to medium-grained sandstones of moderate red (5R 4/6) colour, forming narrow small channel bodies of limited lateral extent, and blackish red (5R 2/2) mudrocks. Interlayered with these sandstones and mudrocks, thin limestones are present. The uppermost succession is characterized by massive, yellowish grey (5Y 7/2) limestones and stromatolitic limestones that

Table 1. Facies associations and their characteristics, defined for the Cerro de las Cabras Formation (Anisian) in the Potrerillos sub-basin, South half-graben, Cuyana Basin.

Facies associations	Facies	Sedimentary structures/fabric	Bed geometry	Vertical and lateral relations	Fossil content	Interpretation
Sandflat and mudflat	Pebbly sandstones (a)	Medium- to coarse-grained sandstone, dusky red (5R 3/4) with dispersed pebbles, Sp (sets: 10 cm thick; cosets: 30 cm thick)	Tabular, 90 cm thick, erosive bases with lags	Overlies massive mudstone facies (c)	–	Proximal sheetfloods to distal alluvial-fan deposits
	Massive intraclastic sandstones (b1)	Fine-grained to medium-grained sandstone, mottling, red brownish dark (10R 3/4), carbonate intraclasts. Calcite cement only, no matrix. Mottling	Tabular, 60 cm thick	Interstratified with pebbly sandstone facies (a)	Rhizoliths and rhizohalos	Proximal sheetfloods with pedogenesis (gleying)
	Mudrocks (e)	Mostly structureless siliciclastic mudstone (Fm) with relict horizontal lamination (Fl) and ripple cross-lamination (Fr). Mottling, mudcrack systems, greyish brown (5YR 3/2), dark green (5G 3/2) or very dark red (5R 2/6). Calcite cement. Smectites. Silica coatings	Tabular-lenticular, 20 to 90 cm thick	Overlies mottled-nodular limestone facies (i) and underlies massive intraclastic sandstone facies (b1) and mottled-nodular limestones (i)	Rhizoliths and rhizohalos	Transition between sandflat (tractive flow) and mudflat (suspension settle-out) with palaeosol development in moderate-good to poor drainage
Palustrine limestones	Mottled-nodular carbonate mudstones (i)	Carbonate mudstone, micrite, mottling, spar-filled crack systems, OM in some cracks, nodules randomly dispersed, yellowish grey (5Y 8/1). Silica coatings	Lenticular-tabular, 75 cm thick	Underlies massive mudstone facies (c)	Rhizoliths and rhizohalos	Palustrine ponds
	Laminated limestones (k)	Micritic boundstone. Plane to domal lamination with crenulated discontinuous micrite laminae (1 to 3 mm thick), olive grey (5Y 4/1) alternating with greyish red mudstone (5R 4/2) laminae (3 mm thick), mudcrack systems, microtepee structures, silica coatings, peloids	Tabular, 70 cm thick	Overlies and underlies massive mudstones (c)	Algae and cyanobacteria Articulated ostracode valves	Stromatolites in carbonate ponds

are olive grey (5Y 4/1) and light olive grey (5Y 6/1). Also, fine-grained very dark red (5R 2/6) sandstones and mudrocks containing carbonate cement are present. They are associated with subordinated greyish green (10G 4/2) tuffs (Figs 7F and 8). The complete unit in its only known outcrop reaches 90 m in thickness. Six facies associations have been defined (Table 3).

Alluvial-fan facies association: Pebbly sandstones (a) form tabular strata 20 to 40 cm thick, with erosive bases and planar cross-stratification (Sp; Fig. 9A) and a moderate red (5R 4/6) colour. Units contain sets 14 cm thick with lenticular to sheet geometry and asymmetrical pinch out (Fig. 9A). Medium-grained to coarse-grained sandstone of this facies is coarser than the similar facies (a) in the Cerro de las Cabras Formation in the south half-graben and is poorly sorted with normal grading and imbricated lag gravel [including volcanic clasts up to 8 cm (cobbles) in diameter] at the base of units. Siliceous granules to pebbles (rock fragments, quartz, feldspar and volcanic clasts) are subangular to subrounded and measure 0·1 to 4 cm. Towards the top of the units, vertical violet halos are filled by finer material, giving the fabric a mottled aspect. Also, tubular branching structures coated by silica (Fig. 9B) are present in plane view of the top of the units, measuring 2 cm wide and up to 40 cm long.

Interpretation: Similar to facies (a) from the south half-graben but contains cobble-sized clasts indicating tractive high-regime flows (Barrier *et al.*, 2010) closer to an alluvial-fan system of moderate development (Beraldi-Campesi *et al.*, 2006). Pedogenesis is much more extensive here than in facies (a) in the south half-graben with the tubular dichotomous structures interpreted as rhizoliths (Klappa, 1980; Owen *et al.*, 2008). Development of incipient palaeosols and pedogenic effects is common in ephemeral subenvironments in which sedimentation is discontinuous (Smoot & Lowenstein, 1991).

Stratified intraclastic sandstones (b2) are medium-grained to coarse-grained and dark reddish brown (10R 3/4). They form lenticular to tabular geometries *ca* 0·5 to 1·5 m thick and contain planar cross-stratification (Sp) and ripple cross-lamination (Sr), normal grading and moderate sorting. Cosets are 20 cm thick and have quartz and feldspar clast lags at the base. Ripple bedforms form a unique bed of medium-grained sandstone with asymmetrical crests 3 cm high and 10 cm spacing. In a few units, flaser bedding and invertebrate traces have been recognized. These traces consist of vertical tubes 8 cm long and 1 cm in diameter in cross-section, filled by calcite (Fig. 9C).

Interpretation: Deposition is similar to that in facies (b1) in the south half-graben but with little palaeosol development. Sr indicates that ripples formed under tractive flow processes (Gierlowski-Kordesch, 1998). The Sp, Sr and flaser bedding characterize deposits dominated by sheetfloods (Gierlowski-Kordesch & Rust, 1994; Fisher *et al.*, 2008). Invertebrate traces have been identified as *Skolithos* and *Scoyenia* (Krapovickas *et al.*, 2008). They are usually attributed to arthropods that thrive in unstable environments (regarding water availability) and are common in marginal subenvironments of playa-lake systems (Gierlowski-Kordesch, 1991; Scott *et al.*, 2009).

Sandflat facies association: Graded sandstones (c) are composed of dark reddish brown (10R 3/4), very fine-grained to medium-grained sandstones with normal grading. They form tabular strata 20 to 45 cm thick with erosive bases. Some layers pinch out and generally are disrupted by massive mudstone lenses up to 2 mm thick. In a few units it is possible to recognize faint horizontal lamination (Sh) 0·1 mm thick. The fabric is mottled and disrupted by cracks and elongated to subcircular halos 0·5 to 2·5 cm in diameter that are pale yellowish orange (10YR 8/6) and greenish grey (5GY 6/1). Vertical cracks are up to 0·1 cm wide and 5 cm long. Horizontal cracks are continuous and 1 mm wide and 8 cm long; they are partially filled by calcite. At the base of the facies units, abundant subangular calcite intraclasts 0·5 to 8 cm long and carbonate lenses of micrite up to 2 cm thick (Fig. 9D) are present. The fabric also contains vertical and anastomosing tubules 6 cm long and 1 cm in diameter, filled by subrounded siliceous grains coarser than the grains in the fabric. The tops of units contain mud drapes with cracks and circular structures of 1 to 3 cm in diameter filled by calcite. In thin section, angular to subangular clasts of quartz, feldspar and rutile 3 mm long are present. Interstitial space is filled by spar cement and siliceous grains show corrosion with their fringes replaced by calcite. Mineralogical analysis of the total rock fraction shows that major components are calcite and quartz while the clay fraction is predominantly illite and mica (Table 4).

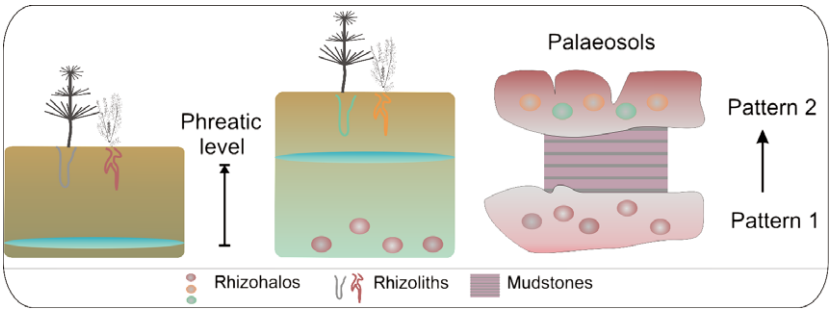

Fig. 6. Rhizohalo patterns and their stratigraphic trends found in palaeosols of mudrock facies (e) of the Cerro de las Cabras Formation (Anisian), Potrerillos sub-basin (South), Cuyana Basin (17 m, Fig. 4). Colour of the halos shows the relative position of the palaeowater table. The change from pattern 1 to pattern 2 in the palaeosols of the succession suggests a rise in the palaeowater table.

Table 2. Mineralogical composition data of the total rock fraction and phyllosilicates composition of the clay fraction from mudstones of the Cerro de las Cabras Formation, Potrerillos sub-basin, Cuyana Basin.

		Total rock fraction								Phyllosilicates clay fraction			
Facies	Sample	Qz	Phy	FK	P	Ca	An	He	Ba	Sm	I/M	Cl	K
e	CC20-12	xx	xx	x	xx	xxx	–	tr	xx	xxx	xx	–	–
	CC19-12	xxx	xx	xx	xx	x	x	–	–	xxx	xx	–	–

Qz, Quartz; Phy, Phyllosilicates; FK, Potasium feldspar; P, Plagioclase; Ca, Calcite; An, Analcime; He, Hematite; Ba, Baritine; Sm, Smectites; I/M, Illite/Mica; Cl, Chlorite; K, Kaolinite; e, Mudrock facies. Estimated relative content: xxx = major components; xx = minor components; x = accessory components; tr = traces.

Interpretation: Faint Sh characterizes sheetflood deposits (Fisher *et al.*, 2007a,b, 2008) in an alluvial plain where confined flows are scarce (Smoot & Lowenstein, 1991). The massive fabric is interpreted as a post-depositional effect of pedogenesis (Gierlowski-Kordesch & Rust, 1994; Retallack, 1994; Wright & Marriott, 2007). Sheetflood deposits are characterized by the interfingering of coarser and finer material (mud drapes), indicating waning flows depositing suspended load over bedload within a sandflat (Smoot & Lowenstein, 1991; Gierlowski-Kordesch & Rust, 1994; Fisher *et al.*, 2008). Mud drapes under subaerial exposure undergo cracking, which provides evidence for the ephemeral nature of this sedimentary system (Smoot & Lowenstein, 1991). Interfingering of fine and coarser sandstone laminae implies fluctuating inflow that is also distinctive of ephemeral flows (Nanson *et al.*, 2002; Fisher *et al.*, 2008). Erosive bases suggest that the initial flow had sufficient competence to erode the underlying deposit (Fisher *et al.*, 2007a). This phenomenon explains how the calcite intraclasts were incorporated into the deposit and why clast angularity suggests minor transport. Halos were formed by roots that generated Fe depletion zones in the rhizosphere (Kraus & Hasiotis, 2006). Colouration indicates incipient palaeosols with moderate to good drainage (Kraus & Hasiotis, 2006). Cracking was probably also caused by root disruption (Retallack, 1994). Vertical and anastomosed tubules are probably due to the infaunal activity of organisms (Bromley, 1996; Buatois & Mángano, 1998) or root activity; the lack of cutans points towards bioturbation. In sandstone, associated claystone sediments rich in smectite and calcite enhance the preservation potential of traces (Scott *et al.*, 2009). Illitic clays are common in semi-arid environments of modern rifts, particularly if associated with smectites (Scott *et al.*, 2007), where they can form from zeolitic precursors (Renaut, 1993). Moreover, illite is abundant in palustrine areas distal from fluvial or alluvial supply (Calvo *et al.*, 1989), pointing to authigenesis under those conditions.

Stratified sandstones (d) are very fine-grained to medium-grained sandstones of moderate reddish brown (10R 4/6) and very pale orange (10YR 8/2). They exhibit faint to conspicuous horizontal lamination (Sh), faint ripple cross-lamination (Sr) and planar cross-stratification (Sp) (Fig. 9E). Geometry is tabular to lobe-like

and facies units are 0·15 to 1·2 m thick and massive towards the top. Sh laminae thickness varies between 0·1 mm and 2 mm in sets 1·5 to 2 cm thick (Fig. 9E); they are disrupted by convolute structures. Sr laminae are 0·1 mm thick and are inclined *ca* 10°. Planar cross-stratification (Sp) is minor in occurrence with sets 2 to 5 cm thick and cosets 15 cm thick. The tops of units show mud drapes with the fabric containing cracks filled by subangular mudstone clasts of up to 1 cm long. Also, angular clasts of calcite 2 mm long are observed at the base of units along with abundant subangular to subrounded grains 2 mm in length of quartz and feldspar. Vertical cracks 0·2 cm wide and 6 cm long are associated with circular yellowish halos with irregular margins 1 cm in diameter (Fig. 9F). Vertical structures up to 0·1 cm wide by 2 cm long, tapering downwards, occur at the top of units. Silica nodules 1·5 cm in diameter are present in the middle of the facies units. Mud chips of 2 cm size with plastic deformation are dispersed in the fabric and are oriented parallel to the stratification surface. Mineralogical analysis indicates that quartz, calcite and analcime are predominant. The clay fraction is dominated by smectites (Table 4).

Interpretation: Sh indicates deposition under upper flow regime conditions, near the boundary between sub-critical and super-critical flows (Miall, 1996). These conditions usually occur during flash floods (Fisher *et al.*, 2007a,b, 2008). The associated convolute structures are the result of deposition of material with different densities (mixed loads) that generate differential loading and consequent synsedimentary deformation (van Loon, 2009). Sr and rare Sp result from sheetflood processes (Smoot & Lowenstein, 1991; Gierlowski-Kordesch, 1998; Leier *et al.*, 2010). Generally, aggradation of these types of successions is slow because of the long periods between flood events (Huerta & Armenteros, 2005; Wakelin-King & Webb, 2007). Cracked mud drapes show the ephemeral nature of sedimentation (Smoot & Lowenstein, 1991; Gierlowski-Kordesch & Rust, 1994) with mud chips resulting from their erosion (Smoot & Lowenstein, 1991; Fisher *et al.*, 2007a). Associated halos and cracks are attributed to root activity (Smoot & Lowenstein, 1991; Kraus & Hasiotis, 2006; Rasbury *et al.*, 2006) and the yellow colouration of the rhizohalos indicates moderate to good drainage (Landon, 1984; Macedo & Bryant, 1987; Kraus & Hasiotis, 2006). Silica nodule development is common in the vadose zone of palaeosols by infiltration of meteoric waters and water table fluctuations (Bustillo, 2010). Smectites characterize soils developed in association with alkaline volcanics, as discussed with facies (c). Analcime characterizes marginal lake areas of alkaline–saline water bodies in association with groundwater input (Renaut, 1993; Cabaleri *et al.*, 2013).

Mudflat facies association: Mudrocks (e) form pale red (5R 6/2) and greyish red (10R 4/2) tabular strata 0·1 to 1·8 m thick. The fabric is partially massive (Fm) with faint horizontal lamination (Fl) and minor low-angle ripple cross-lamination (Fr). Towards the top of the units, the fabric becomes massive (Fm). Horizontal lamination is comprised of alternating laminae of greyish yellow (5Y 8/4) fine sandstone, 3 mm thick, and greyish red (5R 4/2) mudstones, 1·5 mm thick. Low-angle ripple cross-lamination inclines 15° from the stratification plane. Between laminae, circular structures with calcite infilling 1 to 5 mm in diameter are recognized (Fig. 9G). One of the most distinctive features of this facies is the presence of horizontal calcite crystal crusts 4 cm long and 0·4 cm thick with silica laminae 1 mm thick at the base (Fig. 9H). Microtepee structures 0·5 cm high are common in the crusts. Intraclasts of microbial micrite (mat chips) are common; they are subrounded, 2 cm long and 2 mm wide (Fig. 9I) and contain micritic dark laminae 0·5 mm thick and ostracode articulated valves (Fig. 9K).

The muddy fabric is disrupted by diffuse halos of orange, green and grey, which are 0·1 cm wide and 2·5 cm long. Pattern colour changes at the base of units show dominant red fabric containing pink and grey halos 2 cm wide and 6 cm long (Fig. 9J). Lenses composed of angular grains of quartz, feldspar, rutile, biotite and lithic fragments 2 mm long, complete oncolites 2 cm in diameter, fragmented oncolites 1 cm long and circular structures 0·5 cm in diameter recrystallized by spar are dispersed in the middle of facies units. Also dispersed are subrounded micrite intraclasts 1·3 cm long and subangular calcite intraclasts 3 mm long. Tops of facies units contain elongated tubular structures, measuring 1 cm wide by 12 cm long, that taper and branch downwards and exhibit calcite infilling and silica coatings. In thin section, a clay fabric (80%) is observed with patchy micrite and spar. Mineralogical analysis shows that the major components are quartz and analcime and the clay fraction is dominated by smectite (Table 4).

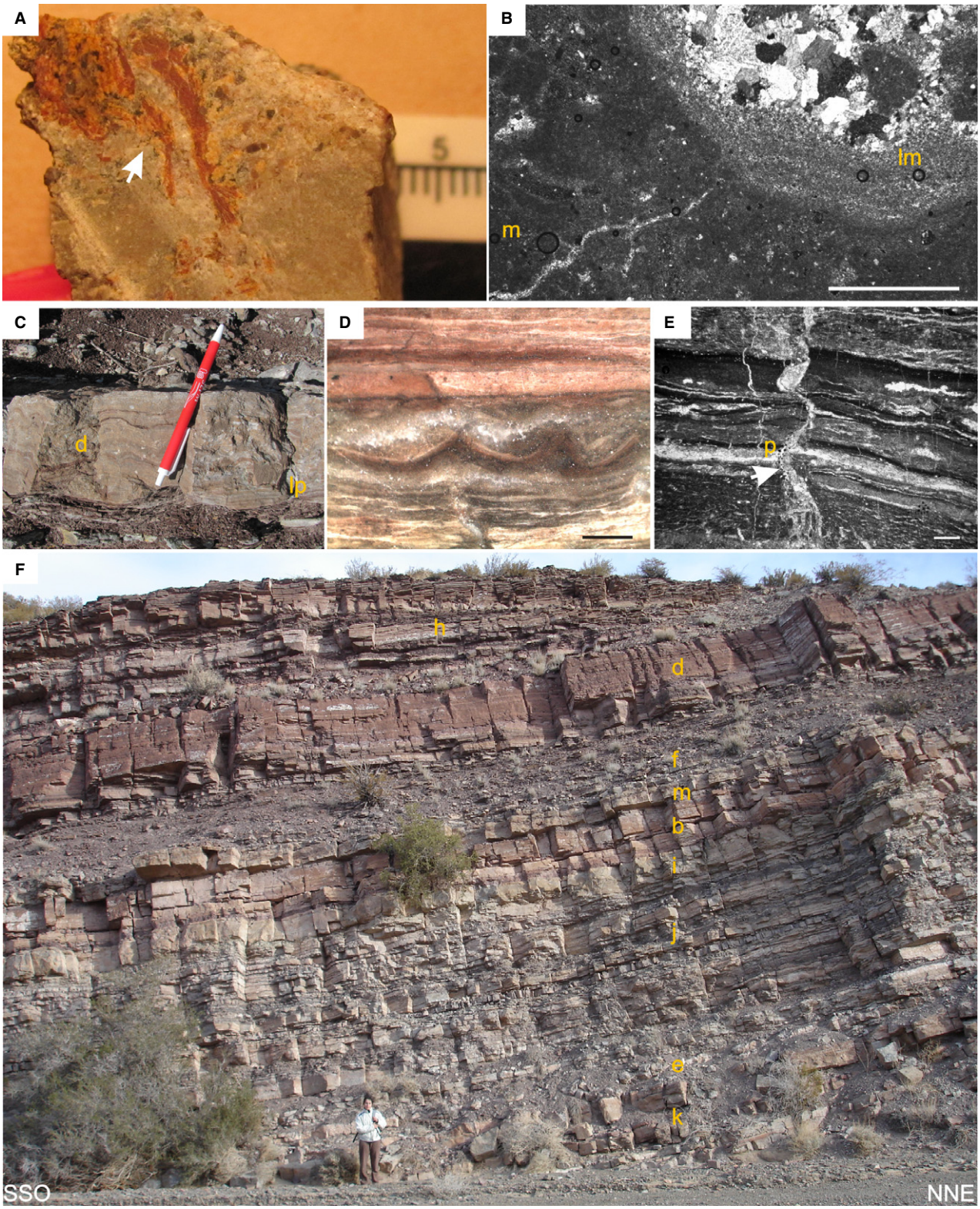

Interpretation: Deposition is similar to that interpreted for facies (e) in the Cerras de las Cabras Formation in the north half-graben: sheetflood muddy bedload (Fr) to suspension settleout lamination (Fl) with post-depositional pedogenic processes giving the fabric a massive cha-

Fig. 7. Outcrop, polished slabs and thin section photographs of the facies defined for the Cerro de las Cabras Formation (Anisian) in the Potrerillos sub-basin (South), Cuyana Basin. (A) Slab photograph of mottled-nodular limestone facies (i) (2·5 m, Fig. 4) showing tubule (rhizolith) filled by spar and coated by silica (arrow). Scale is in millimetres. (B) Thin section microphotograph of (A) showing rhizolith with spar-filled interior immersed in a homogenous micrite (m) with a concentric laminated micrite coating (ml). Planar light (4×). Scale is 2 mm. (C) Outcrop photograph of laminated limestone facies (k) (17·5 m, Fig. 4) showing tabular geometry of this facies and the laminar planar (lp) to domal (d) laminated macrofabric. Length of pen is 14 cm. (D) Slab of C with concave structures and micritic laminae interlaminated with siliciclastic mudstone laminae. Scale is 2 mm. (E) Thin section microphotograph of (D) with a vertical structure disrupting laminated micritic texture interpreted as a rhizolith in association with peloids (p) and cutans (arrow). Parallel light (4×). Scale is 2 mm. (F) General view of the outcrop of the Cerro Puntudo Formation (Anisian), Cerro Puntudo sub-basin, Cuyana Basin (10 to 40 m, Fig. 8) where the mudrock facies (e), stratified sandstone (d), oncolitic laminated sandstone (h), mottled carbonate mudstone (i), nodular wackestone (j), laminated limestone (k) and oncolitic floatstone facies (m) crop out. Person is 1·7 m tall.

racter, disrupting original sedimentary features and producing Vertisols (Gierlowski-Kordesch & Rust, 1994; Gierlowski-Kordesch, 1998). Interfingered sandstone lenses may indicate tractive flows mixed with mud bedload (Maroulis & Nanson, 1996). Halos are the result of pedogenic processes (Catena & Hembree, 2012) and their colours (yellow to grey halos in red soils) indicate moderate to good drainage (Kraus & Hasiotis, 2006) with drainage intermediate in size (Macedo & Bryant, 1987). Elongated tubular structures and calcite circular structures are interpreted as rhizoliths (Klappa, 1980; Huerta & Armenteros, 2005; Catena & Hembree, 2012). Oolites were probably transported, as evidenced by their fragmentation and association with transported siliciclastic grains. Efflorescence crusts are the result of intrasedimentary crystalline growth that occurs in extremely arid periods, commonly in lake margin areas (Hardie *et al.*, 1978; Smoot & Lowenstein, 1991; Rosen, 1994; Scott *et al.*, 2010). It is probable that the limited size of the crusts was controlled by the confinement pressure of the muddy sediment (Lowenstein & Hardie, 1985; Smoot & Lowenstein, 1991). Microbialite intraclasts or micritic mat chips are interpreted as the result of eroded surfaces that were stabilized by biofilms (Cuadrado *et al.*, 2011; Taher & Abdel-Motelib, 2014). It is probable that these surfaces were colonized when they remained wet due to a raised water table after the flood. Eventually, the surfaces suffered desiccation and were eroded in the next flooding event. This facies is typical of the transition area between a muddy sandflat (Gierlowski-Kordesch & Rust, 1994) and the outer zones of the mudflat subenvironment (Surdam & Sheppard, 1978) in throughflow playa lakes (Rosen, 1994; Minter *et al.*, 2007; Scott *et al.*, 2009). Mineralogical composition indicates alkaline–saline waters (Renaut, 1993; Cabaleri *et al.*, 2013) in semi-arid zones or in strongly seasonal climates (Scott *et al.*, 2007).

Laminated siltstones (f) are muddy siltstones that exhibit faint horizontal lamination (Fl) and a partially mottled to massive fabric (Fm) of moderate red (5R 5/4) and greyish red (10R 4/2) colour. Facies units are tabular and measure 0·7 to 1·2 m thick with erosive bases. Laminae are 0·1 mm to 1 cm thick and form units 2 cm thick alternating between red and greyish red. Lamination is disrupted by convolute structures 5 cm long and 3 cm high (Fig. 9L). Grains of subrounded and subangular quartz, feldspar, rutile and biotite measure 0·1 to 2 mm in length and are associated with disrupting tubular structures and halos (Fig. 9M). Fibrous-radial calcite (Fig. 9N) and silica in the carbonate halos surround the tubular structures. There are also subangular calcite intraclasts 3 mm to 1·5 cm long. The massive fabric is disrupted by horizontal structures 5 cm wide and 1·5 cm thick, and vertical tubules of 0·4 cm in diameter and 5·5 cm long that branch and taper downwards, both filled with calcite and coated by silica. Also present are circular pink halos 0·5 cm in diameter with angular grains of quartz and feldspar 0·1 mm in length. In thin section, a detrital texture with angular and subrounded siliciclastic grains contains mostly angular, homogenous micrite intraclasts 80 μm long with straight filaments 20 μm wide and 150 to 250 μm long, and circular structures with two external walls 40 μm in diameter. Other carbonate grains are oolites 800 μm in diameter; the nuclei show spar replacement of algae fragments and the cortex contains parallel filaments arranged radially. Bioclasts include scarce ostracode valves 200 μm long recrystallized by spar. Microspar patches are present in the fabric as well as microgranular silica. Mineralogical analysis of the total rock fraction shows quartz and analcime as major components. The clay fraction is mainly smectite, illite and mica (Table 4).

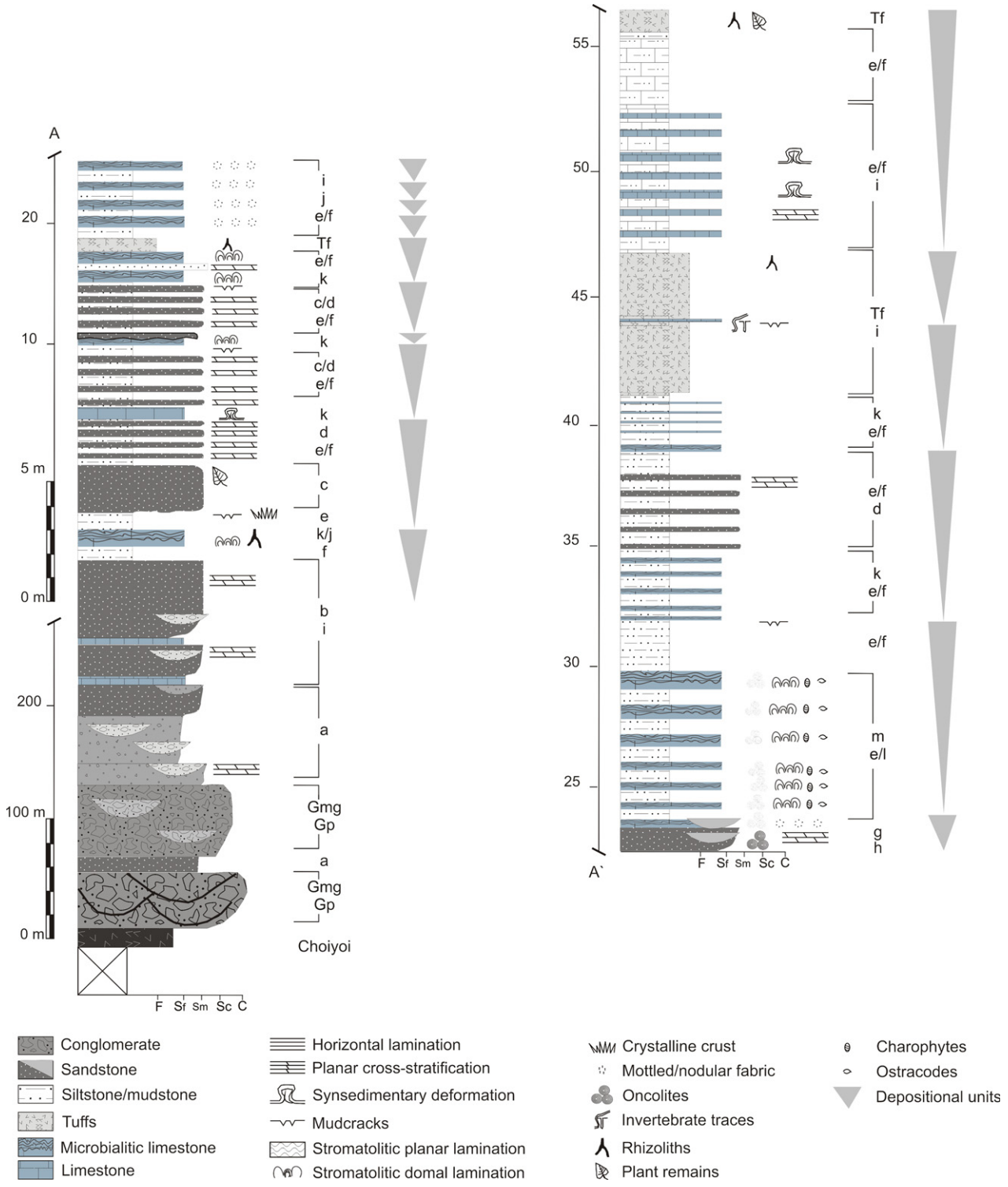

Fig. 8. Detailed log section of the Cerro Puntudo Formation (Anisian), at the Cerro Puntudo sub-basin (North), Cuyana Basin. The facies codes can be found in Table 3. F: fines; Sf: fine sandstones; Sm: medium sandstones; Sc: coarse sandstones; C: conglomerates.

Interpretation: Fl characterizes mudflat sedimentation (Hardie *et al.*, 1978; Gierlowski-Kordesch & Rust, 1994). The thin sandy lenses are formed by low-energy tractive flows. Fm features, including halos and branching tubules, indicate exposure and vegetation forming inci-

Table 3. Facies associations and their characteristics, defined for the Cerro Puntudo Formation (Anisian) in the Cerro Puntudo sub-basin, North half-graben, Cuyana Basin.

Facies associations	Facies	Sedimentary structures/fabric	Bed geometry	Vertical and lateral relationships	Fossil content	Interpretation
Alluvial fan	Pebbly sandstones (a)	Coarse to medium-grained sandstone, moderate red (5R 4/6) with dispersed granules to pebbles. Rare volcanic cobbles. Normal grading, poor sorting, Mottled fabric, many branching tubules and halos	Tabular, 20 to 40 cm thick, erosive bases with lags	Overlies massive mudstone facies (Fm) and underlies stratified intraclastic sandstone facies (b2)	Rhizoliths and rhizohalos	Distal alluvial-fan deposits
	Stratified intraclastic sandstones (b2)	Coarse to medium-grained sandstone, moderate sorting, normal grading, Intraclastic lags of quartz and feldspar, very dark reddish brown (10R 3/4). Sp cosets of 20 cm, Sr and flaser bedding rare	Lenticular to tabular, 0·5 to 1·5 m thick	Overlies and grades laterally with the pebbly sandstone facies (a)	Invertebrate traces: *Skolithos* and *Scoyenia*	Distal alluvial fan to sandflat transition
Sandflat	Graded sandstones (c)	Very fine-grained to medium-grained sandstone, normal grading, Sh faint, dark very reddish brown (10R 3/4). Mottled fabric, cracked mud drapes. Illites	Tabular, 20 to 45 cm thick, erosive bases	Overlies and is interstratified with mudrock facies (e) and underlies laminated limestone facies (k)	Rhizohalos and invertebrate traces: *Skolithos* and *Scoyenia*	Sheetfloods in a low gradient slope with pedogenesis
	Stratified sandstones (d)	Very fine to medium sandstone, moderate sorting, brownish red (10R 4/6) to very pale orange (10YR 8/2), vague Sh and Sr, millimetre-scale laminae, Sp, minor, convolute structures. Unit tops with cracked mud drapes, mud chips randomly dispersed. Analcime. Smectites. Silica nodules	Tabular, 15 to 120 cm thick	Overlies the mudrock facies (e)	Rhizoliths and rhizohalos	Sheetfloods with pedogenesis
Muddy sandflat to mudflat	Mudrocks (e)	Mud siliciclastics (pale red (5R 6/2) and greyish red (10R 4/2). Fl with 0·1 to 1 mm laminae in units 0·2 to 1·5 cm thick of alternating greyish yellow (5Y 8/4) fine sandstone to greyish red (5R 4/2) mudstone. Fr with 0·5 mm thick laminae inclining at 15°. Structureless units (Fm) with diffuse halos. Horizontal calcite crystal crusts (4 cm long and 0·4 cm long) associated with microtepees	Tabular, 10 to 180 cm thick	Underlies oncolitic wackestone facies (g) and is interstratified with stratified sandstone facies (d) (4 cm thick units), laminated siltstones (f), and laminated limestone facies (k)	Rhizohalos. Articulated ostracode valves	Suspension settle-out to tractive flow deposition with pedogenic alteration

Table 3. (continued)

Facies associations	Facies	Sedimentary structures/fabric	Bed geometry	Vertical and lateral relationships	Fossil content	Interpretation
		and micritic intraclasts. Mudcracks and elongated tubular structures up to 12 cm long. Analcime. Smectites. Calcite cement. Silica coatings				
	Laminated siltstones (f)	Muddy siltstone, moderate red (5R 5/4) to greyish red (10R 4/2), faint horizontal lamination (Fl), laminae up to 1 cm thick, convolute structures, mottling, mudcrack systems, tubular structures, pink halos, silica coatings. Analcime, smectites and illites	Tabular, 7 to 120 cm thick, erosive bases	Interstratified with mudrock facies (e)	Rhizohalos. Oolites (cyanobacteria). Rare ostracode valves	Suspension settle-out in vegetated outer mudflat with rare tractive flows
Carbonate channels	Oncolitic wacke-stones (g)	Wackestones are light olive grey (5Y 6/1) to light greenish grey (5GY 8/1). Oncolites 0·1 to 3 cm diameter, randomly distributed in the units, poor sorting, inverse grading, micritic intraclasts and fragmented oncolites. Cracked mud drapes. Halos	Lenticular, 10 to 30 cm thick and 6 m in lateral extent	Overlies and underlies mudrock facies (e)	Rhizohalos. Algae and cyanobacteria	Tractive flows in ephemeral channels on muddy sandflat to mudflat
	Oncolitic laminated sandstones (h)	Very fine sandstone, moderate yellow (5Y 7/6) to dark yellowish orange (10 YR 6/6) with Sl (1 mm thick laminae) and dispersed oncolites (complete and fragmented), ellipsoidal oncolite imbricated lags (0·1 to 1·5 cm diameter) at lower contact. Oncolites have crenulated concentric laminae and nuclei have spar or sandy material. Small vertical cracks at tops of units	Tabular, 20 cm thick	Overlies oncolitic floatstone facies (m) with erosive contact	Algae and cyanobacteria. Rhizoliths	Tractive flows in ephemeral channels
Palustrine limestones	Mottled carbonate mudstones (i)	Mudstone is light bluish grey (5B 7/11) to light greenish grey (5G 8/11). Mottling with yellow orange halos (10YR 8/6) follows cracks and tubular structures, simple mudcrack and tapering crack systems, vertical colouration changes	Lenticular, 75 cm thick and 30 m in lateral extent	Laterally interstratified with laminated siltstone facies (f) and nodular wackestone facies (j)	Rhizoliths and rhizohalos	Palustrine carbonate area in mudflat with pedogenesis
		Light bluish grey (5B 7/11) to light greenish grey (5G 8/11) wackestone,	Tabular, 0·11 to 3 m thick	Overlies stratified sandstone facies (d)	Rhizoliths and rhizohalos	Palustrine carbonate area

Table 3. (continued)

Facies associations	Facies	Sedimentary structures/fabric	Bed geometry	Vertical and lateral relationships	Fossil content	Interpretation
	Nodular wacke-stones (j)	micrite with nodules that are ellipsoidal-subrounded (5 cm diameter), have massive to distinct nuclei, and are associated with pale red (10R 6/2) halos. Cracks are ubiquitous (horizontal and vertical), are lined with clay, and can be filled with spar. Suspended clasts of underlying facies and microbialite fragments		and laminated siltstone facies (f) and grades laterally to mottled carbonate mudstone facies (i)		in mudflat with pedogenesis
	Laminated limestones (k)	Medium dark grey (N5) to dark grey (N3) micrite, plane to domal lamination, crenulated laminae (1 to 2 mm thick), crack systems, mud chips, nodules, tepees, tiny tubular structures with and without OM, peloids, spherulites, silica cementation, OM on laminae surfaces	Tabular to lenticular, 0·5 to 1·05 m thick with 18 to 100 m lateral extent	Overlies and underlies mudrock facies (e) and grades laterally to mottled carbonate mudstone facies (i)	Filamentous algae, Cyanobacteria, Articulated ostracodevalves, Tetrapod tracks Plant or root remains	Palustrine carbonate area with groundwater input and exposure
Lacustrine limestones	Laminated marlstones (l)	Dark blue (5PB 3/2) to pale reddish violet (5RP 6/2) marlstone with very fine lamination (0·1 to 0·2 mm) and interlaminae of fine sandstone and clay (1·7 cm thick). Carbonate portion in thin section: 35%	Tabular, 10 cm thick	Overlies and underlies mudrock facies (e)	–	Settle out in small ponds on the outer mudflat
	Oncolitic floatstones (m)	Medium grey (N5) to dark grey (N3) floatstones with oncolites (1 to 12 cm diameter), silica, carbonate coatings, tiny tubules	Lenticular, 10 to 70 cm thick	Overlies and underlies mudrock facies (e) grades laterally to mottled carbonate mudstone facies (i). Erosive contact with oncolitic laminated sandstone facies (h)	Filamentous algae, Charophyta, articulated ostracode valves, Phytoclasts	Carbonate shallow to deeper ponds on the mudflat

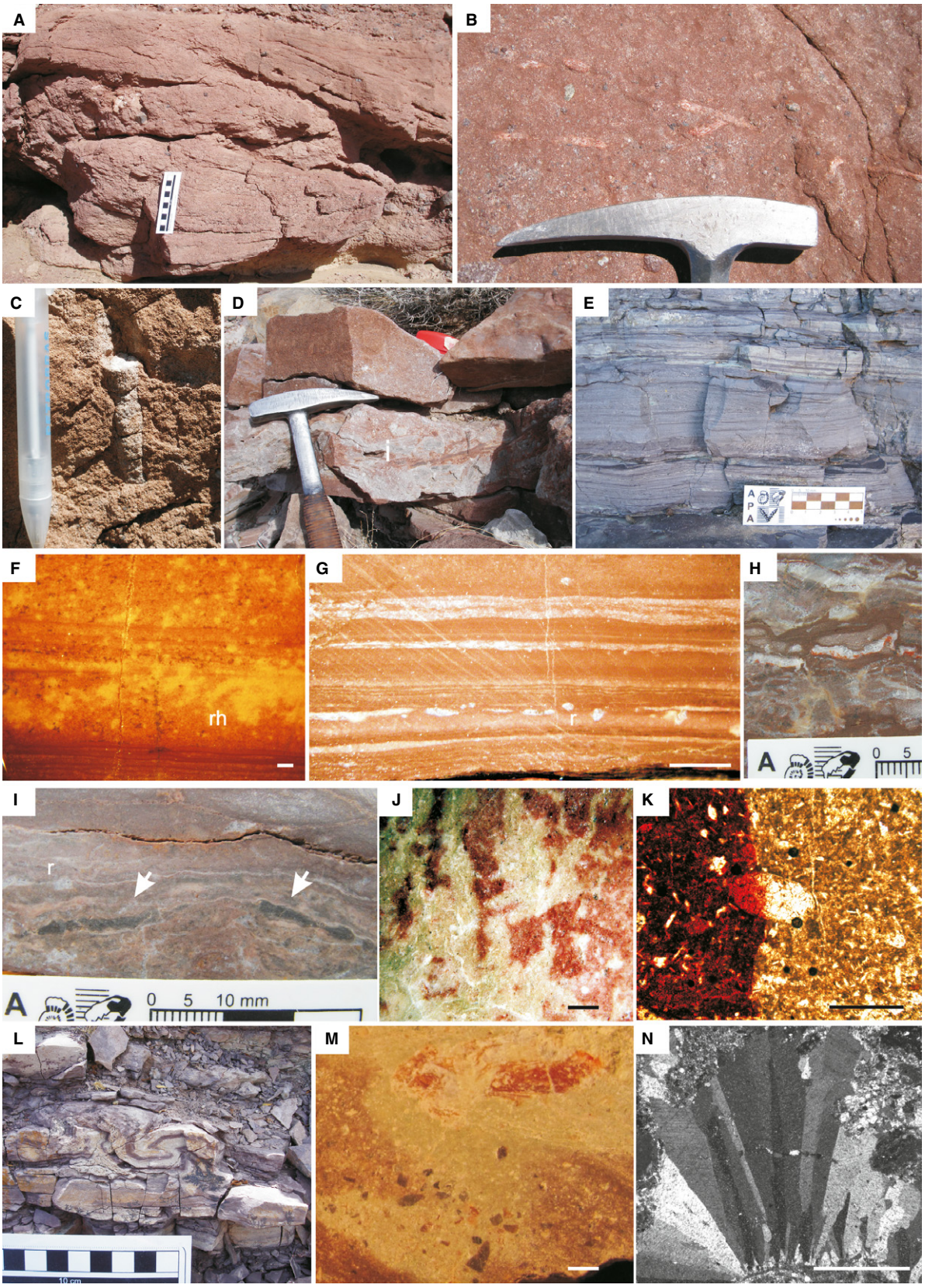

Fig. 9. Outcrop, polished slabs and thin section photographs of the facies defined for the Cerro Puntudo Formation (Anisian) at the Cerro Puntudo sub-basin (North), Cuyana Basin. (A) Outcrop photograph of pebbly sandstone facies (a) (150 m, Fig. 8) with planar cross-stratification (Sp). Scale is in centimetres. (B) Outcrop photograph of pebbly sandstone facies (a) (170 m, Fig. 8) showing rhizoliths coated by silica. Hammer head is 16 cm long. (C) Outcrop photograph of stratified intraclastic sandstone facies (b2) (260 m, Fig. 8) where an invertebrate trace fossil (*Skolithos*) is present. Pen is 1·5 cm wide. (D) Outcrop photograph of graded sandstone facies (c) (1·5 m, Fig. 8) showing intraclasts of carbonate (i) at the base of the sandstone. Hammer is 35 cm long. (E) Outcrop photograph of stratified sandstone facies (d) (5 m, Fig. 8) showing low-angle ripple cross-lamination (Sr) and planar cross-stratification (Sp). Scale is in centimetres. (F) Slab photograph of stratified sandstone facies (d) (5 m, Fig. 8) with faint Sr alternating with massive layers disrupted by mottling and rhizohalos (rh). Scale is 2 mm. (G) Slab photograph of mudrock facies (e) (6 m, Fig. 8) with Fl showing circular structures interpreted as rhizolith cross-sections (r). Scale is 2 cm. (H) Slab photograph of mudrock facies (e) (1·5 m, Fig. 8) with calcitic laminae disrupting the fabric with no displacive textures. Scale is in millimetres. (I) Slab photograph showing microbialite intraclasts interspersed with planar lamination (arrows) and circular structures interpreted as rhizolith cross-sections (r) (2·5 m, Fig. 8). Scale is in millimetres. (J) Slab photograph of diagenetic alteration of mudrock facies (e) (2·5 m, Fig. 8), bioturbation is interpreted as rhizohalos. Scale is 1 cm. (K) Thin section microphotograph of mudrock facies (e) (14 m, Fig. 8) with articulated ostracode valves. Calcite is highlighted by Alizarin Red S staining. Parallel light. Scale is 250 μm (10×). (L) Outcrop photograph of laminated siltstone facies (f) (35 m, Fig. 8) with convolute lamination composed of siltstone and carbonate laminae. Scale is in centimetres. (M) Slab photograph of laminated siltstone facies (f) (1·5 m, Fig. 8) showing a rhizohalo with a silicified rhizotubule. Scale is 1 mm. (N) Thin section microphotograph of the laminated siltstone facies (f) (1·5 m, Fig. 8) of fibrous-radial calcite in the rhizohalos disrupting the siltstone. Scale is 200 μm (5×). Parallel light.

Table 4. Mineralogical composition data of the total rock fraction and phyllosilicates composition of the clay fraction, from sandstones, mudstones and siltstones of the Cerro Puntudo Formation, Cerro Puntudo sub-basin, Cuyana Basin.

		Total rock fraction								Phyllosilicates clay fraction			
Facies	Samples	Qz	Phy	FK	P	Ca	An	He	Ba	Sm	I/M	Cl	K
c	CP14	xxx	xx	x	xx	xxx	x	x			xxx		
d	CP64	xxx	xx	x	xx	xxx	xxx	x		xxx			
e	CP36	xxx	xx	x	xx	xx	xxx	x		xxx	xxx		
f	CP25	xxx	xx	x	xx		xxx	x		xxx			

Qz, Quartz; Phy, Phyllosilicates; FK, Potasium feldspar; P, Plagioclase; Ca, Calcite; An, Analcime; He, Hematite; Ba, Baritine; Sm, Smectites; I/M, Illite/Mica; Cl, Chlorite; K, Kaolinite. Estimated relative content: xxx = major components; xx = minor components; x = accessory components; tr = traces; c, Graded sandstone facies; d, Stratified sandstone facies; e, Mudrock facies; f, Laminated siltstone facies.

pient palaeosols (Gierlowski-Kordesch & Rust, 1994; Gierlowski-Kordesch, 1998; Kraus & Aslan, 1999; Huerta & Armenteros, 2005), similar to the processes forming the massive textures in facies (e). Oolites and bioclasts are considered allochthonous to the facies, and they were probably removed from nearby subenvironments during flooding events. Tubules in the oncolite cortices are interpreted as cyanobacteria (Riding, 1991b). The circular structures with a double external wall are interpreted as transversal sections of microbial filaments. These microorganisms are considered the producers of the microbialites by biologically induced precipitation in adjacent carbonate facies (Freytet & Verrecchia, 1998; Flügel, 2004; Arenas *et al.*, 2007). Fibrous-radial calcite cement indicates diagenesis in a vadose zone (Alonso-Zarza *et al.*, 1992), though this calcite habit has also been associated with geothermal effects in facies related to springs (Jones & Renaut, 2010). These characteristics indicate moderate to good drainage for palaeosols (Landon, 1984; Kraus & Hasiotis, 2006). Long branching structures are interpreted as root moulds (Klappa, 1980). The circular cracking pattern of the fabric suggests that the disruption was caused by mechanical root action (Kraus & Aslan, 1999) with circular calcite structures interpreted as smaller root moulds (Smoot & Lowenstein, 1991). Convolute structures are interpreted as synsedimentary deformation of the substrate by differential load-

ing (van Loon, 2009). Analcime characterizes alkaline and/or saline marginal lake environments (Renaut, 1993; Cabaleri *et al.*, 2013), whereas smectite, illite and mica are typical of deposition and diagenesis in arid depositional settings and seasonal climates (Scott *et al.*, 2007).

Carbonate channel facies association: Oncolitic wackestone (g) is light olive grey (5Y 6/1) to light greenish grey (5GY 8/1) and forms lenticular strata 10 to 30 cm thick and *ca* 6 m in lateral extent. Units show sharp lower contacts and are closely stacked (Fig. 10A). Oncolite layers within a micritic fabric with inverse grading contain oncolites that are 0·1 to 3 cm in diameter, poorly sorted and dispersed. Oncolites are circular and concentric but the biggest ones can be ellipsoidal (Fig. 10B). Their cortex is micritic with a 1 mm thick silica coating. The nuclei have spar recrystallization (Fig. 10B). Dispersed in the fabric, there are abundant subrounded micrite intraclasts 0·25 mm long and fragmented oncolites. The top of the facies units contains mud drapes with numerous vertical cracks 1 mm wide by 2·5 mm long, that branch and taper downwards. The fabric contains circular green and violet halos 1·5 and 2 cm in diameter, respectively. Dispersed in the micritic fabric are grains (2 mm) of quartz, feldspar, rutile and biotite.

Interpretation: The geometry and sharp lower contacts of the facies units indicate channelized tractive flows with oncolites and micritic carbonate transported by high-energy currents as bedload. Genesis of oncolites in fluvial channels has been described in ancient systems (Gierlowski-Kordesch *et al.*, 1991; Verrecchia *et al.*, 1997; Zamarreño *et al.*, 1997; Arenas *et al.*, 2007; Meléndez *et al.*, 2009) as bio-induced by algae and cyanobacteria during flood episodes. The size of the oncolites suggests that the flow had medium competence (Zamarreño *et al.*, 1997; Arenas *et al.*, 2007) with inverse grading indicating a rise in flow energy with time. The association of this facies with the mudrock facies (e) (see Table 3) indicates that deposition was due to tractive flows within the muddy sandflat to mudflat. The formation of mud drapes and their cracking provides evidence for ephemeral channel deposition (Smoot & Lowenstein, 1991). Since the fluvial channels were ephemeral, the oncolites were probably generated in a different subenvironment and were only transported by floods. There are reports of recent oncolite formation in spring-fed ponds where they occur in shallow subenvironments (Winsborough *et al.*, 1994). Also, there are reports of pisoliths forming due to accretion rather than due to rotation in Holocene spring pools (Risacher & Eugster, 1979; Jones & Renaut, 1994). The channel stacking pattern indicates moderate subsidence with exposure allowing some pedogenesis, as indicated by the rhizohalos.

Oncolitic laminated sandstone (h) is very fine-grained sandstone with dispersed oncolites (40% of facies) within horizontal laminae (Sl). The facies units form moderate yellow (5Y 7/6) to dark yellowish orange (10 YR 6/6) tabular units 20 cm thick with an erosive lower contact. Laminae in the sandstone are 1 mm thick and form units 3 mm thick (Fig. 10C) with disruption at the top of the units by vertical cracks 1 cm long. Oncolites are ellipsoidal, 0·1 to 1·5 cm long and are imbricated at the base of the unit (lags; Fig. 10C). There are complete, fragmented and aggregated oncolites. The oncolitic cortices are micritic and show concentric lamination (Fig. 10D) with up to four laminae and alternating light and dark crenulated micritic laminae. External laminae can contain Fe oxides. Oncolitic nuclei can have spar recrystallization, whereas fragmented oncolites contain nuclei filled by sandy material.

Interpretation: Laminated sandstones (Sl) are generated by upper flow regime currents (Miall, 1996) as a result of sheetflooding (Hardie *et al.*, 1978; Smoot & Lowenstein, 1991; Gierlowski-Kordesch, 1998). The sharp erosive base of the facies unit indicates an abrupt change in sedimentation and possible incision of channelized tractive flows (Fisher *et al.*, 2008). The oncolites originated in the channelized streams flowing from adjacent spring ponds. Their formation involves biomineralization of microbes that developed around a precipitation nucleus and caused precipitation of carbonate coatings within Ca-rich waters (Freytet & Verrecchia, 1998; Shiraishi *et al.*, 2008). Therefore, these oncolites are considered allochthonous and were probably transported as bedload by tractive flows (Gierlowski-Kordesch *et al.*, 1991; Miall, 1996; Verrecchia *et al.*, 1997; Zamarreño *et al.*, 1997; Arenas *et al.*, 2007). The size of the oncolites indicates flows of medium competence (Zamarreño *et al.*, 1997; Arenas *et al.*, 2007) and their imbrication within lags shows that the general direction of channel flow was NNE, away from coalescent alluvial fans. These palaeocurrent data differ from the previously determined

palaeocurrent direction of south-east and south at the locality (Sessarego, 1986) in a NNW–SSE aligned basin (López-Gamundí & Astini, 2004). Intergrowth in some oncolites was caused by confinement pressure (Flügel, 2004). Vertical small cracks reflect root disturbance between flood events.

Palustrine limestones facies association: Mottled carbonate mudstones (i) are micritic with a mottled and disrupted fabric of light bluish grey (5B 7/11) and light greenish grey (5G 8/11). They form lenticular beds 75 cm thick and 30 m in lateral extent. The fabric is disrupted by vertical cracks 1 cm wide and 3 cm long (Fig. 10E). Two types of cracks can be recognized. One type shows clay linings and a branching pattern tapering downwards; they are also associated with tubular structures. The other type of crack is devoid of clays and consists of single crack morphology. Pale yellowish orange (10YR 8/6) halos surround tubular structures and cracks. Changes in the colour of the fabric from red to violet and green are present (Fig. 10F). Towards the top of the facies units are concentrations of angular grains of quartz, feldspar and rutile *ca* 3 cm long. In thin section, the fabric is micritic with 30% detrital material including homogenous micrite intraclasts (Fig. 10G).

Interpretation: Lenticular geometry of the units with limited lateral extent and a homogenous micritic fabric indicate that these limestones were precipitated subaqueously within ponds in a mudflat area [associated with facies (f) – see Table 3], probably in shallow low-energy ponds, colonized by plants causing pedogenic alteration, a similar depositional pattern to facies (i) in the Cerro de las Cabras Formation in the South sub-basin. The branching cracks are interpreted as rhizobrecciation (Freytet & Plaziat, 1982) because they are associated with tubular structures interpreted as rhizoliths (Klappa, 1980). Simple cracks are interpreted to be the result of desiccation (Smoot & Lowenstein, 1991). Observed changes in the fabric colour are attributed to changes in groundwater to surface-water levels (Freytet & Plaziat, 1982; Alonso-Zarza & Wright, 2010).

Nodular wackestones (j) are micritic with dispersed nodules of light bluish grey (5B 7/11) to light greenish grey (5G 8/11) (Fig. 10H). They form tabular units 0·11 to 3 m thick with wavy upper contacts with cracked mud drapes filled by calcite. The nodules are ellipsoidal and subrounded and two types have been identified: (i) massive micritic nodules 3 to 5 cm in diameter and (ii) nodules with distinct nuclei (Fig. 10I) calcitic in composition and with silica coating (Fig. 10J). These nodules can contain internal, silicified concentric laminae and are immersed in pale red (10R 6/2) halos. At the top of the facies units, tubular structures protrude from the rock as nodule extensions. Among the nodules, there are horizontal cracks less than 1 mm wide and up to 8 cm long and vertical cracks less than 1 mm wide and 3 cm long. Microbialite fragments with flat alternating light and dark micritic laminae, each 1 mm thick, are dispersed randomly in the wackestone. In addition, fragments of the underlying sandstones (up to 4 cm long) and of the underlying mudrocks (up to 5 cm in length) are suspended in the micrite.

Interpretation: Geometry and sedimentological characteristics of this facies, including nodule development, rhizobrecciation, rhizohalos and rhizoliths, imply similar deposition to that of facies (i) in both half-grabens of the Cuyana Basin: carbonate palustrine areas in a mudflat environment [associated with facies (f) – see Table 3]. The colour of the rhizohalos is characteristic of moderate-well drained palaeosols (Kraus & Hasiotis, 2006; Tanner & Lucas, 2006, 2012). Mud drapes with cracks at the top of the units confirm that the deposit was formed under ephemeral conditions. In this setting, transportation and deposition of the fine sediments by pedogenic mud aggregates, not as suspension settle-out, is the most plausible mechanism that allows carbonate precipitation in a siliciclastic mudflat (Gierlowski-Kordesch, 1998). This even explains the large clasts of underlying facies suspended in the micrite, showing that flooding events moving these clasts were not clouded with suspended siliciclastic mud. Microbial intraclasts clearly were transported from adjacent facies (k).

Laminated limestones (k) are micritic, medium dark grey (N5) to dark grey (N3) with flat or domal lamination (Fig. 10K). The facies units vary in thickness from 5 cm to 1·05 m and their lateral extent is 18 to 100 m. The geometry of the beds is tabular to lenticular. These laminated limestones have vertical, horizontal and polygonal cracks. Vertical cracks are up to 1 mm wide and 4 cm long. Polygonal cracks are 3 to 10 cm long and are filled by angular chips of mudstone 3 cm long (Fig. 10L). A lateral variation in this facies is composed of carbonate lenses and layers with conical structures formed by multiple carbonate layers (Fig. 10M). Tetra-

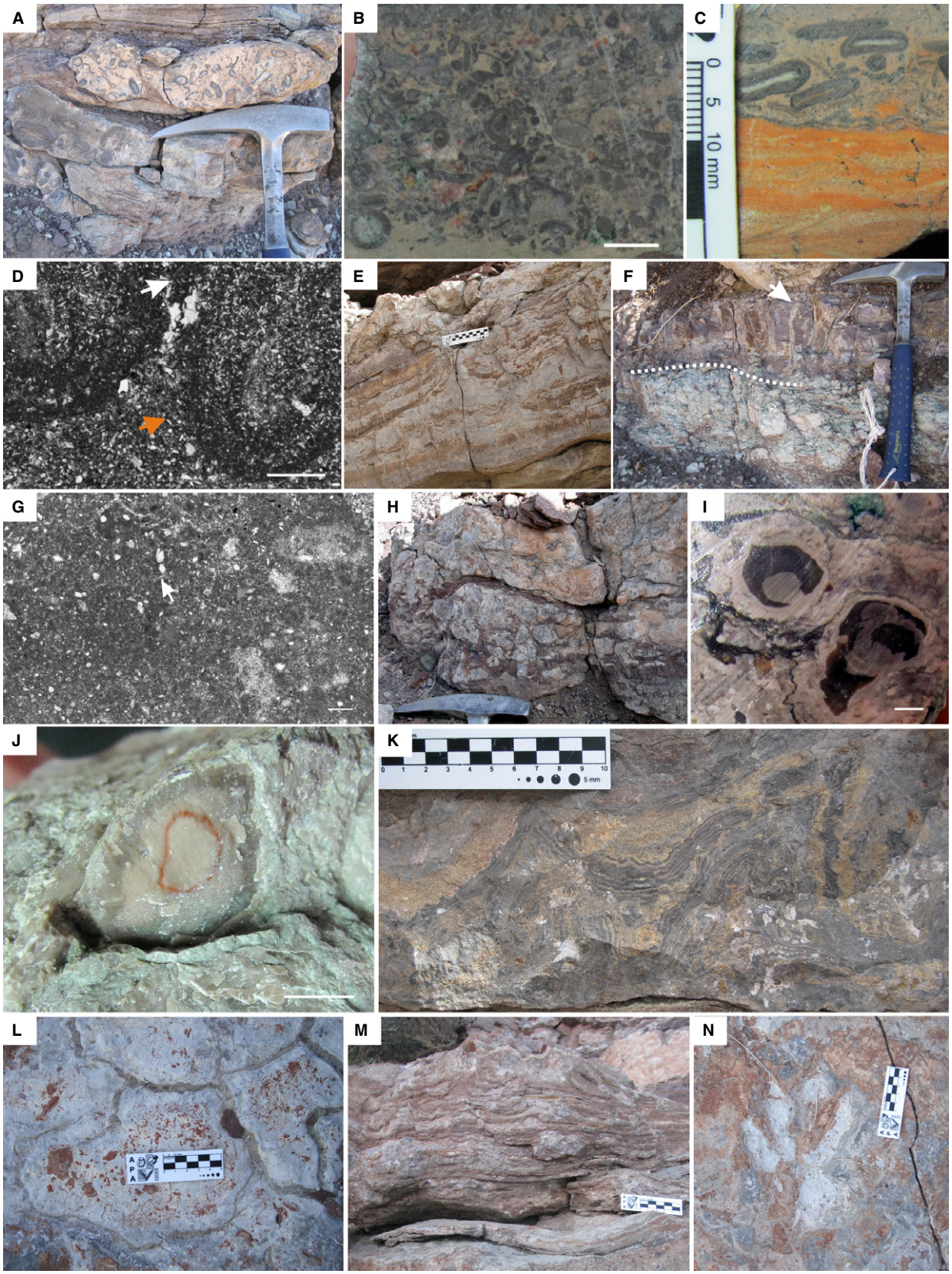

Fig. 10. Outcrop, polished slabs and thin section photographs of the facies defined for the Cerro Puntudo Formation (Anisian) in the Cerro Puntudo sub-basin (North), Cuyana Basin. (A) Outcrop photograph of the oncolitic wackestone facies (g) (22·7 m, Fig. 8) showing complete and fragmented oncolites. Hammer for scale is 33 cm. (B) Slab photograph of oncolitic wackestone facies (g) (22·7 m, Fig. 8) with circular to ellipsoidal, poorly sorted oncolites. Scale is 1 cm. (C) Slab photograph of the oncolitic laminated sandstone facies (h) (22·5 m, Fig. 8) with ellipsoidal oncolites suspended in fine sandstone with underlying horizontal lamination and ripple cross-lamination. Scale is in millimetres. (D) Thin section microphotograph of the oncolitic laminated sandstone facies (h) (22·5 m, Fig. 8) where two intergrown oncolites (white arrow) are suspended in a micrite-detrital matrix. Siliciclastic grains of fibrous shape are probably strontianite (orange arrow). The scale is 5 mm (20×). Plane light. (E) Outcrop photograph of the mottled carbonate mudstone facies (i) (2·5 m, Fig. 8) composed of planar lamination disrupted by vertical cracks attributable to rhizoliths (arrows) and mudcracks. Centimetre scale. (F) Outcrop photograph of the mottled carbonate mudstone facies (i) (21 m, Fig. 8) where two types of diagenetic alteration can be seen, separated by a dotted line. The upper portion of the outcrop is composed of vertical structures interpreted as rhizoliths (arrow) with a green colour within the red silty mudstone interpreted as gleying. Hammer for scale is 33 cm. (G) Thin section microphotograph of the mottled carbonate mudstone facies (i) (2·5 m, Fig. 8) with a micritic–detrital fabric containing subrounded calcite intraclasts (arrow). Scale is 2 mm (4×). Parallel light. (H) Outcrop photograph of the nodular limestone facies (j) (20 m, Fig. 8). Average thickness of the strata is 1·55 m. Hammer for scale is 35 cm. (I) Slab photograph of the nodular wackestone facies (j) (20 m, Fig. 8) with carbonate nodules composed of micrite. Scale is 1 cm. (J) Outcrop photograph of the nodular wackestone facies (j) (20 m, Fig. 8) showing a diagenetically altered nodule with one silicified lamina. Scale is 2 cm. (K) Outcrop photograph of the laminated limestone facies (k) (15·5 m, Fig. 8) with domal structures. Centimetre scale. (L) Outcrop photograph showing cracks of the laminated limestone facies (k) (15·5 m Fig. 8), interpreted as polygonal desiccation cracks. Hammer for scale is 35 cm. (M) Outcrop photograph of the laminated limestone facies (k) (15·5 m, Fig. 8) where a conical structure composed of carbonate and mudstone microbial lamination can be seen. The structure is interpreted as a possible groundwater discharge area. Centimetre scale. (N) Outcrop photograph of bedding plane of the laminated limestone facies (k) observed in (L) (15·5 m, Fig. 8) exhibiting a footprint of a posterior limb of a basal archosaur. Centimetre scale.

pod footprints up to 15 cm long form partial trackways (Fig. 10N). Tepee structures 2 cm high are observed in the laminae of the fabric along with spherical nodules 0·5 mm in diameter and ellipsoidal nodules 1·5 cm wide and 2·2 cm long located towards the top of the units. They have a calcite nucleus of 1·5 cm in diameter and micrite coatings 3 mm thick, and disrupt the fabric. Carbonaceous remains up to 2·5 cm long are preserved on laminae. In thin section, crinkly and domal lamination is composed of discontinuous and crenulated laminae 1 to 2 mm thick and forms units 2 cm thick that alternate between light and dark micritic laminae. Domal lamination shows continuous or discontinuous crenulated micritic laminae up to 2 mm thick.

In thin section, the fabric is micritic with siliciclastic detrital content (35%) as well as bioclasts and is laminated (Fig. 11A). In these micritic laminae, disruptive circular structures with a micrite nucleus are 4 μm in diameter with an external radiating halo 2 μm thick (Fig. 11B). Two types of tiny tubular structures are recognized: (i) hollow tubes with a simple micritized wall, 10 μm wide and up to 100 μm long (Fig. 11C); and (ii) tubes measuring 20 μm wide and 80 μm long with a double external wall that consists of fibrous spar with the tube interior containing dense opaque dark masses of OM. Bioclasts are articulated ostracode valves 10 μm × 200 to 320 μm in width and length with a few being ellipsoidal in shape 600 μm × 350 μm (Fig. 11D). Siliciclastic grains are angular quartz and feldspar, 40 to 400 μm, and oriented parallel to the stratification surface. Spar and microspar, microgranular quartz and chalcedony (Fig. 11E) fill voids and cavities present between the laminae. Silicification in the facies reaches up to 40% by volume. Chalcedony under a microscope with a gypsum plate shows increased birefringence in the north-east and south-west quadrants, diagnostic of length slow chalcedony.

Interpretation: Geometry of the facies indicates deposition in a spatially limited subaqueous shallow environment with low energy. This setting probably received a Ca-rich water supply from springs (Nickel, 1985); this is suggested by the conical carbonate-layered structure interpreted as a possible discharge apron (Jones & Renaut, 2010) preserved in the facies. The laminae were formed by biologically induced carbonate precipitation (Freytet & Verrecchia, 1998; Dupraz *et al.*, 2009; Taher & Abdel-Motelib, 2014). Domal laminae indicate irregularities in the substrate and their recumbent margins indicate that the micro-organisms acted as biostabilizers of the substrate (Hof-

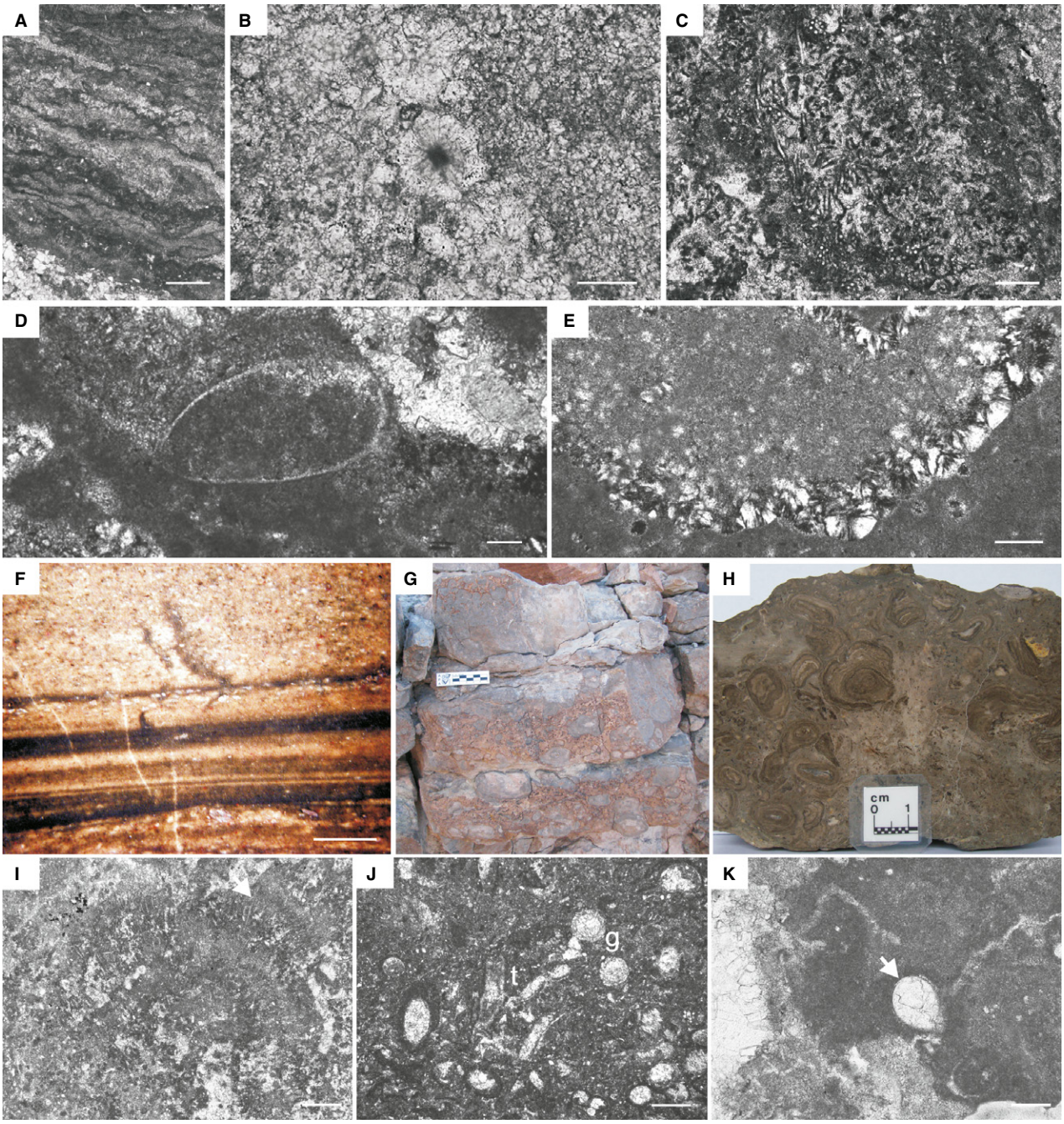

mann, 1975; Arp *et al.*, 2005; Taher & Abdel-Motelib, 2014). Type 1 and type 2 tubules are identified as filamentous algae (Riding, 1991a) and the micrite accumulations (ma) correspond to coccoid cyanobacteria (Hofmann, 1975; Freytet & Verrecchia, 1998; Freytet *et al.*, 1999). Circular structures with a micrite nucleus and external halos are interpreted as spherulites (Freytet & Verrecchia, 2002). These structures form by carbonate precipitation due to rapid degasification (CO_2 loss) usually in hydrothermal settings (Leslie *et al.*, 1992; Perri *et al.*, 2012). This formation and the discharge apron deposit constitute the evidence for groundwater as the principal water supply for this facies. Structures disrupting the fabric are pedogenic nodules and cracks formed from subaerial exposure (Freytet, 1973; Freytet & Plaziat, 1982; Alonso-Zarza & Wright, 2010). Tepee structures were formed during exposure of the microbia-

Fig. 11. Outcrop, polished slabs and thin section photographs of the facies defined for the Cerro Puntudo Formation (Anisian) in the Cerro Puntudo sub-basin (North), Cuyana Basin. (A) Thin section microphotograph of the laminated limestone facies (k) (7 m, Fig. 8) with millimetre-scale discontinuous carbonate laminae alternating with thin mudstone laminae. Scale is 500 m (2·5×). (B) Thin section microphotograph of the laminated limestone facies (k) (10 m, Fig. 8) with a spherulite. Scale is 5 m (40×). (C) Thin section microphotograph of the laminated limestone facies (k) (10 m, Fig. 8) with filamentous cyanobacteria in transversal and longitudinal section. Scale is 80 m (10×). (D) Thin section microphotograph of the laminated limestone facies (k) (15 m, Fig. 8) with an ostracode with articulated valves. Scale is 100 m (40×). (E) Thin section microphotograph of the laminated limestone facies (k) (15 m Fig. 8) where micrite has been replaced by length slow chalcedony (20×). Scale is 100 m. Plane light. (F) Polished slab photograph of the mudrock facies (e) (27 m, Fig. 8) showing subrounded calcite intraclasts within the siltstone and along the thinner laminae of mudstone. Scale is 0·5 cm. (G) Outcrop photograph of the oncolitic floatstone facies (m) (27·5 m, Fig. 8) showing unsorted oncolites of various sizes, both supported and unsupported in micrite. Centimetre scale. (H) Rock slab of the oncolitic floatstone facies (m) (28 m, Fig. 8) showing the oncolitic fabric with simple and composite concentric oncolites. Centimetre scale. (I) Thin section microphotograph of the oncolitic floatstone facies (m) (29 m, Fig. 8) showing an oncolite with filamentous algae (arrow) radially extending from the nucleus-filled cortex. Scale is 100 m (4×). (J) Thin section microphotograph of the oncolitic floatstone facies (m) (29 m, Fig. 8) with spar-filled fragmented thalli (t) and gyrogonites (g) of charophytes suspended in micrite. Scale is 500 m (10×). (K) Thin section microphotograph of the oncolitic floatstone facies (m) (29 m, Fig. 8) with articulated ostracode valves in which hinge is preserved (arrow). Scale is 100 m (20×). Plane light.

lites as a consequence of desiccation (Bernier *et al.*, 1991; Flügel, 2004). The carbonaceous remains are plant or root fragments with preserved OM, perhaps part of the hygrophytes of the palustrine area. Preserved OM and colour of the fabric indicate that the palaeosols formed within very poor drainage (Kraus & Hasiotis, 2006), perhaps near the groundwater table. This is opposite to the moderate to well drained palaeosols identified from the (j) facies. Triassic microbialites developed in flooded areas of the mudflat where there was groundwater supply; similar conditions have been proposed for other ancient examples (Risacher & Eugster, 1979; Smoot & Lowenstein, 1991; Arp *et al.*, 2005; Tanner & Lucas, 2006) and for Recent depositional settings (Winsborough *et al.*, 1994). Circular structures with a micritic nucleus and external radiated halos are cross-sections of rhizoliths (Smoot & Lowenstein, 1991; Gierlowski-Kordesch, 1998).

The tetrapod footprints belong to basal archosaurs probably related to the unique bone remains found in the sub-basin (Mancuso, 2009). For the Middle Triassic (El Portezuelo Formation), in the Rincón Blanco sub-basin (Cuyana Basin; Fig. 1), footprints and trackways have been found as the only evidence of the presence of tetrapods in lake margin areas as well (Marsicano & Barredo, 2004). In this case, the facies that bears the footprints represents a carbonate palustrine setting and preservation of footprints suggests that the water table was near the surface, linked to the nearby lake level. Cracks indicate that microbialites or stromatolites were exposed at times. It is very likely that the footprints were preserved in this facies because of the increased preservation potential provided by the rapid biomineralization triggered by the microbialites (Gehling, 1999; Scott *et al.*, 2007, 2010). Silica indicates environments with alkaline waters (Platt, 1989) and nearby volcanic activity linked to fluids during early diagenesis (Benavente *et al.*, 2015), similar to the silica found in many other facies here.

Lacustrine limestones facies association: Laminated marlstones (l) are dusky blue (5PB 3/2) and pale red purple (5RP 6/2) with horizontal lamination (Fl) forming tabular strata 10 cm thick. Lamination is 0·1 to 0·2 mm thick and forms sets 2 to 9 mm thick and units 2 cm thick (Fig. 11F). Laminae alternate between light and dark calcite and clay and also contain rounded calcite intraclasts 1 mm thick (Fig. 11F). The marlstones can contain mudstone or very fine sandstone 1·7 cm thick. The microfacies show a detrital siliciclastic matrix with 35% carbonate (micrite).

Interpretation: Lithology and the presence of Fl indicate suspension (micrite) with some small-scale tractive flows (sandstone laminae) as the mechanism of transport and deposition in a mixed carbonate and siliciclastic pond setting in the outer area of the mudflat, closer to the siliciclastic alluvial plain.

Oncolitic floatstones (m) contain dispersed oncolites (matrix-supported) within micrite containing gyrogonites of charophytes; units are 10 to 70 cm thick with lenticular geometry and are medium grey (N5) and dark grey (N3). There are

3 cm thick siliciclastic mud drapes and mud lenses between the oncolitic units (Fig. 11G). Oncolites measure 1 to 12 cm in diameter; they are spherical and can be simple or composite (Fig. 11H). Nuclei are replaced by spar and the margins can show a thin lamina of Fe oxides. Cortices of the oncolites are *ca* 50 μm thick and have straight or slightly curved tubules 10 to 20 μm wide, with micrite walls and radial orientations (Fig. 11I). Nuclei consist of charophyte thalli or their reproductive structures (gyrogonites; Fig. 11J). Phytoclasts are dispersed in the micrite and can also be encased within oncolites. Bioclasts (5%) are dispersed in the micrite and consist of ostracode valves 200 μm long, recrystallized by spar (Fig. 11K). In thin section, the micrite contains scarce siliciclastic grains of quartz, biotite, hematite, feldspar and lithic fragments (10%), and abundant carbonate grains represented by the oncolites (75%). Microspar, spar, microgranular quartz and chalcedony are randomly distributed within the micritic texture. Chalcedony is length slow and shows high birefringence in the north-east and south-west quadrants under the gypsum plate; it is present in patches in the micritic texture.

Interpretation: Oncolites of this facies were generated by carbonate precipitation upon charophyte thalli and gyrogonites. The tubules observed in the oncolites and coatings are filamentous algae remains (Benavente *et al.*, 2012); these algae induced carbonate precipitation (Platt & Wright, 1991; Shiraishi *et al.*, 2008; Dupraz *et al.*, 2009). Similar associations between charophytes and filamentous epiphytes have been described previously (Martín-Closas, 1999; Arp *et al.*, 2005). The presence of charophytes in this facies indicates that the palaeoenvironment was a maximum of 10 m deep (Cohen & Thouin, 1987) and that waters were well oxygenated. Phytoclasts with micrite coatings constitute evidence for vegetation cover in adjacent areas, probably hygrophytes with the submerged portion of their stalk coated with carbonate (Liutkus *et al.*, 2005; Arenas *et al.*, 2007; Liutkus & Wright, 2008). This carbonate coating process is ubiquitous in this facies and is common in modern Ca-rich shallow pond settings (Winsborough *et al.*, 1994; Arenas *et al.*, 2000; Alonso-Zarza, 2003; Arenas *et al.*, 2007) and in ancient examples (Freytet & Verrecchia, 2002; Arp *et al.*, 2005; Amezcua *et al.*, 2012). Diagenesis is predominantly spar cementation. Microgranular quartz and chalcedony are the result of very early diagenesis where the deposits interacted with more acidic groundwater fluids (Benavente *et al.*, 2015). Length slow chalcedony indicates sulphate-rich (SO_4) waters (Bustillo, 2010), perhaps hydrothermal. Due to the features described and the lack of evidence for exposure, the facies is interpreted as representing shallow to deeper Ca-rich ponds (Risacher & Eugster, 1979; Calvo *et al.*, 1989).

Subordinate Tuffs (Tf) form tabular strata 25 to 50 cm thick, are very pale blue (5B 8/2) and are interbedded with the facies of the palustrine and lacustrine limestone facies associations (i, j, k, l and m).

Interpretation: These tuffs represent the acidic volcanic activity in the region (López-Gamundí & Astini, 2004; Mancuso, 2009) that contributed to silicification of the carbonate deposits.

Stacking pattern analysis (Markov Chain analysis)

The working hypothesis for both units was H: The facies transitions observed in the Cerro de las Cabras and Cerro Puntudo formations are random. The Markov matrix (Krumbein & Dacey, 1969; Parks *et al.*, 2000) showed that in both cases the facies transitions were random and therefore the hypothesis was accepted (see Supporting Information). Therefore, for the Cerro de las Cabras Formation the most likely transitions to occur were: (b1) – (i) – (k) – (c) – (a). However, no real organized stacking was observed in the log.

For the Cerro Puntudo Formation the most likely transitions to occur were: (e) – (k) – (Tf) – (e) – (b2) – (i) – (j) – (e) – (m). This was not the real stacking pattern observed in the log either. In both cases, this means that the probability that one facies passes to another is the same and is not determined by the underlying lithology.

DISCUSSION

Cerro de las Cabras palaeolake

For the Cerro de las Cabras Formation, two facies associations are proposed: (i) sandflat and mudflat; and (ii) carbonate palustrine subenvironment. These subenvironments form a playa-lake depositional setting (Hardie *et al.*, 1978; Smoot & Lowenstein, 1991; Arp *et al.*, 2005) in the low accommodation transfer zone of the South sub-basin (Fig. 12). In this setting, surface water + sediment supply was through sheetfloo-

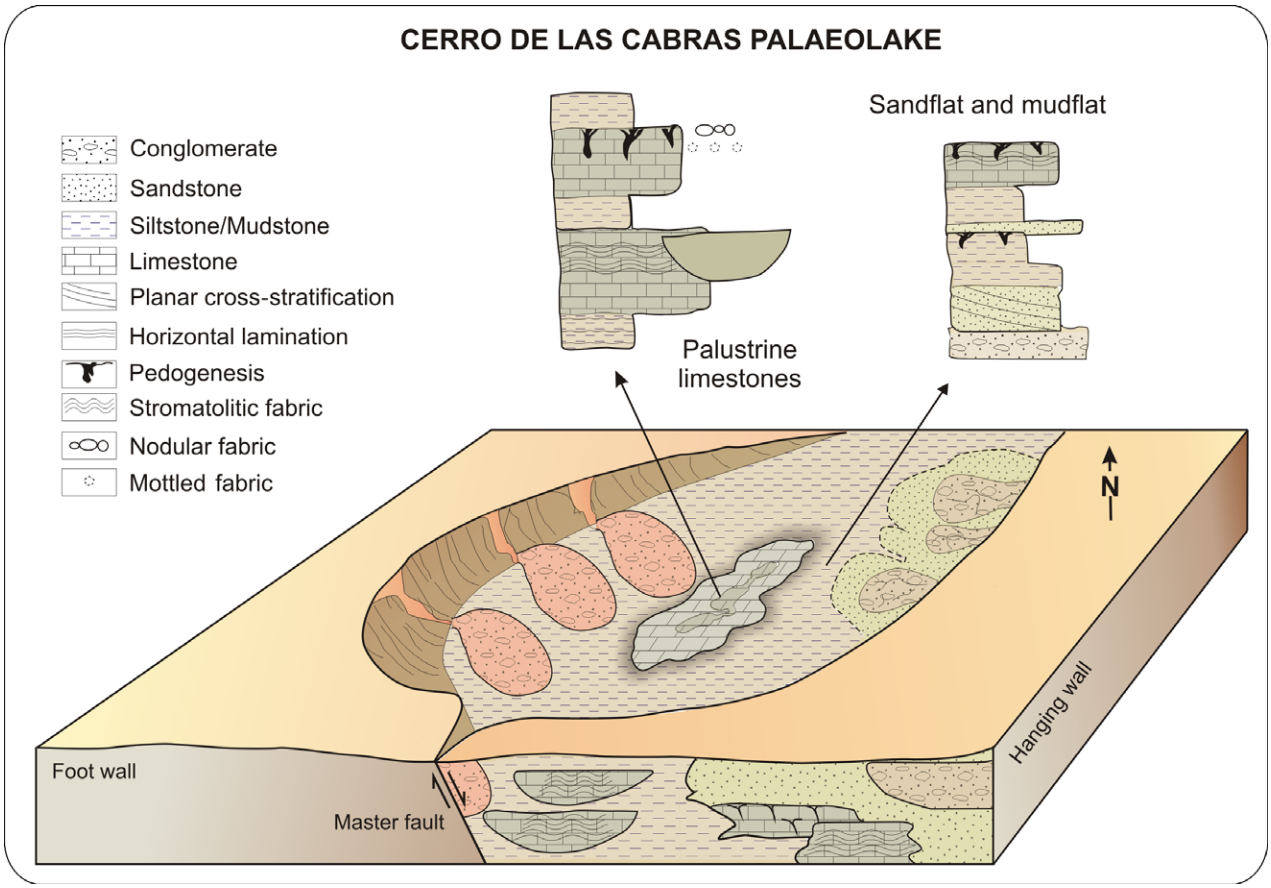

Fig. 12. Diagram (not to scale) of the palaeoenvironmental reconstruction for the lacustrine section of the Cerro de las Cabras Formation (Anisian) at the Potrerillos sub-basin, South area, Cuyana Basin.

ding from a distal alluvial-fan system recorded in the underlying Río Mendoza Formation (Toledo, 1987; Kokogian & Mancilla, 1989).

The sandflat and mudflat deposits have abundant sedimentary features (mud drapes, mudcracks, mud chips and pedogenesis) that indicate subaerial exposure, showing that the surface water + sediment supply was ephemeral (Gierlowski-Kordesch & Rust, 1994; Gierlowski-Kordesch, 1998). Between sedimentation episodes, palaeosol development was dominant. These palaeosols developed under good to moderate drainage and vegetation cover (Klappa, 1980; Kraus & Hasiotis, 2006; Liutkus & Wright, 2008). Mineralogy of the fine siliciclastic sediments was dominated by smectites that characterize vertic soils (Gierlowski-Kordesch & Rust, 1994; Gierlowski-Kordesch, 1998; Paik & Lee, 1998). Smectites are common in depositional settings, where there is an alkaline volcanic provenance (Scott *et al.*, 2007) under seasonal climate (Wakelin-King & Webb, 2007). This interpretation agrees with the tectonic and climatic setting described for the Triassic Cuyana rift basin (Artabe *et al.*, 2001; Spalletti, 2001).

Carbonate palustrine subenvironments are characterized by the primary biogenic precipitation of carbonates (Alonso-Zarza, 2003; Gierlowski-Kordesch, 2010). These carbonates have abundant subaerial exposure features indicating deposition in a very shallow palustrine setting (Freytet & Plaziat, 1982; Alonso-Zarza & Wright, 2010). In these limestones different degrees of pedogenesis are recognized. The mottled-nodular limestone facies (d) has abundant pedogenic features such as rhizoliths, rhizohalos and crack systems. According to the classification proposed by Alonso-Zarza *et al.* (1992), this facies characterizes an intermediate situation between a palustrine and a pedogenic subenvironment. In that classification, the laminated limestone facies (e) represents stromatolitic or microbialitic development under subaqueous conditions, but with subsequent exposure features (microtepee structures and rhizobrecciation). This corresponds to a palustrine subenvironment of shal-

low carbonate ponds of limited extent that developed in the distal zone of an alluvial-fan system, fed mainly by groundwater supply (Calvo *et al.*, 1989; Huerta & Armenteros, 2005; Meléndez *et al.*, 2009). With the siliciclastic mud probably bound up in pedogenic mud aggregates, the carbonates were able to precipitate in clear water within the basin (Talbot *et al.*, 1994; Gierlowski-Kordesch, 1998); although no direct evidence of these peds has been found at this time. The conditions for their formation are all met in this rift basin, namely volcanic activity, smectitic mineralogy of clays and seasonal climate (Gierlowski-Kordesch & Gibling, 2002). Generally, playa-lake systems form in the lowest areas of the basin and can be open or closed hydrological systems (Hardie *et al.*, 1978; Rosen, 1994). For the Cerro de las Cabras palaeolake, the nearby location of rift shoulders generated probable rainshadow areas (after Gierlowski-Kordesch & Gibling, 2002). This explains the dominance of groundwater supply to the system and suggests that the pedogenic and subaerial exposure features were caused by phreatic level fluctuations (Meléndez *et al.*, 2009) or regional water table level oscillations from lake level changes (Renaut *et al.*, 2013).

There are discrete intervals (Fig. 6) of facies repetitions that would be expected to result from cyclic patterns in the stacking pattern of this succession. However, the Markov analysis confirmed that the facies transitions observed are random. This is logical in a playa-lake system where facies transitions and stacking patterns reflect the palaeohydrology and its fluctuations through time through non-Walterian patterns (Rosen, 1994). These palaeohydrological changes connected to the synrift stage of the half-graben are interpreted as being controlled by tectonics and regional climate, reflecting pulses of subsidence and aggradation alternating with pulses of little to no sedimentation, erosion and palaeosol development (Alonso-Zarza *et al.*, 2012). In the succession, it is possible to determine an overall increasing subsidence shown by an increase in strata thickness preservation and predominance of palustrine facies associations (Pla-Pueyo *et al.*, 2009) with stromatolite development towards the top (Fig. 4). This succession shows mostly aggradation. Coarser facies (a and b1) of the sandflat facies association show evidence for bedload transport (flat bed and sheetfloods). These deposits represent the episodic inflow of siliciclastics and water from a distal alluvial fan (Vandervoort, 1997) and aggradationally interstratify with the biogenic and pedogenic limestone facies (d and k). Palaeosol development suggests a constant subsidence with few unaltered sediments. In this succession, the limestone units record the subaqueous processes of carbonate precipitation marking the flooding events (Fig. 4), but these units also show features of subaerial exposure. These short frequency variations in single units are diagnostic of an evaporative facies association where flooding and exposure events are condensed into a thin deposit; thus, this evaporative facies association corresponds to an underfilled lake type (Bohacs *et al.*, 2000). This is also in agreement with other geological features, including low OM preservation and low-diversity biotic assemblages. However, the truly characteristic feature of an evaporative facies association that has not been found is evaporite development (Bohacs *et al.*, 2000). Rosen (1994) points out that in playa-lake systems the development of evaporites occurs when a hydrological system is closed for surface water and groundwater. An open groundwater system will not allow the accumulation of ions to produce evaporites, even though the surface drainage is closed. This implies open groundwater flow for the Cerro de las Cabras palaeolake, as has been confirmed from geochemical data (Benavente, 2014). According to the Bohacs *et al.* (2000) lake-type model, underfilled lakes have persistently closed hydrology for surface water. Rosen (1994) confirms that very few playa lakes are actually closed to all water supply; playas that do not accumulate evaporites have open throughflow in subsurface groundwater. An example of ephemeral underfilled lakes without thick evaporite layers is the Jurassic East Berlin Formation from the Hartford rift basin of the USA (Gierlowski-Kordesch & Rust, 1994; Bohacs *et al.*, 2000).

Cerro Puntudo palaeolake

This system developed in the low gradient plain of the ramp or platform margin of the rift at its northern tip (López-Gamundí & Astini, 2004) with wide lateral drainage networks supplying water + sediment. In these areas of moderate to low subsidence (Gawthorpe & Leeder, 2000), shallow lakes of very low gradient commonly develop (Platt & Wright, 1991; Alonso-Zarza *et al.*, 1992; Pla-Pueyo *et al.*, 2009; Alonso-Zarza & Wright, 2010). Usually, these lakes are fed by groundwater in arid and dry areas (Billi, 2007). Six facies associations have been identified

(Fig. 13): (i) distal alluvial fan; (ii) sandflat; (iii) muddy sandflat to mudflat; (iv) carbonate channels; (v) palustrine limestones; and (vi) lacustrine limestones. These facies associations represent six subenvironments that form part of a lacustrine depositional system (Hardie *et al.*, 1978; Smoot & Lowenstein, 1991).

The alluvial-fan facies association is characterized by coarse deposits that reflect the transition from tractive processes in confined flows of the proximal fan to the more distal zone dominated by sheetfloods (Fisher *et al.*, 2008). The supply of water and sediment was ephemeral, as indicated by the abundant pedogenic features (Fisher *et al.*, 2007a). The sandflat is characterized by sheetflood deposits that reflect the expansion of the turbulent flow from channelized flow near the source area to a distal flow deceleration as water enters the lake margin (Fisher *et al.*, 2007a,b). The ichnofacies *Skolithos* and *Scoyenia* described by Krapovickas *et al.* (2008) have been identified as part of the most distal zone of the alluvial fan in transition to the sandflat. These ichnofacies are composed of opportunistic organisms in soft and firm substrates that allow them to thrive during flooding periods (Gierlowski-Kordesch, 1991; Scott *et al.*, 2012). This is consistent with an unstable environment that alternates between wet and arid periods.

It is presumed that the thicker siliciclastic mudrock to siltstone successions of the muddy portion of the sandflat formed by accumulation of tractive pedogenic aggregate transport (Gier-

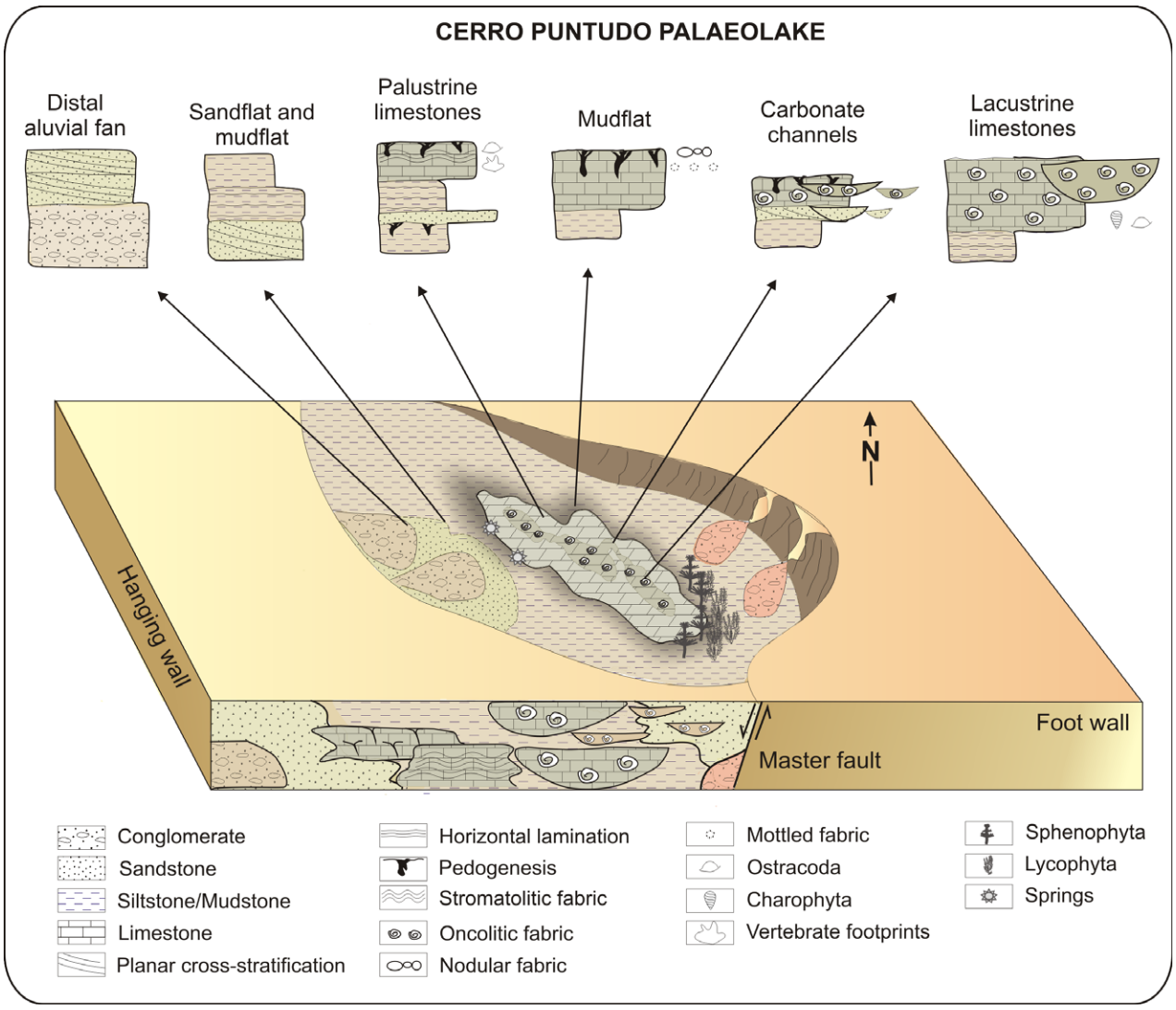

Fig. 13. Diagram (not to scale) with the palaeoenvironmental interpretation of the Cerro Puntudo Formation (Anisian), Cerro Puntudo sub-basin (North), Cuyana Basin.

lowski-Kordesch & Rust, 1994). Pedogenic mud aggregates are formed in rift basins because of the formation of expandable clays (smectite) found in Vertisols that typically produce the sand-sized peds (Talbot, 1994; Gierlowski-Kordesch & Gibling, 2002). In the Cerro Puntudo sub-basin (north half-graben), the clay assemblage is dominantly smectitic and the climate conditions are inferred as an arid regime with seasonality. Deposits of the muddy sandflat are thick (Fig. 8) which suggests equilibrated subsidence and water + sediment supply along with bedload transport of mud. These mudrocks were previously interpreted as deposits of a deep lake setting (Sessarego, 1986) and the lack of lamination was explained as a result of a non-stratified palaeolake (López-Gamundí & Astini, 2004). However, the study of the mudrocks and muddy siltstones at a microscale level has revealed abundant pedogenic features (cracked mud drapes, mudcrack systems and rhizoliths) and interbedded sandy and muddy bedload, indicating that the fines were deposited from waning flows as tractive pedogenic aggregates. Also, microbialites imply that biofilms stabilized the substrate and were associated with Ca-rich fluids. This supports a Ca-rich groundwater supply probably linked to basement Palaeozoic limestones or alkaline volcanics at very specific points in the system, possibly through springs linked to the half-graben faults (Scott *et al.*, 2007; Renaut *et al.*, 2013). This groundwater input is consistent with a humid playa lake (Liutkus & Wright, 2008).

Mineralogy corresponds to smectitic and illitic clays with high analcime content. It is likely that smectite was formed from diagenesis of the abundant alkaline volcanic rocks in the area (Cuadros *et al.*, 1999; Deocampo, 2004) and its presence points to an extremely seasonal palaeoclimate (Scott *et al.*, 2007; Wakelin-King & Webb, 2007). Analcime also formed from diagenetic alteration of alkaline volcanic rocks, within alkaline waters (Boles & Surdam, 1979), supporting the alkaline chemistry of the Cerro Puntudo palaeolake.

Scarce channel bodies in the system are sandy to micritic and their bedload is dominantly oncolites. Orientation of the channels is normal to the rift bounding faults (Gawthorpe & Leeder, 2000), which implies that the channels were secondary, not axial. These channels formed as connections between the oncolitic ponds sourced by groundwater and related to topography (Winsborough *et al.*, 1994; Amezcua *et al.*, 2012) with high water supply transporting the oncolites as bedload (Nichols & Fisher, 2007).

The palustrine limestones precipitated under subaqueous conditions but were subsequently exposed (Freytet & Plaziat, 1982; Alonso-Zarza *et al.*, 2012) in the proximal carbonate mudflat, in contrast to the lacustrine limestones that show no features of subaerial exposure and diagenesis under subaqueous conditions. These two subenvironments characterize the Ca-rich water supply setting. Due to the tectonic context of the sub-basin, including active faulting during the early synrift, it is likely that the Ca-rich waters were supplied through springs (Liutkus *et al.*, 2010). Presence of sedimentary structures interpreted as possible discharge aprons in the palustrine facies (k) supports this possibility (Renaut & Tiercelin, 1994; Jones & Renaut, 2010). Carbonate precipitation in spring areas is favoured by rapid degasification (CO_2 loss; Renaut *et al.*, 2002) and also in this case the micro-organisms would have been involved in the process through induced biogenic precipitation (Arp *et al.*, 2005; Dupraz *et al.*, 2009). Moreover, in this spring-sourced facies (k), the presence of spherulites might indicate the possibility of hydrothermal groundwater (Renaut *et al.*, 2013).

The subenvironments described form part of a playa-lake system (Rosen, 1994). Development of crystalline efflorescent crusts suggests that the water discharge at the surface was balanced by evaporation. Contrary to what is commonly thought, crystalline crusts depend on the amount of discharged water to the surface from shallow groundwater; this commonly occurs in throughflow playa lakes (Rosen, 1994).

In the sedimentological log (Fig. 8), a dominantly aggradational stacking pattern is identified. The distal alluvial-fan facies (a and b) and the sandflat facies (c and d) accumulate aggradationally with the biogenic limestones in the ramp or platform margin of the basin. In general, in the succession a minor retrogradational tendency can be seen from metres 0 to 2·5 of the log (Fig. 8) which can be linked to an increase in subsidence. From that point towards the top (point A, Fig. 8) several shallowing-upward assemblages can be seen, where the sediments with pedogenic and exposure features (e and f) represent shallowing and the limestones (k) represent deepening that allowed stromatolite formation. However, towards the top of the sedimentological log (point A, Fig. 8), limestone units thin and exhibit exposure features (i and

j). This trend could indicate a decrease in subsidence. Towards the top of the lake succession (point A′, Fig. 8), the channelized flows (g and h) reflect spring water flowing downhill, perhaps as a result of a series of block faults along the margin of the basin (Winsborough *et al.*, 1994; Amezcua *et al.*, 2012). Subsequent units of the lacustrine limestone facies association (l and m) provide evidence of the most significant deepening of the lake system (22 to 30 m, Fig. 8), corresponding to the highest subsidence recorded in the succession. The thickening-upward units of facies (m) also indicate increasing subsidence. Minor progradation might be recorded as sheetflood deposits reach the subaqueous deposits of the margin of the palaeolake, as in two points in the sedimentological log (5 to 10 m and 35 to 38 m, Fig. 8). An aggradational–progradational stacking pattern commonly defines a fluctuating profundal facies association diagnostic of a balanced-fill lake type (Bohacs *et al.*, 2000). This is in agreement with the freshwater to salinity tolerant biotic assemblage found for the unit composed of cyanobacteria, charophytes and ostracods. Geochemical data point to an open hydrology for the lake system (Benavente, 2014) that characterizes balanced-fill lakes during the time when the accommodation space mainly equilibrated with the water + sediment supply. More detailed sampling is needed to recognize the occasionally closed hydrology. Nevertheless, the progradation in this succession is minor but is commonly linked with palustrine systems in playa lakes (Fregenal-Martínez & Meléndez, 2010). The restricted areal extent of the studied succession cannot confirm this lake-type interpretation. More studies are required to determine whether the Cerro Puntudo indeed can be interpreted as a balanced-fill lake type.

Development of palaeosols and their thicknesses are linked to times when subsidence surpasses water + sediment supply with considerable periods of exposure (Pla-Pueyo *et al.*, 2009; Alonso-Zarza *et al.*, 2012). However, palaeosol thickness does not increase towards the top of the succession while the development of subaqueous facies does increase (k and m). This indicates a balance between the increment in subsidence and the water + sediment supply up to a point (A′ to 30 m, Fig. 8), and then again a diminution in the water + sediment supply. These variations in subsidence were probably linked to the tectonic pulses of the synrift stage.

Markov Chain analysis has shown that the facies transitions are random here as well. This is probably related to particular characteristics of playa-lake systems, in which the hydrology and groundwater supply are very important factors in the variations of the setting. In this system, it is most likely that the facies transitions are determined by the hydrological fluctuations rather than by Walter's Law (Rosen, 1994). Hydrological fluctuations were probably related to the tectonic instability of the synrift stage as well as climate variations through time.

Tectonic versus climatic sedimentary control

The portion of the Cuyana rift studied here consisted of two half-grabens (north and south; Legarreta *et al.*, 1992; López-Gamundí, 2010; Barredo *et al.*, 2011) with opposing master fault positions (López-Gamundí, 2010). This pattern is similar to the tectonic structure of the East Africa rift system (Cohen, 1990; Renaut & Tiercelin, 1994). In this context, in the Potrerillos sub-basin (southern half-graben) the master fault is located to the west and in the Cerro Puntudo sub-basin (northern half-graben) it is located to the east.

The Cerro de las Cabras palaeolake developed in the Potrerillos sub-basin near the transfer zone of the basin (southern half-graben) while the Cerro Puntudo palaeolake developed at the ramp or platform margin of the (northern half-graben) rift. These zones are similar from a tectonic point of view since both represent the lowest subsidence ratios in the basin (Cohen, 1990; Fig. 14). López-Gamundí & Astini (2004) interpreted the Cerro Puntudo Formation as the infilling of a relatively low accommodation zone in the rift. Moreover, this low accommodation zone most probably represents the northern tip of the rift (López-Gamundí & Astini, 2004).

Patterns observed in both studied formations can be caused by tectonics combined with climatic factors (Carroll & Bohacs, 1999; Bohacs *et al.*, 2000; Alonso-Zarza *et al.*, 2012). In the studied successions, the stacking pattern reveals mostly aggradation alternating with minor progradation indicating moderate increasing subsidence with accompanying water + sediment supply. Aggradational and minor progradational patterns reflect pulses of major subsidence accompanied by the supply and pulses of subsidence surpassing the supply, respectively. Changes in subsidence controlled by tectonics during the synrift influenced palaeohydrological

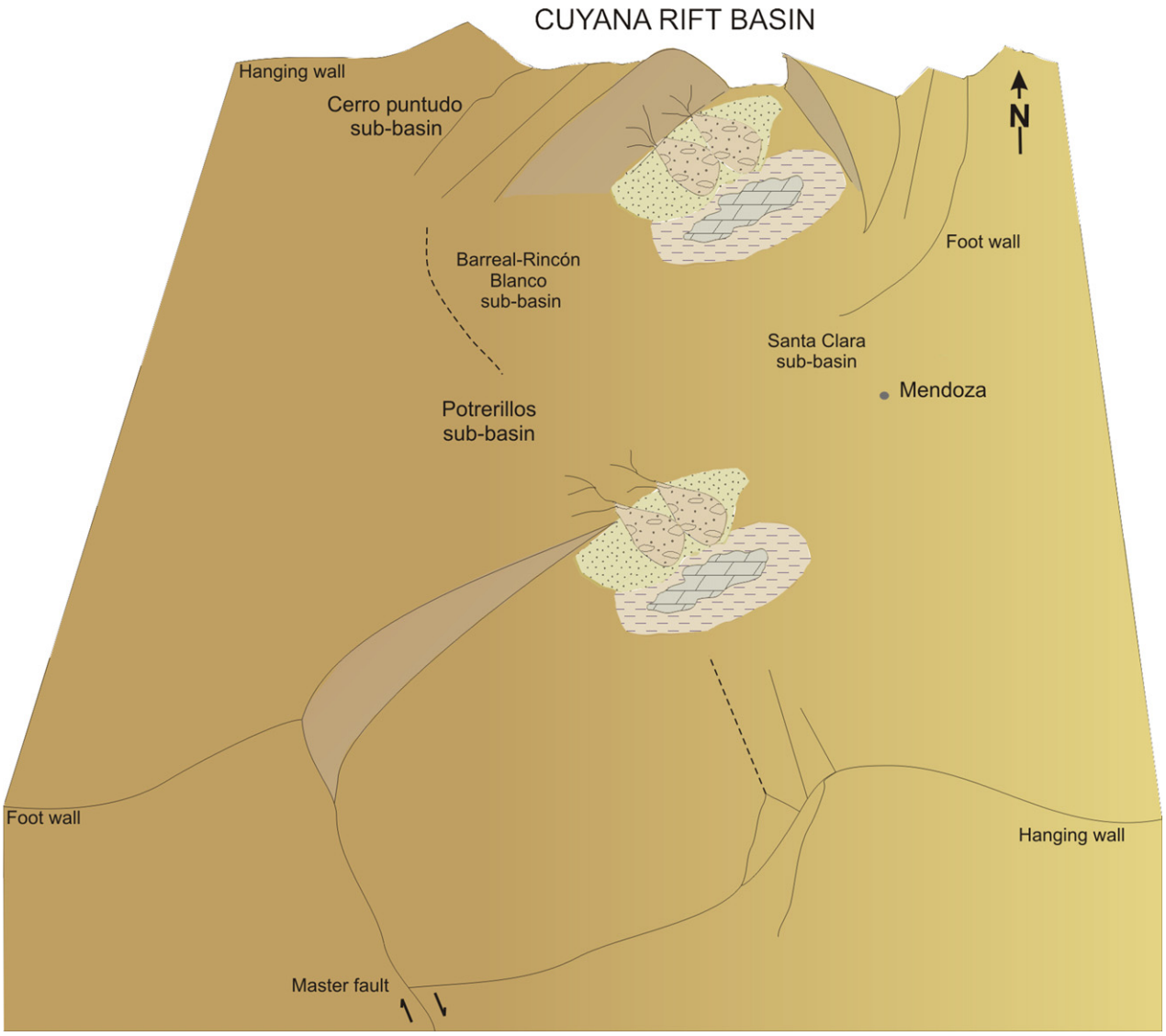

Fig. 14. Diagram (not to scale) of the Potrerillos sub-basin (South) and Cerro Puntudo sub-basin (North) with carbonate lacustrine systems development in the tectonic setting of the Cuyana Basin rift, Mendoza and San Juan provinces, Argentina. Only the sedimentary infill that represents the studied systems has been included. Modified after Legarreta *et al.* (1992).

fluctuations and affected the variable stacking pattern and facies transitions. In this stage, the existence of numerous isolated sub-basins of limited extent is common (Gawthorpe & Leeder, 2000). Tectonics influenced the drainage networks, the palaeotopography and the location of springs, among other features. However, this does not rule out a climatic influence most probably affecting the phreatic level fluctuations and surface-water input. Additional geochemical studies will aid in clarifying climatic influence. Nevertheless, the evidence provided points to a strong tectonic control reflected in subsidence pulses that conditioned sedimentation. The strong seasonal climate with extensive subaerial exposure may have been influenced by a regional rain shadow in a subsiding basin.

In order to frame a model for carbonate accumulation in continental rifts, a comparison to two other examples in the geological record from Europe is summarized in Table 5: the Miocene deposits of the Teruel Graben (Spain; Alonso-Zarza *et al.*, 2012) and a Triassic succession in the Germanic Basin (Arp *et al.*, 2005). Calcium-rich lakes associated with alluvial red siliciclastic mudrocks in the Teruel Basin contains facies similar to those in the Cuyana Basin, including similar palustrine structures, like

Table 5. Comparison of the carbonate deposits of the Triassic Cuyana rift (Cerro de las Cabras and Cerro Puntudo Formations), Unit II of the Teruel Graben (Spain), and the Arnstadt Formation of the Germanic Basin (Germany).

Features	Teruel Basin	Germanic Basin	Cuyana Basin	
Units	Unit II	Arnstadt	Cerro de las Cabras	Cerro Puntudo
Lacustrine system	Ca-rich shallow lakes on alluvial plain	Ca-rich perennial to playa lake	Ca-rich playa lake	Ca-rich perennial to playa lake
Age	Vallesian-Turolian	Norian	Anisian	Anisian
Position in rift	Escarpment area (half-graben)	?	Ramp/platform (half-graben)	Transfer zone (half-graben)
Subsidence rate	Relatively high	?	Relatively low-medium	Relatively low-medium
Paleolake features	High-energy ramp-like lake	Low-energy lake	Low-energy ramp-like lake	Low-energy ramp-like lake
Facies	Alluvial: red mudrocks Palustrine: marginal to shallow carbonate lake Lacustrine: shallow to deeper lake	Alluvial: channel and floodplain Palustrine: dry playa mudflat, saline playa mudflat Lacustrine: Ca-rich perennial	Alluvial: muddy sandflat to sandflat Palustrine: dry siliciclastic mudflat, Ca-rich palustrine	Alluvial: outer fan, channels, muddy sandflat to sandflat Palustrine: dry siliciclastic mudflat, Ca-rich palustrine Lacustrine: Ca-rich perennial
Carbonate facies	Lacustrine: wackestone to packstones, rudstones to floatstones. Palustrine: brecciated limestones, mottled limestones, limestones with root traces, clayey limestones, granular limestones, micro-karstified limestones, laminar calcretes, carbonate mounds	Lacustrine: massive dolomite mudstone, stromatolitic boundstone, intraclastic dolomite Alluvial: Calcisol-Vertisol, dolocretes – both groundwater and pedogenic	Palustrine: mottled-nodular carbonate mudstones, laminated limestones	Lacustrine: oncolitic floatstones. Palustrine: mottled carbonate mudstones, nodular wackestone, laminated limestones. Fluvial: carbonate channels
Paleoenvironments	Palustrine, lacustrine	Alluvial, evaporitic (gypsum), palustrine, lacustrine	Alluvial, palustrine	Alluvial, palustrine, lacustrine
Water chemistry	Freshwater	Freshwater to saline	Alkaline–saline	Alkaline–saline
Ca supply	Surface/groundwater input	Surface/groundwater input	Dominantly groundwater input	Dominantly groundwater input
Biota	Stromatolites, insect trace fossils, ostracods, charophytes, mammals	Stromatolites, bivalves, conchostracans, plant remains, fish scales, vertebrate bones	Microbialites, ostracods	Microbialites, tetrapod tracks, charophytes, ostracods, invertebrate trace fossils, plant remains
Basement	Triassic siliciclastics, carbonates, and evaporites and Jurassic carbonates	Palaeozoic greywackes, shales, and volcanics below lower Triassic Mg-rich evaporites, limestones, and dolostones	Palaeozoic carbonates and siliciclastics and volcanics	Palaeozoic carbonates and siliciclastics and volcanics

cracks, mottling and nodules, and lacustrine wackestones and floatstones; however, they also record some high-energy carbonates as well (packstones and rudstones). The interpreted high energy, ramp-like Miocene palaeolake is located in the escarpment region along the border fault. This is opposite to the location with a lower gradient palaeoenvironment of the two studied palaeolakes of the Triassic Cuyana rift basin. Calcium-rich playa-lake systems also are present in the Triassic Arnstadt Formation in the extensional Germanic Basin (Arp *et al.*, 2005). The Arnstadt Formation carbonates are dominated by mainly dolomitic facies, especially the pedogenic and groundwater dolocretes. Clearly the Mg-rich lower Triassic sediments influenced the chemistry of the Norian lake waters in this German basin. All of three the rift basins have carbonate source rocks to supply the Ca needed for thick carbonate accumulations (after Gierlowski-Kordesch, 1998; Gierlowski-Kordesch *et al.*, 2008; Gierlowski-Kordesch, 2010; Alonso-Zarza *et al.*, 2012) whether through surface water or groundwater. Variability in the locations of palustrine and lacustrine carbonate deposits within two of the rift basins (Table 5) show that carbonate environments can exist anywhere in a rift basin as long as the sediment input is dominated by localized spring activity or overland erosion of a mostly carbonate landscape, perhaps linked with the binding of fine siliciclastic muds into pedogenic mud aggregates (Gierlowski-Kordesch, 1998; De Wet *et al.*, 2002; Renaut *et al.*, 2013). Clearly provenance and hydrology are key controls in carbonate accumulation in continental rift basins.

Palaeohydrology

Although the Cerro de las Cabras and Cerro Puntudo palaeolakes provide abundant evidence indicating subaerial exposure, the described palaeosols contain remains of a well-developed vegetation cover including herbaceous hygrophytes, sphenophytes and lycopsids (Mancuso, 2009). This suggests that, even though the local conditions in the half-grabens were arid, the palaeosols contained sufficient humidity to allow such vegetation cover (i.e. a high groundwater table in that area of the rift); which supports humid playa-lake types (Liutkus & Wright, 2008) with differing hydrological balances (Rosen, 1994). However, the rift context was arid and the surface water + sediment supply was scarce and ephemeral (Hardie *et al.*, 1978). The Cerro de las Cabras underfilled palaeolake probably had an open subsurface hydrology allowing throughflow of ions. This condition prevented the accumulation of thick evaporites because usually, in this type of system, the evaporation and the water supply ratio are in equilibrium (Rosen, 1994). The Cerro Puntudo palaeolake was also a hydrological open system at some time during its lifetime, both to surface water and to groundwater supply. In both cases, the groundwater fluctuations that controlled the changes in the palaeolake level could be linked to tectonics as well as climate.

The extensive carbonate sedimentation can be linked to groundwater sources because of the sedimentary features confirming groundwater discharge at the surface and a lack of limestone deposits in proximal sandflat areas, ruling out a clastic overland supply of carbonate (see Gierlowski-Kordesch, 2010). This fact points to springs linked to faulting (Winsborough *et al.*, 1994; Amezcua *et al.*, 2012) because groundwater circulation in rifts is affected by fault geometry (Jones & Renaut, 2010). Moreover, springs sustain limited lakes and ponds in areas affected by volcanism as is the case for some lakes of the East Africa rift (Renaut *et al.*, 2002). In the case of the Cerro Puntudo Formation, a discharge apron area has been identified, supporting a groundwater supply through springs and a complex palaeohydrology of the sub-basin (Renaut *et al.*, 2002). It is most likely that these systems formed in the lowest areas of the basin fed by a high water table in the nearby rift shoulders (Renaut *et al.*, 2013). Groundwater level fluctuations caused pedogenesis and subaerial exposure of the deposits (Meléndez *et al.*, 2009).

Palaeoclimate

Microflora studies for the Middle Triassic of Argentina show an affinity with the Ipswich microflora assemblage defined for Australia (Zavattieri & Batten, 1996; Zamuner *et al.*, 2001). This type of flora has been linked to temperate–warm to colder climate conditions (Zamuner *et al.*, 2001). A subtropical seasonal regime with wet summers and dry winters (Artabe *et al.*, 2001; Stipanicic & Volkheimer, 2002) has been proposed for the central-west Triassic basins of Argentina. However, for the Cuyana Basin, complex rift tectonics pushed the local climate conditions towards aridity (Stipanicic & Volkheimer, 2002). In the Cerro de las Cabras

and Cerro Puntudo formations, the abundant vertic soils indicate seasonality most probably caused by the rift topographic features inducing a rain shadow effect. Nevertheless, the presence of sphenophytes and lycopsids (Mancuso, 2009) confirm the existence of a wet season sustaining a high water table in some areas. This is indeed in agreement with the sedimentological, mineralogical and palaeontological data found for the half-grabens of the Cuyana Basin. Moreover, in the southernmost point of the Southern Hemisphere (Patagonia), during the Triassic, a typical warm–temperate climate (dry summers–wet winters) is recognized through the reconstruction of phytogeographic provinces (Scotese *et al.*, 1999; Quattrocchio *et al.*, 2011).

CONCLUSIONS

In the Potrerillos (southern) and Cerro Puntudo (northern) sub-basins of the Cuyana rift basin two carbonate palustrine–lacustrine depositional systems have been characterized as playa lakes with abundant microbialites. These systems were independent, were fed by a spring system and developed in moderate subsidence areas of the rift. Development of the lake systems in low to moderate accommodation tectonic settings with a Ca-rich hydrological provenance contributes new information on facies modelling for carbonate sedimentation in rift basins.

The Cerro de las Cabras system represents a sandflat and mudflat, and a carbonate palustrine setting with evidence of ephemeral conditions. However, the palaeosol characteristics indicate a rising water table. The Cerro Puntudo system, linked with a distal alluvial fan, formed a sandflat, muddy sandflat to mudflat, a carbonate palustrine setting, carbonate channels and a carbonate lacustrine subenvironment. The evidence for ephemeral conditions is widespread, except in the lacustrine facies where mineralogy supports alkalinity of lake waters. Mineralogy supports seasonally arid conditions for both palaeolake systems (wet and dry periods); this agrees with global palaeoclimatic models for the Triassic, taking into account the local effects in the rain shadow areas of the Cuyana rift. In both palaeolake successions, it is possible to recognize increasing subsidence through time.

The Cerro de las Cabras and Cerro Puntudo microbialites were formed by filamentous cyanobacteria. Autotrophic algae were found in association with Charophyta algae and ostracods. These micro-organisms passively induced the biomineralization of the structures (biologically induced precipitation). The limiting factor for the process was the availability of Ca, primarily sourced by Ca-rich groundwater, not by eroding limestone in the surface drainage area.

The dominantly aggradational stacking patterns of the Cerro de las Cabras succession characterize an underfilled playa lake with open subsurface hydrology. In this case, the stacking pattern and biota strengthen the interpreted underfilled lake type. Underfilled lakes without thick evaporite accumulations may be closed to surface-water supply but open to groundwater movement. The Cerro Puntudo aggradational–minor progradational succession is difficult to interpret due to lack of outcrop exposure across the basin to confirm a balanced-filled lake interpretation, although palaeontological and geochemical data support it. Nevertheless, both cases show that playa-lake systems have facies arrangements forming complex mosaics (random successions as confirmed by Markov Chain analysis) mainly determined by palaeohydrological fluctuations dependent on climate and tectonics in concert (see Bohacs *et al.*, 2003).

Comparison of the Ca-rich systems studied with similar ones in other extensional basins strengthens the need for an integrated sedimentary model considering palaeohydrology and provenance as important controls on sedimentation patterns. Application of these concepts to other rift basins globally will aid in developing new carbonate sedimentation models for freshwater limestones in extensional settings.

ACKNOWLEDGMENTS

Funding for this research was provided by two grants from CONICET (CAB) and projects PICT 32236 (Responsible ACM), PIP 11420090100209 (Responsible ACM) and PIP 11220100100034 (Responsible NGC). CAB wishes to thank Geól. Guillermo Cozzi for the mineralogical analysis and Mr Gabriel Giordanengo for two figures in this article. Technicians at INGEIS and Mr Joel Bertoglio and Mrs Silvana Dadán from the Secretaría de Minería de Mendoza provided help with sample processing. Drs Dina López and Sila Pla-Pueyo are thanked for providing logistical support during this research. The authors thank two anonymous reviewers and Associate Editor Daniel Ariztegui for help that improved the quality of the manuscript.

REFERENCES

Alonso-Zarza, A.M. (2003) Palaeoenvironmental significance of palustrine carbonates and calcretes in the geological record. *Earth-Sci. Rev.*, **60**, 261–298.

Alonso-Zarza, A.M. and **Wright, V.P**. (2010) Palustrine carbonates. In: *Carbonates in Continental Settings. Facies, Environments and Processes* (Eds A.M. Alonso-Zarza and L. Tanner), *Dev. Sedimentol.*, **61**, 103–131.

Alonso-Zarza, A.M., **Calvo, J.P.** and **García del Cura, M.A.** (1992) Palustrine sedimentation and associated features, grainification and pseudomicrokarst, in the Middle Miocene (Intermediate Unit) of the Madrid Basin, Spain. *Sed. Geol.*, **76**, 43–61.

Alonso-Zarza, A.M., **Meléndez, A.**, **Martín-García, R.**, **Herrero, M.J.** and **Martín-Pérez, A.** (2012) Discriminating between tectonism and climate signatures in palustrine deposits: lessons from the Miocene of the Teruel Graben, NE Spain. *Earth-Sci. Rev.*, **113**, 141–160.

Amezcua, N., **Gawthorpe, R.** and **MacQuaker, J.** (2012) Cascading carbonate lakes of the Mayrán Basin system, northeast México: the interplay of inherited structural geometry, bedrock lithology, and climate. *Geol. Soc. Am. Bull.*, **124**, 975–988.

Arenas, C., **Gutiérrez, F.**, **Osácar, C.** and **Sancho, C.** (2000) Sedimentology and geochemistry of fluvio-lacustrine tufa deposits controlled by evaporite solution subsidence in the central Ebro Depression, NE Spain. *Sedimentology*, **47**, 883–909.

Arenas, C., **Cabrera, Ll** and **Ramos, L.** (2007) Sedimentology and tufa facies and continental microbialites from the Palaeogene of Mallorca Island (Spain). *Sed. Geol.*, **197**, 1–22.

Armenteros, I. and **Daley, B.** (1998) Pedogenetic modification and structure evolution in palustrine facies as exemplified by the Bembridge Limestone (Late Eocene) of Isle of Wight, southern England. *Sed. Geol.*, **119**, 275–295.

Arp, G., **Bielert, F.**, **Hoffmann, V.-E.** and **Löffler, T.** (2005) Palaeoenvironmental significance of lacustrine stromatolites of the Arnstadt Formation (''Steinmergelkeuper'', Upper Triassic, N-Germany). *Facies*, **51**, 433–455.

Artabe, A.E., **Morel, E.M.** and **Spalletti, L.A**. (2001) Paleoecología de las floras triásicas argentinas. In: *El Sistema Triásico en la Argentina* (Eds A. Artabe, E. Morel and A. Zamuner), pp. 199–225. Fundación Museo de La Plata "Francisco Pascasio Moreno", La Plata.

Ávila, J.N., **Chemale, F., Jr**, **Mallmann, G.**, **Kawashita, K.** and **Armstrong, R.A.** (2006) Combined stratigraphic and isotopic studies of Triassic strata, Cuyo Basin, Argentine Precordillera. *Geol. Soc. Am. Bull.*, **118**, 1088–1098.

Barredo, S.P. (2005) Análisis estructural y tectosedimentario de la subcuenca de Rincón Blanco. PhD Dissertation, Precordillera Occidental, provincia de San Juan. Universidad de Buenos Aires, 325 pp.

Barredo, S.P., **Chemale, F.**, **Marsicano, C.**, **Ávila, J.N.**, **Ottone, E.G.** and **Ramos, V.A.** (2011) Tectono-sequence stratigraphy and U-Pb zircon ages of the Rincón Blanco Depocenter, northern Cuyo Rift, Argentina. *Gondwana Res.*, **21**, 624–636.

Barrier, L., **Proust, J.-N.**, **Nalpas, T.**, **Robin, C.** and **Guillocheau, F.** (2010) Control of alluvial sedimentation at foreland-basin active margins: a case study from the northeastern Ebro Basin (southeastern Pyrenees, Spain). *J. Sed. Res.*, **80**, 728–749.

Bellosi, E.S., **Jalfin, G.A.**, **Bossi, G.E.**, **Boggetti, D.**, **Chebli, P.** and **Muruaga, C**. (2001) Facies y sedimentación. In: *El Sistema Triásico en la Argentina* (Eds A.E. Artabe, E.M. Morel and A.B. Zamuner), pp. 103–129. Fundación Museo de La Plata "Francisco Pascasio Moreno", La Plata.

Benavente, C.A. (2014) Microbialitas lacustres de secuencias triásicas de Argentina. PhD Dissertation, Universidad de Buenos Aires, 264 pp.

Benavente, C.A., **Mancuso, A.C.** and **Cabaleri, N.G.** (2012) First occurrence of charophyte algae from a Triassic paleolake in Argentina and their paleoenvironmental context. *Palaeogeogr. Palaeocl.*, **363–364**, 172–183.

Benavente, C.A., **D'Angelo, J.A.**, **Crespo, E.M.** and **Mancuso, A.C**. (2015) Chemometric approach to Charophyte preservation (Triassic Cerro Puntudo Formation, Argentina): paleolimnologic implications. *Palaios*, **9**, 449–459, in press.

Beraldi-Campesi, H., **Cevallos-Ferriz, S.R.S.** and **Chacón-Baca, E.** (2004) Microfossil algae associated with Cretaceous stromatolites in the Tarahumara Formation, Sonora, Mexico. *Cretaceous Res.*, **25**, 249–265.

Beraldi-Campesi, H., **Cevallos-Ferriz, S.R.S.**, **Centeno-Garcia, E.**, **Arenas-Abad, C.** and **Fernández, L.P.** (2006) Sedimentology and paleoecology of an Eocene-Oligocene alluvial-lacustrine arid system, southern México. *Sed. Geol.*, **191**, 227–254.

Bernier, P., **Gaillard, C.**, **Gall, J.C.**, **Barales, G.J.**, **Bourseau, P.**, **Buffetauts, E.** and **Wenz, S.** (1991) Morphogenetic impact of microbial mats on surface structures of Kimmeridgian micritic limestones (Cerin, France). *Sedimentology*, **38**, 127–136.

Bertani, R.T. and **Carozzi, A.V.** (1985) Lagoa Feia Formation (Lower Cretaceous) Campos Basin, offshore Brazil: rift-valley stage carbonate reservoirs – I and II. *J. Petrol. Geol.*, **8**, 199–220.

Billi, P. (2007) Morphology and sediment dynamics of ephemeral stream terminal distributary systems in the Kobo Basin (northern Welo, Ethiopia). *Geomorphology*, **85**, 98–113.

Bohacs, K.M., **Carroll, A.R.**, **Neal, J.E.** and **Mankiewicz, P.J**. (2000) Lake-basin type, source potential, and hydrocarbon character: an integrated sequence-stratigraphic-geochemical framework. In: *Lake Basins Through Space and Time* (Eds E.H. Gierlowski-Kordesch and K.R. Kelts), *AAPG Stud. Geol.*, **46**, 3–34.

Bohacs, K.M., **Carroll, A.R.** and **Neal, J.E**. (2003) Lessons from large lake systems: thresholds, nonlinearity, and strange attractors. In: *Extreme Depositional Environments: Mega End Members in Geologic Time* (Eds M.A. Chan and A.W. Archer), *Geol. Soc. Am. Spec. Pap.*, **370**, 75–90.

Boles, J.R. and **Surdam, R.C.** (1979) Diagenesis of volcanogenic sediments in a Tertiary saline lake: Wagon Bed Formation, Wyoming. *Am. J. Sci.*, **279**, 832–853.

Bromley, R.G. (1996) *Trace Fossils. Biology, Taxonomy and Applications*. Chapman and Hall, London.

Buatois, L.A. and **Mángano, M.G.** (1998) Trace fossil analysis of lacustrine facies and basins. *Palaeogeogr. Palaeocl.*, **140**, 367–382.

Bustillo, M.A. (2010) Silicification of continental carbonates. In: *Carbonates in Continental Settings. Facies, Environments and Processes* (Eds A.M. Alonso-Zarza and L. Tanner), *Dev. Sedimentol.*, **61**, 153–178.

Bustillo, M.A. and **Alonso-Zarza, A.M.** (2007) Overlapping of pedogenesis and meteoric diagenesis in distal alluvial

and shallow lacustrine deposits in the Madrid Miocene Basin, Spain. *Sed. Geol.*, **198**, 255–271.

Cabaleri, N.G. and **Armella, C.** (1999) Facies lacustres de la Formación Cañadón Asfalto (Caloviano-Oxfordiano), en la quebrada Las Chacritas, Cerro Cóndor, provincia del Chubut. *Rev. Asoc. Geol. Argentina*, **54**, 375–388.

Cabaleri, N.G. and **Armella, C.** (2005) Influence of biothermal belt on the lacustrine sedimentation of the Cañadon Asfalto Formation (Upper Jurassic, Chubut province, Southern Argentina). *Geol. Acta*, **3**, 205–214.

Cabaleri, N.G. and **Benavente, C.A.** (2013) Sedimentology and paleoenvironments of the Las Chacritas carbonate paleolake, Cañadón Asfalto Formation (Jurassic,) Patagonia, Argentina. *Sed. Geol.*, **284–285**, 91–105.

Cabaleri, N.G., **Armella, C.** and **Silva Nieto, D.G.** (2005) Saline paleolake of the Cañadón Asfalto Formation (Middle-Upper Jurassic), Cerro Cóndor, Chubut province (Patagonia), Argentina. *Facies*, **51**, 350–364.

Cabaleri, N.G., **Benavente, C.A.**, **Monferrán, M.**, **Narváez, P.L.**, **Volkheimer, W.**, **Gallego, O.F.** and **Do Campo, M.D.** (2013) Palaeoenvironmental and climatic significance of the Puesto Almada Member (Upper Jurassic, Cañadón Asfalto Formation), at the Fossati sub-basin, Patagonia Argentina. *Sed. Geol.*, **296**, 103–121.

Calvo, J.P., **Alonso-Zarza, A.M.** and **García del Cura, M.A.** (1989) Models of Miocene marginal lacustrine sedimentation in response to varied depositional regimes and source areas in the Madrid Basin (Central Spain). *Palaeogeogr. Palaeocl.*, **70**, 199–214.

Camoin, G., **Casanova, J.**, **Rouchy, J.M.**, **Blanc-Valleron, M.M.** and **Deconinck, J.F.** (1997) Environmental controls on perennial and ephemeral carbonate lakes: the central palaeo-Andean Basin of Bolivia during Late Cretaceous to early Tertiary times. *Sed. Geol.*, **113**, 1–26.

Carroll, A.R. and **Bohacs, K.M.** (1999) Stratigraphic classification of ancient lakes: balancing tectonic and climatic controls. *Geology*, **27**, 99–102.

Catena, A. and **Hembree, D.** (2012) Recognizing vertical and lateral variability in terrestrial landscapes: a case study from the paleosols of the Late Pennsylvanian Casselman Formation (Conemaugh Group), southeast Ohio, USA. *Geosciences*, **2**, 178–202.

Chebli, G.A., **Ploszkiewicz, J.V.** and **Azpiroz, G.M.** (2001) El Sistema Triásico y los hidrocarburos. In: *El Sistema Triásico en la Argentina* (Eds A.E. Artabe, E.M. Morel and A.B. Zamuner), pp. 283–315. Fundación Museo de La Plata "Francisco Pascasio Moreno", La Plata.

Cohen, A.S. (1990) A tectonostratigraphic model for sedimentation in Lake Tanganyika, Africa. In: *Lacustrine Basin Exploration. Case Studies and Modern Analogs* (Ed. B. Katz), *AAPG Mem.*, **50**, 137–150.

Cohen, A.S. and **Thouin, C.** (1987) Nearshore carbonate deposits in Lake Tanganyika. *Geology*, **15**, 414–418.

Cuadrado, D.G., **Carmona, N.B.** and **Bournod, C.** (2011) Biostabilization of sediments by microbial mats in a temperate siliciclastic tidal flat, Bahia Blanca estuary (Argentina). *Sed. Geol.*, **237**, 95–101.

Cuadros, J., **Caballero, E.**, **Huertas, J.**, **Jiménez de Cisneros, C.**, **Huertas, F.** and **Linares, J.** (1999) Experimental alteration of volcanic tuff: smectite formation and effect on O isotope composition. *Clay Clay Mineral.*, **47**, 769–776.

De Wet, C.B., **Mora, C.I.**, **Gore, P.J.W.** and **Gierlowski-Kordesch, E.H.** (2002) Deposition and geochemistry of lacustrine and spring carbonates in Mesozoic Rift Basins, Eastern North America. In: *Sedimentation in Continental Rifts* (Eds R.W. Renaut and G.M. Ashley), *SEPM Spec. Publ.*, **73**, 309–325.

Deocampo, D.M. (2004) Authigenic clays in East Africa: regional trends and paleolimnology at the Plio-Pleistocene boundary, Olduvai Gorge, Tanzania. *J. Paleolimnol.*, **31**, 1–9.

Dupraz, C., **Reid, R.P.**, **Braissant, O.**, **Decho, A.W.**, **Norman, R.S.** and **Visscher, P.T.** (2009) Processes of carbonate precipitation in modern microbial mats. *Earth-Science Rev.*, **96**, 141–162.

Durand, N., **Gunnell, Y.**, **Curmi, P.** and **Ahmad, S.M.** (2006) Pathways of calcrete development on weathered silicate rocks in Tamil Nadu, India: mineralogy, chemistry and paleoenvironmental implications. *Sed. Geol.*, **192**, 1–18.

Fisher, J.A., **Nichols, G.J.** and **Waltham, D.A.** (2007a) Unconfined flow deposits in distal sectors of fluvial distributary systems: examples from the Miocene Luna and Huesca Systems, northern Spain. *Sed. Geol.*, **195**, 55–73.

Fisher, J.A., **Waltham, D.A.**, **Nichols, G.J.**, **Krapf, C.B.E.** and **Lang, S.C.** (2007b) A quantitative model for deposition of thin fluvial sand sheets. *J. Geol. Soc. London*, **164**, 67–71.

Fisher, J.A., **Krapf, C.B.E.**, **Lang, S.C.**, **Nichols, G.J.** and **Payenberg, T.H.D.** (2008) Sedimentology and architecture of the Douglas Creek terminal splay, Lake Eyre, central Australia. *Sedimentology*, **55**, 1915–1930.

Flügel, E. (2004) *Microfacies and Carbonate Rocks. Analysis, Interpretation and Application*. Springer, Berlin.

Folguera, A. and **Etcheverría, M.** (2004) Hoja Geológica 3369-15 Potrerillos, Provincia de Mendoza. Programa Nacional de Cartas Geológicas de la República Argentina, 1:100.000. Servicio Geológico Minero Argentino. Instituto de Geología y Recursos Minerales, Buenos Aires, **301**, 1–136.

Fregenal-Martínez, M.A. and **Meléndez, N.** (2010) Lagos y sistemas lacustres. In: *Sedimentología: del Proceso Físico a la Cuenca Sedimentaria* (Ed. A. Arche), pp. 299–395. Consejo Superior de Investigaciones Científicas, Madrid.

Freytet, P. (1973) Petrography and paleonvironment of continental carbonate deposits with particular reference to the Upper Cretaceous and Lower Eocene of Languedoc (southem France). *Sed. Geol.*, **10**, 25–60.

Freytet, P. and **Plaziat, J.C.** (1982) Continental carbonate sedimentation and pedogenesis. Late Cretaceous and Early Tertiary of Southern France. In: *Contributions to Sedimentology* (Ed. B.H. Purser), , Vol. **12**, pp. 1–213. E. Schweitzerbartsche Verlagsbuchhandlung, Stutgart

Freytet, P. and **Verrecchia, E.P.** (1998) Freshwater organisms that build stromatolites: a synopsis of biocrystallization by prokaryotic and eukaryotic algae. *Sedimentology*, **45**, 535–563.

Freytet, P. and **Verrecchia, E.P.** (2002) Lacustrine and palustrine carbonate petrography: an overview. *J. Paleolimnol.*, **27**, 221–237.

Freytet, P., **Toutin-Morin, N.**, **Broutinc, J.**, **Debriette, P.**, **Durand, M.**, **El Wartiti, M.**, **Gand, G.**, **Kerp, H.**, **Orzag, F.**, **Paquette, Y.**, **Ronchi, A.** and **Sarfati, J.** (1999) Palaeoecology of nonmarine algae and stromatolites: Permian of France and adjacent countries. *Ann. Paléontologie*, **85**, 99–153.

Gawthorpe, R.L. and **Leeder, M.R.** (2000) Tectono-sedimentary evolution of active extensional basins. *Basin Res.*, **12**, 195–218.

Gehling, J.G. (1999) Microbial mats in terminal proterozoic siliciclastics: Ediacaran death masks. *Palaios*, **14**, 40–57.

Ghosh, P. (1997) Geomorphology and palaeoclimatology of some Upper Cretaceous palaeosols in central India. *Sed. Geol.*, **110**, 25–49.

Gierlowski-Kordesch, E.H. (1991) Ichnology of an ephemeral lacustrine/alluvial plain system: Jurassic East Berlin Formation, Hartford Basin, USA. *Ichnos*, **1**, 221–232.

Gierlowski-Kordesch, E.H. (1998) Carbonate deposition in an ephemeral siliciclastic alluvial system: Jurassic Shuttle Meadow Formation, Newark Supergroup, Hartford Basin, USA. *Palaeogeogr. Palaeocl.*, **140**, 161–184.

Gierlowski-Kordesch, E.H. (2010) Lacustrine carbonates. In: *Carbonates in Continental Settings. Facies, Environments and Processes* (Eds A.M. Alonso-Zarza and L. Tanner), *Dev. Sedimentol.*, **61**, 1–102.

Gierlowski-Kordesch, E.H. and **Gibling, M.R**. (2002) Pedogenic mud aggregates in rift sedimentation. In: *Sedimentation in Continental Rifts* (Eds R. Renaut and G.M. Ashley), *SEPM Spec. Publ.*, **73**, 195–206.

Gierlowski-Kordesch, E.H. and **Rust, B.R**. (1994) The Jurassic East Berlin Formation, Hartford Basin, Newark Supergroup (Connecticut and Massachusetts): a saline lake-playa-alluvial plain system. In: *Sedimentology and Geochemistry of Modern and Ancient Saline Lakes* (Eds R.W. Renaut and W.M. Last), *SEPM Spec. Publ.*, **50**, 249–265.

Gierlowski-Kordesch, E.H., **Gómez Fernández, J.C.** and **Meléndez, N**. (1991) Carbonate and coal deposition in an alluvial-lacustrine setting: Lower Cretaceous (Weald) in the Iberian Range (east-central Spain). In: *Lacustrine Facies Analysis* (Eds P. Anadón, Ll. Cabrera and K. Kelts), *IAS Spec. Publ.*, **13**, 109–125.

Gierlowski-Kordesch, E.H., **Jacobson, A.D.**, **Blum, J.D.** and **Valero Garcés, B.L.** (2008) Watershed reconstruction of a Paleocene-Eocene lake basin using Sr isotopes in carbonate rocks. *Geol. Soc. Am. Bull.*, **120**, 85–95.

Gierlowski-Kordesch, E.H., **Finkelstein, D.B.**, **Truchan, J.J.** and **Kallini, K.D.** (2013) Carbonate lakes associated with distal siliciclastic perennial-river systems. *J. Sed. Res.*, **83**, 1114–1129.

Gómez-Gras, D. and **Alonso-Zarza, A.M.** (2003) Reworked calcretes: their significance in the reconstruction of alluvial sequences (Permian and Triassic, Minorca, Balearic Islands, Spain). *Sed. Geol.*, **158**, 299–319.

Gómez-Pérez, I. (2003) An early Jurassic deep-water stromatolitic bioherm related to possible methane seepage (Los Molles Formation, Neuquén, Argentina). *Palaeogeogr. Palaeocl.*, **201**, 21–49.

Hardie, L.A., **Smoot, J.P.** and **Eugster, H.P**. (1978) Saline lakes and their deposits: a sedimentological approach. In: *Modern and Ancient Lake Sediments* (Eds A. Matter and M.E. Tucker), *IAS Spec. Publ.*, **2**, 7–41.

Hargrave, J.E., **Hicks, M.K.** and **Scholz, C.A.** (2014) Lacustrine carbonate from Lake Turkana, Kenya: a depositional model of carbonates in an extensional basin. *J. Sed. Res.*, **84**, 224–237.

Harris, P.M., **Ellis, J.** and **Purkis, S.J.** (2013) Assessing the extent of carbonate deposition in early rift settings. *AAPG Bull.*, **97**, 27–60.

Hofmann, H.J. (1975) Stratiform Precambrian stromatolites, Belcher Islands, Canada: relations between silicified microfossils and microstructure. *Am. J. Sci.*, **275**, 1121–1132.

Huerta, P. and **Armenteros, I.** (2004) Asociaciones de carbonatos continentales en el Eoceno de la Cuenca de Almazán. *Geo-Temas*, **6**2, 75–78.

Huerta, P. and **Armenteros, I.** (2005) Calcrete and palustrine assemblages on a distal alluvial-floodplain: a response to local subsidence (Miocene of the Duero basin, Spain). *Sed. Geol.*, **177**, 253–270.

Jones, B. and **Renaut, R.W.** (1994) Crystal fabrics and microbiota in large pisoliths from Laguna Pastos Grandes, Bolivia. *Sedimentology*, **41**, 1171–1202.

Jones, B. and **Renaut, R.W**. (2010) Calcareous spring deposits in continental settings. In: *Carbonates in Continental Settings. Facies, Environments and Processes* (Eds A.M. Alonso-Zarza and L. Tanner), *Dev. Sedimentol.*, **61**, 177–224.

Klappa, C.F. (1980) Rhizoliths in terrestrial carbonates: classification, recognition, genesis and significance. *Sedimentology*, **27**, 613–629.

Kokogian, D.A. and **Mancilla, O**. (1989) Análisis estratigráfico secuencial de la Cuenca Cuyana. In: *Cuencas Sedimentarias Argentinas* (Eds G.A. Chebli and L.A. Spalletti), *Ser. Correlación Geol.*, **6**, 169–201.

Kokogian, D.A., **Seveso, S.S.** and **Mosquera, A**. (1993) Capítulo I-7 Las secuencias sedimentarias triásicas. In: *Relatorio Geología y Recursos Naturales de Mendoza* (Ed. V. Ramos), pp. 65–78. XII Congreso Geológico Argentino and II Congreso de Exploración de Hidrocarburos.

Krapovickas, V., **Mángano, M.G.**, **Mancuso, A.C.**, **Marsicano, C.A.** and **Volkheimer, W.** (2008) Icnofaunas triásicas en abanicos aluviales distales: evidencias de la Formación Cerro Puntudo, Cuenca Cuyana, Argentina. *Ameghiniana*, **45**, 463–472.

Kraus, M.J. (1999) Paleosols in clastic sedimentary rocks: their geologic applications. *Earth-Science Rev.*, **47**, 41–70.

Kraus, M.J. and **Aslan, A.** (1999) Palaeosol sequences in floodplain environments: a hierarchical approach. *IAS Spec. Publ.*, **27**, 303–321.

Kraus, M.J. and **Hasiotis, S.T.** (2006) Significance of different modes of rhizolith preservation to interpreting paleoenvironmental and paleohydrologic settings: examples from Paleogene paleosols, Bighorn Basin, Wyomi NG, U.S.A. *J. Sed. Res.*, **76**, 633–646.

Krause, J.M., **Bellosi, E.S.** and **Raigemborn, M.S.** (2010) Lateritized tephric palaeosols from Central Patagonia, Argentina: a southern high-latitude archive of Palaeogene global greenhouse conditions. *Sedimentology*, **57**, 1721–1749.

Krumbein, W.C. and **Dacey, M.F.** (1969) Markov chains and embedded Markov chains in geology. *Math. Geol.*, **1**, 79–96.

Landon, J.R. (1984) *Booker Tropical Soil Manual*. Booker Agricultural International Limited, Bath.

Legarreta, L., **Kokogian, D.A.** and **Dellapé, D.A.** (1992) Estructura terciaria de la Cuenca Cuyana: Cuánto de inversión tectónica? *Rev. Asoc. Geol. Argentina*, **47**, 83–86.

Leier, A.L., **Mcquarrie, N.**, **Horton, B.K.** and **Gehrels, G.E.** (2010) Upper Oligocene conglomerates of the Altiplano, Central Andes: the record of deposition and deformation along the margin of a Hinterland Basin. *J. Sed. Res.*, **80**, 750–762.

Leslie, A.B., **Tucker, M.E.** and **Spiro, B.** (1992) A sedimentological and stable isotopic study of travertines and associated sediments within Upper Triassic lacustrine limestones, South Wales, UK. *Sedimentology*, **39**, 613–629.

Liutkus, C.M. and **Wright, J.D.** (2008) The influence of hydrology and climate on the isotope geochemistry of playa carbonates: a study from Pilot Valley, NV, USA. *Sedimentology*, **55**, 965–978.

Liutkus, C.M., **Wright, J.D.**, **Ashley, G.M.** and **Sikes, N.E.** (2005) Paleoenvironmental interpretation of lake-margin deposits using $d^{13}C$ and $d^{18}O$ results from early Pleistocene carbonate rhizoliths, Olduvai Gorge, Tanzania. *Geology*, **33**, 377–380.

Liutkus, C.M., **Beard, J.S.**, **Fraser, N.C.** and **Ragland, P.C.** (2010) Use of fine-scale stratigraphy and chemostratigraphy to evaluate conditions of deposition and preservation of a Triassic Lagerstätte, south-central Virginia. *J. Paleolimnol.*, **44**, 645–666.

Llambías, E.J. (2001) Complejos magmáticos triásicos al norte de los 40° S. In: *El Sistema Triásico de la Argentina* (Eds A. Artabe, E. Morel and A. Zamuner), pp. 55–68. Fundación Museo de La Plata "Francisco P. Moreno", La Plata.

van Loon, A.J. (2009) Soft-sediment deformation structures in siliciclastic sediments: an overview. *Geólogos*, **15**, 3–55.

López-Gamundí, O. (2010) Sedimentation styles and variability of organic matter types in the Triassic, non-marine half-grabens of west Argentina: implications for petroleum systems in rift basins. *Petrol. Geosci.*, **16**, 267–272.

López-Gamundí, O.R. and **Astini, R.** (2004) Alluvial fan lacustrine association in the fault tip end of a half-graben, northern Triassic Cuyo Basin, western Argentina. *J. S. Am. Earth Sci.*, **17**, 253–265.

Lowenstein, T.K. and **Hardie, L.A.** (1985) Criteria for the recognition of salt-pan evaporites. *Sedimentology*, **32**, 627–644.

Lynn, W. and **Williams, D.** (1992) The making of a Vertisol. *Soil Surv. Horizons*, **33**, 45–51.

Macedo, J. and **Bryant, R.B.** (1987) Morphology, mineralogy, and genesis of a hydrosequence of Oxisols in Brazil. *Soil Sci. Soc. Am. J.*, **51**, 690–698.

Mancuso, A.C. (2009) Taphonomic analysis in lacustrine environment: two very different Triassic lake paleoflora contexts from Western Gondwana. *Sed. Geol.*, **222**, 149–159.

Mancuso, A.C., **Chemale, F.**, **Barredo, S.**, **Ávila, J.N.**, **Ottone, E.G.** and **Marsicano, C.A.** (2010) Age constraints for the northernmost outcrops of the Triassic Cuyana Basin, Argentina. *J. S. Am. Earth Sci.*, **30**, 97–103.

Maroulis, J.C. and **Nanson, G.C.** (1996) Bedload transport of aggregated muddy alluvium from Cooper Creek, central Australia: a flume study. *Sedimentology*, **43**, 771–790.

Marsicano, C.A. and **Barredo, S.P.** (2004) A Triassic tetrapod footprints assemblage from southern South America: palaeobiogeographical and evolutionary implications. *Palaeogeogr. Palaeocl.*, **203**, 313–335.

Martín-Closas, C. (1999) Epiphytic overgrowth of Charophyte thalli by stromatolite-like structures and fungi in the Lower Cretaceous of the Iberian Ranges (Spain). *Aust. J. Botany*, **47**, 305–313.

Meléndez, N., **Liesa, C.L.**, **Soria, A.R.** and **Meléndez, A.** (2009) Lacustrine system evolution during early rifting: El Castellar Formation (Galve subbasin, Central Iberian Chain). *Sed. Geol.*, **222**, 64–77.

Miall, A.D. (1996) *The Geology of Fluvial Deposits: Sedimentary Facies, Basin Analysis and Petroleum Geology*. Springer Verlag, Berlin.

Minter, N.J., **Krainer, K.**, **Lucas, S.G.**, **Braddy, S.J.** and **Hunt, A.P.** (2007) Palaeoecology of an Early Permian playa lake trace fossil assemblage from Castle Peak, Texas, USA. *Palaeogeogr. Palaeocl.*, **246**, 390–423.

Müller, R., **Nysteun, J.P.** and **Wright, V.P.** (2004) Pedogenic mud aggregates and paleosol development in ancient dryland river systems: criteria for interpreting alluvial mudrock origin and floodplain dynamics. *J. Sed. Res.*, **74**, 537–551.

Nanson, G.C., **Tooth, S.** and **Knighton, D.** (2002) A global perspective on dryland rivers: perceptions, misconceptions and distinctions. In: *Dryland Rivers: Hydrology and Geomorphology of Semi-Arid Channels* (Eds M.J. Kirkby and L.J. Bull), pp. 17–54. John Wiley & Sons, Chichester.

Nichols, G.J. and **Fisher, J.A.** (2007) Processes, facies and architecture of fluvial distributary system deposits. *Sed. Geol.*, **195**, 75–90.

Nickel, E. (1985) Carbonates in alluvial fan systems. An approach to physiography, sedimentology, and diagenesis. *Sed. Geol.*, **42**, 83–104.

Owen, R.A., **Owen, R.B.**, **Renaut, R.W.**, **Scott, J.J.**, **Jones, B.** and **Ashley, G.M.** (2008) Mineralogy and origin of rhizoliths on the margins of saline, alkaline Lake Bogoria, Kenya Rift Valley. *Sed. Geol.*, **203**(1–2), 143–163.

Paik, I.S. and **Lee, Y.I.** (1998) Desiccation cracks in vertic palaeosols of the Cretaceous Hasandong Formation, Korea: genesis and palaeoenvironmental implications. *Sed. Geol.*, **119**, 161–179.

Parks, K.P., **Bentley, L.R.** and **Crowe, A.S.** (2000) Capturing geological realism in stochastic simulations of rock systems with Markov statistics and simulated annealing. *J. Sed. Res.*, **70**, 803–813.

Perri, E., **Manzo, E.** and **Tucker, M.E.** (2012) Multi-scale study of the role of the biofilm in the formation of minerals and fabrics in calcareous tufa. *Sed. Geol.*, **263–264**, 16–29.

Pla-Pueyo, S., **Gierlowski-Kordesch, E.H.**, **Viseras, C.** and **Soria, J.M.** (2009) Major controls on sedimentation during the evolution of a continental basin: Pliocene-Pleistocene of the Guadix Basin (Betic Cordillera, southern Spain). *Sed. Geol.*, **219**, 97–114.

Platt, N. (1989) Lacustrine carbonates and pedogenesis: sedimentology and origin of palustrine deposits from the Early Cretaceous Rupelo Formation, W Cameros Basin, N Spain. *Sedimentology*, **36**, 665–684.

Platt, N. and **Wright, P.** (1991) Lacustrine carbonates: facies models, facies distributions and hydrocarbon aspects. In: *Lacustrine Facies Analysis* (Eds P. Anadón, Ll. Cabrera and K. Kelts), *IAS Spec. Publ.*, **13**, 57–74.

Quattrocchio, M.E., **Volkheimer, W.**, **Borromei, A.M.** and **Martínez, M.A.** (2011) Changes of the palynobiotas in the Mesozoic and Cenozoic of Patagonia: a review. *Biol. J. Linn. Soc.*, **103**, 380–396.

Ramos, V.A. and **Kay, S.M.** (1991) Triassic rifting and associated basalts in the Cuyo Basin, central Argentina. In: *Andean Magmatism and its Tectonic Setting* (Eds R.S. Harmon and C.W. Rapela), *Geol. Soc. Am. Spec. Pap.*, **265**, 79–91.

Rasbury, T.E., **Gierlowski-Kordesch, E.H.**, **Cole, J.M.**, **Sookdeo, C.**, **Spataro, G.** and **Nienstedt, J.** (2006) Calcite cement stratigraphy of a nonpedogenic calcrete in the Triassic New Haven Arkose (Newark Supergroup). In: *Paleoenvironmental Record and Applications of Calcretes and Palustrine Carbonates* (Eds A.M. Alonso-Zarza and L.H. Tanner), *Geol. Soc. Am. Spec. Pap.*, **416**, 203–221.

Renaut, R.W. (1993) Zeolitic diagenesis of late Quaternary fluviolacustrine sediments and associated calcrete formation in the Lake Bogoria Basin, Kenya Rift Valley. *Sedimentology*, **40**, 271–301.

Renaut, R.W. and **Tiercelin, J.-J**. (1994) Lake Bogoria, Kenya Rift Valley – a sedimentological overview. In: *Sedimentology and Geochemistry of Modern and Ancient Saline Lakes* (Eds R.W. Renaut and W.M. Last), *SEPM Spec. Publ.*, **50**, 101–123.

Renaut, R.W., **Morley, C.K.** and **Jones, B**. (2002) Fossil hot-spring travertine in the Turkana Basin, northern Kenya: structure, facies, and genesis. In: *Sedimentation in Continental Rifts* (Eds R.W. Renaut and G.M. Ashley), *SEPM Spec. Publ.*, **73**, 123–141.

Renaut, R.W., **Owen, R.B.**, **Jones, B.**, **Tiercelin, J.-J.**, **Tarits, C.**, **Ego, J.K.** and **Konhauser, K.O.** (2013) Impact of lake-level changes on the formation of thermogene travertine in continental rifts: evidence from Lake Bogoria, Kenya rift valley. *Sedimentology*, **60**, 428–468.

Retallack, G.J. (1994) A pedotype approach to latest Cretaceous and earliest Tertiary paleosols in eastern Montana. *Geol. Soc. Am. Bull.*, **106**, 1377–1397.

Riding, R. (1991a) Classification of microbial carbonates. In: *Calcareous Algae and Stromatolites* (Ed. R. Riding), pp. 21–54. Elsevier, Berlin.

Riding, R. (1991b) Calcified cyanobacteria. In: *Calcareous Algae and Stromatolites* (Ed. R. Riding), pp. 52–87. Elsevier, Berlin.

Risacher, F. and **Eugster, H.P.** (1979) Holocene pisoliths and encrustations associated with spring-fed surface pools, Pastos Grandes, Bolivia. *Sedimentology*, **26**, 253–270.

Rosen, M.R. (1994) The importance of groundwater in playas: a review of playa classifications and the sedimentology and hydrology of playas. *Geol. Soc. Am. Spec. Pap.*, **289**, 1–18.

Rouchy, J.M., **Servant, M.**, **Fournier, M.** and **Causse, C.** (1996) Extensive carbonate algal bioherms in upper Pleistocene saline lakes of the central Altiplano of Bolivia. *Sedimentology*, **43**, 973–993.

Rust, B.R. and **Nanson, G.C.** (1991) Bedload transport of mud as pedogenic aggregates in modern and ancient rivers: discussion. *Sedimentology*, **38**, 157–160.

Scholle, P.A. and **Ulmer-Scholle, D.S.** (2003) A color guide to the petrography of carbonate rocks: grains, textures, porosity diagenesis. *AAPG Mem.*, **77**, 1–461.

Scotese, C.R., **Boucot, A.J.** and **McKerrow, W.S.** (1999) Gondwanan palaeogeography and palaeoclimatology. *J. Afr. Earth Sci.*, **28**, 99–114.

Scott, J.J., **Renaut, R.W.R.**, **Owen, B.** and **Sarjeant, W.A.S**. (2007) Biogenic activity, trace formation, and trace taphonomy in the marginal sediments of saline, alkaline Lake Bogoria, Kenya Rift Valley. In: *Sediment–Organism Interactions: A Multifaceted Ichnology* (Eds R.G. Bromley, L.A. Buatois, G. Mángano, J.F. Genise and R.N. Melchor), *SEPM Spec. Publ.*, **88**, 311–332.

Scott, J.J., **Renaut, R.W.R.**, **Buatois, L.A.** and **Owen, B.** (2009) Biogenic structures in exhumed surfaces around saline lakes: an example from Lake Bogoria, Kenya Rift Valley. *Palaeogeogr. Palaeocl.*, **272**, 196–198.

Scott, J.J., **Renaut, R.W.R.** and **Owen, B.** (2010) Taphonomic controls on animal tracks at saline, alkaline Lake Bogoria, Kenya Rift Valley: impact of salt efflorescence and clay mineralogy. *J. Sed. Res.*, **80**, 639–665.

Scott, J.J., **Buatois, L.A.** and **Mángano, M.G**. (2012) Lacustrine environments. In: *Trace Fossils as Indicators of Sedimentary Environments* (Eds D.R. Knaust and G. Bromley), *Dev. Sedimentol.*, **64**, 379–417.

Sessarego, H.L. (1986) Nuevos depósitos triásicos en la margen norte del río San Juan, Quebrada del Tigre, Provincia de San Juan. Estratigrafía y paleoambientes sedimentarios. *Revista de la Asociación Argentina de Mineralogía, Petrología y Sedimentología*, **17**, 67–79.

Shiraishi, F., **Reimer, A.**, **Bisset, A.**, **de Beer, D.** and **Arp, G.** (2008) Microbial effects on biofilm calcification, ambient water chemistry and stable isotope records in a highly supersaturated setting (Westerhöfer Bach, Germany). *Palaeogeogr. Palaeocl.*, **262**, 91–106.

Smoot, J.P. and **Lowenstein, T.K**. (1991) Depositional environments of nonmarine evaporites. In: *Evaporites, Petroleum, and Mineral Resources* (Ed. J.L. Melvin), *Dev. Sedimentol.*, **50**, 189–347.

Spalletti, L.A. (1997) Cuencas triásicas del oeste argentino: origen y evolución. *Acta Geol. Hisp.*, **32**, 29–50.

Spalletti, L.A. (2001) Evolución de las cuencas sedimentarias. In: *El Sistema Triásico en la Argentina* (Eds A.E. Artabe, E.M. Morel and A.B. Zamuner), pp. 81–101. Fundación Museo de La Plata "Francisco Pascasio Moreno", La Plata.

Spalletti, L.A., **Fanning, C.M.** and **Rapela, C.W.** (2008) Datting the Triassic continental rift in the southern Andes: the Potrerillos Formation, Cuyo Basin. *Argentina. Geol. Acta*, **6**3, 267–283.

Stipanicic, P.N. (2001) Antecedentes geológicos y paleontológicos. In: *El Sistema Triásico en la Argentina* (Eds A.E. Artabe, E.M. Morel and A.B. Zamuner), pp. 1–21. Fundación Museo de La Plata "Francisco Pascasio Moreno", La Plata.

Stipanicic, P.N. and **Marsicano, C**. (2002) Léxico Estratigráfico de la Argentina. *Asoc. Geol. Argentina*. Serie «B» (Didáctica y Complementaria), **26**(8), 1–343.

Stipanicic, P.N. and **Volkheimer, W**. (2002) Paleoclimatología y paleorrelieve. In: *Léxico Estratigráfico de la Argentina, Triásico* (Eds P.N. Stipanicic and C.A. Marsicano), *Rev. Asoc. Geol. Argent.*, **58**(3), 22–23.

Suárez, M. and **Bell, C.M.** (1994) Braided rivers, lakes and sabkhas of the upper Triassic Cifuncho Formation, Atacama region, Chile. *J. S. Am. Earth Sci.*, **7**, 25–33.

Surdam, R.C. and **Sheppard, R.A.** (1978) Zeolites in saline, alkaline-lake deposits. In: *Natural Zeolites Occurrence, Properties, Use* (Eds L.B. Sand and F.A. Humpton), pp. 145–174. Pergamon Press, Elmsford, NY.

Taher, A.G. and **Abdel-Motelib, A.** (2014) Microbial stabilization of sediments in a recent salina, Lake Aghormi, Siwa Oasis, Egypt. *Facies*, **60**, 45–52.

Talbot, M.R. (1994) Paleohydrology of the late Miocene Ridge basin lake, California. *Geol. Soc. Am. Bull.*, **106**, 1121–1129.

Talbot, M.R., **Holm, K.** and **Williams, M.A.J**. (1994) Sedimentation in low gradient desert margin systems: a comparison of the late Triassic of north-west Somerset (England) and margin systems: a comparison of the late Triassic of north-west Somerset (England) and the late Quaternary of east-central Australia. In: *Paleoclimate and Basin Evolution of Playa Systems* (Ed. M.R. Rosen), *Geol. Soc. Am. Spec. Pap.*, **289**, 97–117.

Tanner, L.H. and **Lucas, S.G**. (2006) Calcretes of the Upper Triassic Chinle Group, Four Corners region, southwestern U.S.A.: climatic implications. In: *Paleoenvironmental Record and Applications of Calcretes and Palustrine*

Carbonates (Eds A.M. Alonso-Zarza and L.H. Tanner), *Geol. Soc. Am. Spec. Pap.*, **416**, 53–74.

Tanner, L.H. and **Lucas, S.G.** (2012) Carbonate facies of the Upper Triassic Ojo Huelos Member, San Pedro Arroyo Formation (Chinle Group), southern New Mexico: paleoclimatic implications. *Sed. Geol.*, **273–274**, 73–90.

Toledo, M.J. (1987) Análisis de facies e interpretación paleoambiental de las sedimentitas triásicas del área Co. Bayo – Co. Melocotón, Departamento de Las Heras, Provincia de Mendoza. PhD Dissertation, Universidad Nacional de Buenos Aires, 108 pp.

Tunik, M.A. (2003) Interpretación paleoambiental de los depósitos de la Formación Saldeño (Cretácico superior), en la alta Cordillera de Mendoza, Argentina. *Rev. Asoc. Geol. Argentina*, **58**, 417–433.

Uliana, M.A. and **Biddle, K.** (1988) Mesozoic-Cenozoic paleogeographic and geodynamic evolution of southern South America. *Rev. Brasil. Geociênc.*, **18**, 172–190.

Vandervoort, D.S. (1997) Stratigraphic response to saline lake-level fluctuations and the origin of cyclic nonmarine evaporite deposits: the Pleistocene Blanca Lila Formation, northwest Argentina. *Geol. Soc. Am. Bull.*, **109**, 210–224.

Verrecchia, E.R., **Freytet, P.**, **Julien, J.** and **Baltzer, F.** (1997) The unusual hydrodynamical behaviour of freshwater oncolites. *Sed. Geol.*, **113**, 225–243.

Wakelin-King, G.A. and **Webb, J.A.** (2007) Threshold-dominated fluvial styles in an arid-zone mud-aggregate river: the uplands of Fowlers Creek, Australia. *Geomorphology*, **85**, 114–127.

Wilding, L.P. and **Tessier, D**. (1988) Genesis of Vertisols: shrink swell phenomena. In: *Vertisols: Their Distribution, Properties, Classification and Management* (Eds L.P. Wilding and R. Puentes), Texas A&M University Printing Center, College Station, TX.

Winsborough, B.M., **Seeler, J-.S.**, **Golubic, S.**, **Folk, R.L.** and **Maguire, B. Jr**. (1994) Recent freshwater lacustrine stromatolites, stromatolitic mats and oncoids from northeastern Mexico. In: *Phanerozoic Stromatolites II* (Eds J. Bertrand-Sarfati and C. Monty), pp. 71–100. Kluwer Academic Publishers, Dordrecht.

Wright, P.V. (2012) Lacustrine carbonates in rift settings: the interaction of volcanic and microbial processes on carbonate deposition. In: *Advances in Carbonate Exploration and Reservoir Analysis* (Eds J. Garland, J.E. Neilson, S.E. Laubach and K.J. Whidden), *Geol. Soc. London Spec. Publ.*, **370**, 39–47.

Wright, P.V. and **Marriott, S.B.** (2007) The dangers of taking mud for granted: lessons from Lower Old Red Sandstone dryland river systems of South Wales. *Sed. Geol.*, **195**, 91–100.

Young, M.J., **Gawthorpe, R.L.** and **Sharp, I.R.** (2003) Normal fault growth and early syn-rift sedimentology and sequence stratigraphy: Thal Fault, Suez Rift, Egypt. *Basin Res.*, **15**, 479–502.

Zamarreño, I., **Anadón, P.** and **Utrilla, R.** (1997) Sedimentology and isotopic composition of Upper Palaeocene to Eocene non-marine stromatolites, eastern Ebro Basin, NE Spain. *Sedimentology*, **44**, 159–176.

Zamuner, A.B., **Zavattieri, A.M.**, **Artabe, A.E.** and **Morel, E.M**. (2001) Paleobotánica. In: *El Sistema Triásico en la Argentina* (Eds A.E. Artabe, E.M. Morel and A.B. Zamuner), pp. 143–184. Fundación Museo de La Plata "Francisco Pascasio Moreno", La Plata.

Zavattieri, A.M. and **Batten, D.J**. (1996) Miospores from Argentinian Triassic deposits and their potential for intercontinental correlation. In: *Palynology Principles and Applications* (Eds J. Jarsonius and D.C. McGregor), *Am. Assoc. Strat. Palynol.*, **2**, 767–778.

Manuscript received 16 July 2014; revision accepted 24 February 2015

Supporting Information

Additional Supporting Information may be found in the online version of this article:

Data S1. Markov Chain Analysis.
Data S2. Cerro de las Cabras Formation.
Data S3. Cerro Puntudo Formation.